

COSMIC RAYS OVER
THE UPPER MID-WEST

by

**CASE FILE
COPY**

Thomas A. Rygg

Technical Report No. 73-081

December 1972



UNIVERSITY OF MARYLAND
DEPARTMENT OF PHYSICS AND ASTRONOMY
COLLEGE PARK, MARYLAND

Space Physics Group

This is a preprint of research carried out at the University of Maryland. In order to promote the active exchange of research results, individuals and groups at your institution are encouraged to send their preprints to

**PREPRINT LIBRARY
DEPARTMENT OF PHYSICS AND ASTRONOMY
UNIVERSITY OF MARYLAND
COLLEGE PARK, MARYLAND
20742
U.S.A.**

COSMIC RAYS OVER
THE UPPER MID-WEST[†]

by

Thomas A. Rygg

Technical Report No. 73-081

December, 1972

Dissertation submitted to the Faculty of the Graduate School
of the University of Maryland in partial fulfillment
of the requirements for the degree of
Doctor of Philosophy
1972

[†]This research was supported by the Office of Naval Research Grant
Nonr-710 (19) and National Aeronautics and Space Administration Grants
NGR-21-002-066 and NSG-398. *NA-21-002-008*

APPROVAL SHEET

Title of Thesis: Cosmic Rays Over the Upper Mid-West

Name of Candidate: Thomas A. Rygg
Doctor of Philosophy, 1972

Thesis and Abstract Approved:

James A. Earl

James A. Earl
Associate Professor of Physics
Department of Physics and Astronomy

Date Approved: Nov. 27, 1972

VITA

Name: Thomas A. Rygg.

Permanent address: [REDACTED], [REDACTED], [REDACTED].

Degree and date to be conferred: Ph. D. 1972.

Date of birth: [REDACTED]

Secondary education: Murray High School, St. Paul, Minnesota, June, 1960.

Collegiate institutions attended	Dates	Degree	Date of Degree
University of Minnesota Minneapolis, Minnesota	1960-1965	B. Phys.	June, 1964
University of Maryland College Park, Maryland	1965-1972	M. S. Ph. D.	June, 1970 December, 1972

Major: Physics.

Minor: Astronomy.

Publications:

Rygg, T. A., and J. A. Earl, Balloon measurements of cosmic ray protons and helium over half a solar cycle 1965-1969, *J. Geophys. Res.*, 76, 7445, 1971.

Earl, J. A., D. E. Neely, and T. A. Rygg, Balloon measurements of the energy spectrum of cosmic ray electrons between 1 and 25 GeV, *J. Geophys. Res.*, 77, 1087, 1972.

Positions held: NASA Trainee, Physics Department,
University of Minnesota, 1964-1965.

Graduate Research Assistant, Physics Department,
University of Maryland, 1965-1972.

N. R. C. - N. A. S. A. Post Doctoral Fellow,
Space Science Laboratory, Marshall Space Flight Center,
Huntsville, Alabama, 1972.

ABSTRACT

Title of Thesis: Cosmic Rays Over the Upper Mid-West

Thomas A. Rygg, Doctor of Philosophy, 1972

Thesis directed by: James A. Earl, Associate Professor of Physics

Differential energy spectra of cosmic ray protons and helium nuclei in the energy range 100 - 260 MeV/nucleon were measured on balloon flights from Minneapolis, Minnesota and from Sioux Falls, South Dakota. The detector was a Geiger tube hodoscope operated in conjunction with two scintillation counters and lead absorbers totalling 75 gms/cm^2 in thickness. The energy spectrum of re-entrant albedo protons was found to be essentially flat in the 100 - 200 MeV interval as is predicted by theoretical calculations of the equilibrium spectrum of secondary protons emerging from thick layers of air. Geomagnetic cutoff rigidities obtained during quiet times from the spectra of helium nuclei were variable from day to day averaging 23% below the level predicted by detailed orbit calculations that invoke only internal sources of the earth's magnetic field. Correlation of the cutoff with the earth's equatorial field suggested that the source of the variation is a fluctuating ring current located within the radiation belt at $\sim 7 R_E$. During the magnetic storm of August 30, 1966, the cutoff was observed to be depressed at times below 40% of its quiet time level, but it was restored to nearly the normal level during the positive phase of the storm. Because of the depressed cutoffs, it was possible to measure the spectrum of primary protons just before and during the Forbush decrease of August 30, 1966

and thus to show that the form of these spectra was indential to that observed throughout the solar cycle with the same instrument. Specifically, the spectrum of protons during the most deeply modulated period that was observed followed the same law, $J=AT$, where J is the differential intensity, T is kinetic energy, and A is a parameter independent of energy but variable in time, that characterizes the modulated spectrum of primary protons. The solar cycle variation of atmospheric secondary protons was investigated. It was found that the intensity of secondary protons varied by 40% over the solar cycle and was in good agreement with a theoretical model of atmospheric propagation.

ACKNOWLEDGEMENTS

I must express my sincere gratitude to my thesis advisor Professor James A. Earl who has guided me through the peaks and valleys of my graduate career. One could not imagine an advisor more intensely interested in his students.

The enthusiasm, guidance, and help of my co-advisor Professor Joseph J. O'Gallagher is also gratefully acknowledged.

Most sincere thanks go to Richard and Barbara Stafford whose southern hospitality has enabled me to complete this thesis. Their optimism and encouragement have kept me going through these final stages.

Special thanks go to Mary Louise Snidow, Rose Pryor, and Ira Tannenbaum who cheerfully and competently typed the many versions of the manuscript.

I also wish to thank Janet Luhmann whose research into the August 28 solar flare I found most valuable.

Assistance in many aspects of data processing provided by the staff of the Goddard Space Flight Center is also gratefully acknowledged. The Office of Naval Research, Raven Industries, and Winzen Research arranged and provided many fine balloon flights for the hodoscope. I am also grateful to the staffs of the Cornell Electron Synchrotrons, the Brookhaven AGS, the Cal Tech Synchrotron, and the Naval Research Lab Linac for their cooperative efforts in the detector calibrations.

Thanks also go to Steve Gustafson, Chuck Carlson, John Rockstroh, Dennis Neely, Greg Burrows, Maurice Pairel, Harvey Novak, George Umberger, Julius Brecht, Chip Meegan, Larry Bagg, Bob Smith, Bill Leech,

Larry Votta, and Janet Luhmann for assistance in the balloon operations over these many years.

Computer time for this project was supported in part through the facilities of the University of Maryland's Computer Science Center.

Work on this project began at the University of Minnesota where support was provided by the Office of Naval Research Grant Nonr-710(19). Support at the University of Maryland was provided by the National Aeronautics and Space Administration Grants NGR-21-002-066 and NsG 398. I would also like to acknowledge receipt of a N.A.S.A. Traineeship that supported my graduate studies at the University of Minnesota.

TABLE OF CONTENTS

Chapter	Page
ACKNOWLEDGEMENTS	ii
LIST OF TABLES	vi
LIST OF FIGURES	vii
I. INTRODUCTION	1
II. APPARATUS AND BALLOON FLIGHTS	6
A. Description of the Instrument	6
B. Data Analysis	8
C. Balloon Flights	12
III. ATMOSPHERIC SECONDARY PROTONS	13
IV. RE-ENTRANT ALBEDO PROTONS	18
A. Introduction	18
B. Observed Fluxes	21
C. Model Calculations	22
D. Discussion	29
V. QUIET TIME GEOMAGNETIC CUTOFFS	34
A. Introduction	34
B. Empirical Determination of Geomagnetic Cutoffs	45
C. Narrative Description of Cutoff Variations	49
1.) Flight 1038-W	49
2.) Flight 1056-W	49
3.) Flight 1057-W	50
4.) Flights 974-N and 975-N	51
5.) Flights 1078-W and 1079-W	53
D. Discussion	55

Chapter	Page
VI. AUGUST 28, 1966 FLARE — INTERPLANETARY AND GEOMAGNETIC DISTURBANCE	64
A. Introduction	64
B. Observations During the August 28, 1966 Disturbance	70
C. Geomagnetic Cutoff Variations During Flight 1057-W	74
1.) Analysis Procedure	74
2.) Cutoff Determinations	76
3.) Discussion	80
D. Forbush Decrease of August 30, 1966	88
VII. SUMMARY AND CONCLUSIONS	97
APPENDIX A ATMOSPHERIC SECONDARY PROTONS REVISION FOR BEHAVIOR AT LARGE DEPTHS	101
APPENDIX B INDUCTIVE EFFECT OF THE EARTH ON OBSERVED D_{st} VALUES	104
APPENDIX C ENERGY DENSITY IN THE EARTH'S FIELD AND LIMITATIONS ON RING CURRENT STRENGTH	105
REFERENCES	108

LIST OF TABLES

Table	Page
I. Ionization Depths in the Detector	115
II. Summary of Flight Data	116
III. Re-entrant Albedo Scale Factors	117
IV. Tabulation of Observed Cutoff Rigidities	118
V. Coefficients A_{ij} for Fitting Shea et al. (1968) cutoff grid	119

LIST OF FIGURES

Figure	Page
1. Schematic Diagram of the Hodoscope Detector	120
2. Sample Pulse Height Distributions	121
3. Calculated Secondary Proton Spectra	122
4. Growth Curve of Atmospheric Secondary Protons	123
5. Regression Analysis of Secondary Proton Intensity	124
6. Observed Spectra of Re-entrant Albedo Protons	125
7. Regression Analysis of Re-entrant Albedo Proton Intensity	126
8. Schematic Diagram of Albedo Trajectories and Angular Distribution of Secondary Production	128
9. Comparison of Observed and Predicted Re-entrant Albedo Spectra	129
10. Regression Analysis of Penetrating Proton Intensity	130
11. Illustration of the Smoothing Effect of the Hodoscope's Rigidity Windows on the Penumbral Cutoff Structure	132
12. Flight 1038-W Helium Rigidity Spectrum	133
13. Contours of Constant Geomagnetic Cutoff	134
14. Flight 1038-W Trajectory	136
15. Flights 1056-W and 1057-W Trajectories	137
16. Flight 1056-W Helium Rigidity Spectrum	138
17. Flight 974-N Trajectory	139
18. Flight 974-N Helium Rigidity Spectra	140
19. Flight 975-N Trajectory	141
20. Flight 975-N Helium Rigidity Spectra	142
21. Flights 1078-W and 1079-W Trajectories	143
22. Flights 1078-W and 1079-W Helium Rigidity Spectra	145

Figure	Page
23. P_o vs. P_c for Six Upper Mid-West Flights	146
24. P_{cx} vs. P_c for Six Upper Mid-West Flights	148
25. Cutoff Depression vs. D_{st}	150
26. Histogram of Hourly D_{st} Values	151
27. Comparison of Cutoffs Measured Over Minneapolis	152
28. Time History of August 28, 1966 Solar Flare	154
29. Flight 1057-W Proton Rigidity Spectra	156
30. Flight 1057-W Helium Rigidity Spectra	157
31. Flight 1057-W Regression Analysis of Penetrating Proton Flux	159
32. Flight 1057-W Comparison of Cutoff Depression and D_{st}	160
33. Idealized Magnetospheric Configurations	162
34. Neutron Monitor Rates for the Canadian Net for August, 1966 (Steljes, 1966)	164
35. Flight 1057-W Regression Analysis of Low Energy Protons	166
36. Flight 1057-W Regression Analyses of Helium Nuclei	168

I. INTRODUCTION

Cosmic rays provide a useful tool for studying a variety of astrophysical and geophysical phenomena. They appear to permeate most of our galaxy and thus serve as probes of magnetic fields over scales ranging from those of geophysical and interplanetary interest to those related to the structure of our galaxy. Studies of cosmic ray propagation in the interplanetary medium have yielded information concerning the large and small scale structure of the magnetic field carried into space by the expanding solar wind plasma. Though far from being completely understood, studies of the modulation of cosmic ray intensity which is correlated with the eleven-year cycle of solar activity have been used to estimate the volume of space occupied by the solar plasma and to determine the degree of turbulence of the field. Studies of the temporal behavior of the intensity of energetic particles released during solar flares provide independent estimates of the degree of magnetic disorder in the interplanetary medium and confirm the large scale spiral structure of the interplanetary magnetic field. Studies of short term cosmic ray modulation phenomena (Forbush decreases) which are also associated with solar activity help identify changes in the interplanetary medium caused by these disturbances.

On a small scale, cosmic rays show a remarkable sensitivity to the structure of the earth's magnetic field manifested through the geomagnetic cutoff effect. At a given latitude particles below a particular rigidity (the cutoff rigidity) are deflected away by the earth's magnetic field and, consequently, are denied access to the top of the atmosphere. High order expansions of the earth's internal field are required to resolve anomalies in the low latitude cosmic ray intensity

distribution revealed in neutron monitor surveys. Exceptionally low cutoff rigidities and day-night cutoff variations observed at high latitudes are sensitive to the shape of the cavity (the magnetosphere) in which the earth's field is confined by the solar plasma and to the topology of the field within. When the solar wind plasma flow is enhanced by solar activity, the response of the magnetosphere (a magnetic storm) is strongly evident in reduced cosmic ray cutoffs at middle latitudes. Since the time scale of these disturbances is only several hours, cosmic rays provide one of the few ways of observing the effects of the magnetic storm on a global basis.

This thesis deals experimentally with these geophysical questions with the aid of a balloon borne Geiger tube hodoscope which measures the differential energy spectra of cosmic ray protons and helium nuclei in the energy range 100-260 MeV/nucleon and integral intensities above 260 MeV/nucleon. Electrons in the energy range 16-150 MeV are also resolved but their analysis has already been presented elsewhere (Luhmann, 1971; Luhmann and Earl, 1973). The term hodoscope is derived from the Greek roots hodos, meaning path, and scopos, meaning to watch. Thus the term hodoscope is used in particle physics to describe any device (usually electronic) that determines and displays the trajectory of a charged particle. The same instrument provided data for an M. S. thesis (Rygg, 1970) which dealt with the long term solar modulation of primary protons and helium nuclei observed during nine high latitude flights covering the entire increasing phase of solar activity (1965-1969). While the results discussed here are quite independent of the M. S. thesis, it would be unnecessarily repetitious to present more

than a cursory review of the already available description of the detector and data analysis scheme. Furthermore, extensive use is made here of major conclusions reached in the earlier work. Consequently, the interested reader is referred to the M. S. thesis and to a published paper based on it (Rygg and Earl, 1971).

Since the data on which this thesis is based were obtained from seven balloon flights over the Upper Mid-West, where the geomagnetic cutoff normally excludes most primaries within the energy range covered by the detector, the discussion will focus on geomagnetic effects and on the modulation of secondary components. However, some observations of low-rigidity primaries were made during a period of reduced cutoff associated with a large magnetic storm on August 29-30, 1966. Specific topics include the geomagnetic cutoff during magnetically quiet and highly disturbed periods, short term cosmic ray modulation (Forbush decrease), re-entrant proton albedo, and atmospheric secondary protons. The mapping of geomagnetic cutoffs was facilitated by winds at balloon altitudes which resulted in flight trajectories entering Minnesota, Wisconsin, Iowa, Nebraska, and South Dakota.

Since the above topics are quite diverse, the text that follows is organized so that each chapter is more or less self contained and begins with an introduction that presents a background for the topic and reviews the pertinent literature. Chapter II. summarizes the data and gives a brief description of the detector and data analysis scheme. Chapter III. extends and verifies calculations of the propagation of secondary protons in the atmosphere (Rygg, 1970) and discusses the solar modulation of this component. Atmospheric secondaries do not

possess great intrinsic significance, but they constitute a background that must be subtracted before more interesting processes affecting the intensity of primary cosmic rays can be studied. The empirical demonstration in Chapter III. that the intensity of atmospheric secondary protons at Churchill and Minneapolis varies by 40% over the solar cycle together with the verification of a propagation model puts this subtraction on a more firm theoretical and observational basis than has been available previously. Chapter IV. deals with another secondary component, the re-entrant albedo protons which are upward moving secondaries that are reflected back toward earth by the geomagnetic field. The observed differential energy spectrum of re-entrant albedo protons is essentially flat from 100-250 MeV. This new result does not agree with some earlier reports (Teegarden, 1967; Ormes and Webber, 1968; Bingham et al., 1968), but it is expected as a consequence of the model for calculating the intensity of direct secondaries which is applied in Chapter IV. to the production of re-entrant albedo protons.

Observations of the latitude and temporal variations of the geomagnetic cutoff during magnetically quiet times are presented in Chapter V. On some occasions the cutoff is consistent with that expected from the earth's internal field, but the cutoff is variable from day to day and is usually depressed. This observation demonstrates, for the first time, a significant effect of external currents upon mid-latitude cutoffs. The day to day variability appears to be correlated with small changes ($\pm 15\gamma$) in the equatorial magnetic field, but diurnal variations, if present at all, are smaller than the day to day variation.

Chapter VI. presents observations obtained on August 30, 1966 from a 24 hour balloon flight during which the geomagnetic cutoff at Minneapolis was depressed below 40% of its quiet time value. However, the cutoff was restored to nearly its full quiet time value during the positive phase of a magnetic storm which began with the sudden commencement of 1112 U. T. August 30, 1966. Because of the depressed cutoffs, it was possible to observe primary protons during portions of the flight and thus to demonstrate that the $J=AT$ spectral behavior that is characteristic of the eleven-year modulation below 200 MeV is also a characteristic of the Forbush modulation.

II. APPARATUS AND BALLOON FLIGHTS

A. Description of the Instrument

The detector, shown in Figure 1, consists of a Geiger tube hodoscope, a dE/dx detector and a sandwich of lead and plastic scintillator plates which comprise a total energy calorimeter. Five pairs of crossed trays of Geiger tubes, shown end on, define the range and geometry of a particle and detect nuclear interactions occurring in the lead. The combined light output of the five calorimeter plates is a sample of the total energy deposited in the lead absorber. The amplitudes of the dE/dx and calorimeter signals are determined by 18 channel logarithmic pulse height analyzers which have channel widths of 33% and a dynamic range of 100. The trays of Geiger tubes measure 15 cm by 15 cm, and the apparatus is 32 cm high. The total absorber thickness is equivalent to 76 gms/cm^2 of lead. A modified version of the detector containing an additional 38 gms/cm^2 of lead distributed evenly throughout was flown on two flights in late 1967.

As indicated in Figure 1, eleven two-fold coincidences select particle trajectories which pass through tray 10 when extended. An event is registered only when such a coincidence occurs between both pairs of upper trays. This use of multiple telescopes defines a beam collimated to $\pm 16^\circ$ with a geometric factor of 10.3 cm^2 steradian before it enters the main body of the detector.

The technical details of how pulse height and Geiger tube information was processed by the flight apparatus, telemetered to the ground, tape-recorded and finally analyzed by computer do not bear

repeating as they are found in Rygg (1970). Nonetheless, the end result is a computer compatible record of all information pertaining to each event including the pulse heights, the waiting time from the previous event and a list of those geiger tubes that were discharged.

B. Data Analysis

In the present experiment the energy spectra of cosmic ray protons and helium nuclei from 66 - 250 MeV/nucleon are determined by the range, dE/dx , and calorimeter responses to the various particles. Events are first sorted to restrict the analysis to particles firing one Geiger tube per tray. This criterion rejects electron showers and obvious nuclear interactions. Those events satisfying this criterion are then accumulated in a three dimensional histogram whose coordinates are dE/dx pulse height, calorimeter pulse height and the number of the last tray of Geiger tubes in which a discharge occurred (RANGE). The parameter RANGE delineates definite, non-drifting energy intervals when the appropriate range-energy relation is applied. Table I lists the ionization depths and energy intervals thus defined for both configurations of the detector.

In addition to distinguishing the particle's charge, the dE/dx and calorimeter pulse heights also separate out a background of electrons and nuclear interactions which did not fire extra Geiger tubes. Figure 2 shows two representative histograms for RANGE 10 and RANGE 7 obtained by summing the dE/dx and calorimeter pulse heights for events selected as described above. The proton and helium curves shown in that figure are synthetic distributions constructed by folding the known detector resolution (due basically to photoelectron statistics) into the expected pulse height response function for that range interval. The broad peak near minimum ionization for RANGE 7 is the distribution of electrons plus fast proton background as determined from accelerator calibrations.

The number of particles for each component - protons, helium nuclei, and background - is obtained from a computer analysis which adjusts the amplitude of the three synthetic distributions to obtain a best fit to the observed pulse height distribution. The raw numbers of protons and helium nuclei must then be corrected for a variety of effects which tend to remove valid particles from the analysis. These include nuclear interactions, Geiger tube inefficiency, and extra discharges due to "knock-on" electrons and inclined trajectories all of which are treated rather extensively in Rygg (1970).

Calculation of fluxes is then a simple matter of dividing the number of particles by the detector exposure, subtracting the atmospheric secondary contamination to the protons, applying an atmospheric absorption correction ($\lambda_p=150 \text{ gms/cm}^2$, $\lambda_{\text{He}}=54 \text{ gms/cm}^2$) and dividing by the energy intervals appropriate to the top of the atmosphere. Errors quoted are a combination of the 3% error in determination of the geometric factor and particle statistics.

In addition to the spectral determination using stopping particles the RANGE 10 distribution in Figure 2 was resolved into a minimally ionizing peak (fast protons $E \geq 720 \text{ MeV}$) plus a more heavily ionizing component (slow protons 260-720 MeV) using the curve fitting techniques previously described.

In the original analysis scheme, once the computer had sorted all the events and had printed out the appropriate matrices all further analysis was done by hand. Since this thesis is basically concerned with time variations of the cosmic ray flux on scales as small as one

hour, the order of magnitude increase in required calculations made it necessary to implement the entire analysis procedure into a single computer program which accumulates matrices over any desired time interval and then prints out the fully corrected particle fluxes and the experimental errors.

C. Balloon Flights

The data available for analysis consists of 20 balloon flights, summarized in Table II, and calibration exposures to protons and pions at the Brookhaven Alternating Gradient Synchrotron and to electrons at the Cornell 2 and 10 GeV Synchrotrons, and the Naval Research Lab Linac. This thesis will be concerned primarily with the flights made from Minneapolis, Minnesota and Sioux Falls, South Dakota.

Twelve balloon flights launched from Fort Churchill, Manitoba cover nearly the entire period from cosmic ray maximum in May, 1965 through cosmic ray minimum in 1969 and 1970 and halfway back to maximum in July, 1971 with one or two flights each summer. Since the geomagnetic cutoff rigidity at the latitude of Churchill remains below 100 MV, well below the atmospheric cutoff at 2 gms/cm^2 for protons, 300 MV, protons and helium nuclei seen at Churchill are galactic cosmic rays plus atmospheric secondaries. Data from eight Churchill flights through 1969 were used earlier to study solar modulation throughout the increasing phase of the cycle of solar activity (Rygg, 1970; Rygg and Earl, 1971).

Seven balloon flights launched at intermediate latitudes (Minneapolis and Sioux Falls) during 1965-68 are analyzed here for geomagnetic cutoff effects, proton albedo intensities and atmospheric secondaries. The geomagnetic cutoff in the region covered by these flights (1 to 2GV) excludes primary protons so that protons stopping in the detector consist of atmospheric secondaries plus re-entrant albedo. The rigidities of stopping helium nuclei, however, span the cutoff region and provide quite accurate determinations of cutoff rigidities since there

are very few secondary or albedo helium nuclei. One of these flights, 1057-W, occurred during a period of geomagnetic and interplanetary activity associated with an importance 3 solar flare occurring at 1521 U.T. on August 28, 1966 providing new information on cutoff variations and short term modulation phenomena.

Calibration data obtained at the Brookhaven A.G.S. were used to study proton interactions and their visibility in the detector so that suitable interaction corrections could be made to flight data. Electron calibration data from 105 to 8200 MeV obtained at the Cornell 2 and 10 GeV Synchrotrons were used to demonstrate that electrons around 300 MeV can give a single particle signature in the Geiger tubes and therefore account for most of the background at low ionization as in Figure 2 (Rygg, 1970).

III ATMOSPHERIC SECONDARY PROTONS

Before discussing observations at the top of the atmosphere some attention must be devoted to the dominant correction that must be applied to low energy particle data obtained within the atmosphere - the subtraction of atmospheric secondary protons. Considerable effort was devoted to this correction in earlier work (Rygg, 1970) because the secondary flux amounted to half that observed in the lowest energy bin. In that paper a model describing atmospheric secondary production and propagation was presented with some experimental verifications of the predictions; specifically, the depth and solar cycle dependence of the absolute intensity. In this thesis we will be interested in rather small changes in the low energy proton flux observed at varied conditions of solar modulation and latitude which are likely to affect the contribution of secondaries. Furthermore, earlier predictions of this model (Rygg, 1970) concerning the solar cycle and latitude dependence contradict to a certain extent the analysis presented by Teegarden (1967). Hence further verification of these effects is necessary.

Energetic cosmic rays interacting with air nuclei above the detector produce a spectrum of low energy secondary protons. Before reaching the detector however, the secondary beam is degraded by ionization loss and nuclear absorption. In the model discussed by Rygg, particles arising from a constant production function (per gram) at all depths above the detector are propagated through the intervening air using standard equations for energy loss (Rossi, 1952) and an absorption mean free path of 150 gms./cm^2 . A constant production is consistent

with the observation of a constant flux (+20%) of penetrating particles up to depths of 200 gms./cm^2 . Except for energies below those considered here, particle trajectories are not significantly affected by multiple scattering (Rossi, 1952) nor magnetic deflection in the relatively short distance to the detector.

The energy spectra and depth dependence of the secondary protons as predicted by the model (Rygg, 1970; and slight revisions in Appendix A. are shown in Figures 3 and 4, respectively. The absolute intensity and energy spectrum at 3 gms/cm^2 agrees very well with the direct measurements made by Teegarden (1967) and Freier and Waddington (1968) when corrections of the order of 20% for solar modulation are applied (Rygg, 1970).

As an aid to understanding assumptions that will be made later in this chapter and in the following chapter we must consider two equilibrium situations reflected in the solutions presented in Figure 3. Consider for example the flux of secondary particles at 80 MeV. Since 1) the production spectrum is peaked strongly towards low energy and 2) the range of an 80 MeV proton is only 6 gms/cm^2 , the bulk of the particles seen at 80 MeV are generated within a depth above the detector comparable to that range. For depths in the atmosphere greater than this characteristic depth, the expected linear depth/intensity relation rounds off to a constant when the equilibrium between production and ionization loss is reached. An example of this situation is depicted in Figure 4 for RANGE 4 protons (66 - 106 MeV) where the equilibrium beyond 20 gms/cm^2 predicted by the model (solid curve) is verified

using the observed "growth" curve of four flights made in 1968 and 69 (experimental points).

As one goes to higher energies, the characteristic depth interval in which particles are generated also becomes larger explaining the increased fluxes of high energy particles even though the production spectrum has a steeply falling energy dependence. A second equilibrium situation is reached when the particle range becomes comparable to the nuclear absorption mean free path. In that case the bulk of the secondary flux at all energies originates within one or two mean free paths of the detector. This equilibrium accounts for the persistent negative slope of the spectra beyond 100 MeV and the depth independent energy spectra beyond 300 gms/cm². This latter discussion has little relevance to the observations of primary particles discussed in this thesis but it will be invoked in the following chapter concerning re-entrant proton albedo.

It can be seen in Figure 4 that the RANGE 4 protons in the 20 - 100 gms/cm² depth interval are predominantly secondary even at high latitudes with the flux being sensitive to neither small changes in depth nor energy (see Figure 3). Because of these facts the RANGE 4 flux is an appropriate indicator of the solar cycle and latitude dependence of the secondary component. Since the model predicts that the secondary flux is most sensitive to the incident proton flux in the 1 - 2 GeV range, both solar modulation and geomagnetic effects should be important. Figure 5 is a regression plot of the RANGE 4 fluxes obtained in the 20 - 100 gms/cm² ascent portion of every flight made from Churchill

(solid circles) and Minneapolis/Sioux Falls (open circles) vs. Deep River Neutron Monitor (Steljes, 1972). The solid lines indicate the prediction obtained from the model assuming that the secondary production scales as

$$\int_0^{\infty} M(E) J(E) dE \quad (\text{III-1.})$$

where $M(E)$ is the multiplicity of secondary particles initiated by a particle of energy E and $J(E)$ is the appropriate cosmic ray spectrum. At Churchill $J(E)$ was assumed to be the primary spectrum given by Meyer (1969) for solar minimum and Rygg (1970) for solar maximum. At Minneapolis the cosmic ray spectrum was assumed identical to the Churchill spectrum above the geomagnetic cutoff. A flat albedo spectrum at the level of the RANGE 7-9 and RANGE 10 (slow) components was assumed below cutoff. Assuming a zero albedo flux results in a 10% reduction of the Minneapolis results.

The weighted least squares fits to each of the groups of data in Figure 5 coincide with the theoretical predictions within 2-3%. However, the errors involved do not allow a statistically significant demonstration of the latitude effect. Nevertheless since the Minneapolis/Churchill difference is only 8% it will do little harm to assume that the theoretical result applies. The solar cycle variation is more clearly significant. Teegarden (1967) placed an upper limit of 13% on the variation of secondary intensity at Sioux Falls for two flights having Mt. Washington Neutron Monitor hourly readings of 2180

and 2405. The more extensive survey reported here gives a variation of $21 \pm 9\%$ for the same conditions. Although there is a little overlap in the limits placed on the variation, the marked solar cycle effect evident in Figure 5 for both Sioux Falls/Minneapolis and Churchill fails to support Teegarden's assertion that the secondary flux is sensitive to the primary flux near 3.6 GeV rather than the 1.5-2 GeV obtained from the model used here.

To obtain a measure of confidence with which the theory can be applied, we take the observed RMS deviation of the points in Figure 5 which is 6%. This error will be included in all fluxes quoted in the following sections.

IV. RE-ENTRANT ALBEDO PROTONS

A. Introduction

Were it not for the copious production of secondary protons in the earth's atmosphere, there would be essentially no low energy protons at low latitudes where primaries are excluded by the geomagnetic field. Protons observed at rigidities below the geomagnetic cutoff consist of direct secondary protons produced in the atmosphere above the balloon plus protons produced as upward moving secondaries (splash albedo) in one hemisphere which, guided by the earth's field, re-enter the atmosphere at the conjugate region in the opposite hemisphere. This second component - the re-entrant proton albedo - can never coexist with the primary flux. The albedo is observed only when the orbits traced by particles traveling through the geomagnetic field intersect the earth, whereas the primary flux is observed only when the particle orbits connect to interplanetary space. In both cases Liouville's theorem requires that the observed differential intensity is the same as that existing at the source. Above cutoff the proton intensity at the top of the atmosphere is the same as that of the primary beam outside the magnetosphere. Below cutoff the re-entrant albedo intensity at the top of the atmosphere is the same as that of the splash albedo leaving the atmosphere.

Energetic cosmic ray particles undergoing nuclear interactions with air nuclei produce a beam of secondary protons which is collimated in the forward direction. Those that are produced above the balloon traveling vertically downward are observed as directly produced atmospheric secondaries. At low latitudes, the small fraction that is produced with a vertically upward velocity component is confined to the

flux tube on which it was produced and re-enters the atmosphere at the magnetic conjugate point in the opposite hemisphere with the same intensity it had upon escaping the atmosphere. Although the fraction of upward moving secondaries is quite small (20-30% of the downward secondaries), the albedo flux exceeds the directly produced secondaries at energies above 150 MeV because upward moving particles produced at all depths in the atmosphere contribute to the re-entrant albedo while direct secondaries come only from the thin layer of atmosphere above the balloon.

In the succeeding sections of this chapter, observations of the energy spectrum and solar cycle dependence of the albedo flux observed over the Upper Mid-West will be presented. In contrast to previously reported work, both the observed spectra and model calculations show a very flat energy spectrum reflecting the equilibrium nature of the albedo component. The absolute fluxes obtained here also exceed previously reported levels. The albedo spectra will be used later in this thesis to provide a reference level for the proton flux below the geomagnetic cutoff so that the cutoff variations that occurred during Flight 1057-W can be identified. The albedo observations also provide further verification of the secondary proton propagation model discussed in the preceding chapter. Furthermore, a clear definition of the albedo flux level is needed since the proton albedo is an incessant source of background particles in cosmic ray studies using integral detectors. For example, if there were no proton albedo, the energy spectrum of the primary proton beam could be determined from a latitude survey using an integral detector by taking the derivative of the observed flux with

respect to geomagnetic cutoff energy. However, the albedo flux adds a background variation which, using the fluxes obtained here, cancels out most of the latitude variation.

B. Observed Fluxes

The spectra of re-entrant albedo protons as measured at the top of the atmosphere for six quiet time mid-latitude flights are shown in Figure 6. The differential flux is only weakly dependent on energy and lies in the range .5-.8 protons/M² sec ster MeV. The positive slope exhibited by Flights 1038W and 1056-W probably results from a slight overestimation of the secondary proton correction at the relatively large ceiling depths (9gms/cm²) of these flights. Here the secondary flux accounts for 75% of the observed RANGE 4 flux but only 30% of the RANGE 9 flux. Flights 974-N and 975-N yield the best estimates of the albedo spectra. At their ceiling altitude of 3.5 gms/cm², the RANGE 4 secondary correction is only 50%, and the RANGE 9 correction is 10%. The fluxes obtained above 200 MeV from these flights are then as well determined as those obtained from the Churchill flights where the secondary contribution averages 16%.

The solar modulation of the re-entrant albedo intensity should be the same as the modulation of the direct secondary intensity because of their common origin. The regression analysis of the albedo intensity at 200 MeV (RANGE 7, 8 and 9) vs. Deep River Neutron Monitor (Steljes, 1972) shown in Figure 7, however, fails to show conclusively the expected solar cycle variation. The dashed line, which has been normalized to fit the average flux level indicates the expected variation. The poor statistical accuracy of the data allows any variation from flat to something of the order of the predicted form. The wide variations appear to be purely random since there is no latitude variation. The RMS deviation from the dashed line is 20%. Further discussion of these data follows the presentation of calculations of the albedo intensity, energy spectrum and solar cycle variation.

C. Model Calculations

Published determinations of the proton albedo spectra (Teegarden, 1967; Bingham et al., 1968; Ormes and Webber, 1968) differ by almost a factor of 10. Some theoretical basis for comparison is needed first to predict the flux and second to sort out the possible effects of latitude and solar cycle that might account for the observed differences. Two versions of a model used to predict albedo intensity will be presented here. Both assume that the shape of the energy spectrum of albedo particles is the same as that obtained for atmospheric secondary protons in the limit of large depths (see Figure 3). Since only a small fraction of the atmospheric secondary flux is projected upward, this equilibrium spectrum must be reduced by the "back to front ratio" of the angular distribution of secondary particles generated in the atmosphere. The two models differ only in the determination of this ratio.

Since the origin of the proton albedo is identical to that of the direct secondaries, the model of particle generation and propagation discussed in Chapter III and Appendix A will also be used here. For all atmospheric depths, it is assumed that each differential element of the atmosphere is illuminated over the upper hemisphere by a constant flux of energetic cosmic rays. Through the mechanism of nuclear interaction with the air nuclei each differential element becomes a constant source (per gram) of low energy protons. Both those going downward (which are direct secondaries) and those going upward (which constitute the albedo flux) propagate according to Equation A-1 (see Appendix A). The albedo flux leaving the top of the atmosphere is composed of those

upward moving particles generated at all depths which survived the nuclear absorption and ionization loss processes. To the extent that the production of albedo particles is independent of atmospheric depth, the albedo component can thus be identified with the equilibrium spectrum at large depths obtained from the secondary particle model. The nature of this equilibrium is discussed in the preceding chapter.

The assumption of a constant illuminating flux and therefore a constant source of secondary particles is required only down to depths of 200 - 250 gms/cm² because the spectrum of secondary particles reaches its equilibrium level within that depth. The secondary particle spectrum at 200 gms/cm² obtained from the model matches the equilibrium form within 3% at all energies. The penetrating proton flux ($E > 260 \text{ MeV}$) observed by the hodoscope varies by less than $\pm 20\%$ down to a depth of 200 gms/cm². Since the mean energy of these particles (2 GeV) is characteristic of those particles that generate most of the secondary flux (Rygg, 1970), the production of secondary particles down to 200 gms/cm² must also be constant within similar limits. It is argued therefore that reasonable conditions for application of the equilibrium propagation model are satisfied.

The most critical factor in calculating the overall albedo intensity is determining the fraction of secondary particles that is projected upwards. Figure 8b shows the angular distribution of secondary protons, $E \gtrsim 90 \text{ MeV}$, calculated by assuming that a volume element of air is illuminated by a flux of high energy particles uniformly distributed over the upper hemisphere. Since most atmospheric secondary particles are produced by cosmic rays in the 1.5 - 2 GeV interval (Rygg, 1970),

the angular distribution of protons of energy greater than 90 MeV emitted by ^{27}Al illuminated by 1840 MeV protons, calculated by Metropolis et al. (1958) was assumed to be representative of albedo particles. Note that there is a strong downward peaking so that the determination of which particles actually can escape upward can have a strong effect on the albedo intensity.

It is apparent from Figure 8b that the bulk of the albedo flux is generated nearly horizontal. Deflection of the secondary particle trajectories by the earth's magnetic field can, therefore, have a definite effect on the fraction that escape upward. Figure 8a depicts the atmosphere as a thin sheet confined to the NSEW plane. The vector \vec{B} denotes the magnetic field with a dip angle δ , which, given the cutoff rigidity P_c , can be obtained from the solution of

$$P_c = 15.96 \cos^4 \lambda \text{ (GV.)} \quad (\text{Smart and Shea, 1967}) \quad (\text{IV-1.})$$

$$\delta = \tan^{-1} \left(\frac{\cot \lambda}{2} \right) \quad (\text{IV-2.})$$

assuming the earth's field is a simple dipole. Since an equilibrium situation exists, the problems of escape can be effectively separated from energy loss or further interactions so that the situation presented in Figure 8a can be applied to the last interaction generating a particle no matter where it happens. Orbits of particles produced with angular inclinations of 20° to the horizon are indicated in four typical directions. Assuming an energy of 200 MeV, these orbits will all lie on a flux tube having a diameter of 80 km. They will, however, have differing pitch angles depending on the direction in which they are produced. Note that the north moving particle, produced at point E,

dives back into the atmosphere and that the particle directed westward at point N skims the atmosphere for nearly one-half turn before it finally escapes. Particles directed southward and eastward easily escape.

In quantitative terms, particles produced in the azimuthal direction ϕ at a zenith angle α have a pitch angle μ with respect to the magnetic field given by

$$\mu = \cos^{-1}(-\sin \delta \sin \alpha \cos \phi + \cos \delta \cos \alpha) \quad (\text{IV-3.})$$

Maximum and minimum pitch angles occur when $\phi = 0^\circ, 180^\circ$ so that

$$\alpha - \delta \leq \mu \leq \alpha + \delta \quad (\text{IV-4.})$$

Assuming for the moment that the guiding center approximation describes the motion along the flux tube, the pitch angle distribution of the particles arriving in the opposite hemisphere will be the same as that of the emerging particles. Since the particles will typically make many orbits around the field line before their re-entry, the points of impact will be uniformly distributed around the flux tube so that their zenith angles at impact ν will be spread over the interval

$$\text{maximum } \begin{cases} \alpha - 2\delta \\ 0^\circ \end{cases} \leq \nu \leq \text{minimum } \begin{cases} \alpha + 2\delta \\ 90^\circ \end{cases} \quad (\text{IV-5.})$$

For example, particles emitted at zenith angles of $\alpha = 70^\circ$ (20° above the horizon) at Minneapolis ($\delta \sim 18^\circ$) will appear spread over $34^\circ \leq \nu \leq 90^\circ$ at the conjugate point in the Southern Hemisphere.

In model #1, the assumption is made that all particles that meet the geometric conditions for escape have an equal probability of being detected as albedo particles upon re-entry. This case applies when the albedo detector accepts a wide range of zenith angles or when smoothing

effects owing to large dip angles or non-adiabatic particle motion predominate. For $\delta \approx 45^\circ$ in Equation IV-5., vertically detected particles ($\nu=0^\circ$) could have been generated at any zenith angle α . For rigidities near cutoff, failure of the guiding center approximation allows particles escaping in nearly horizontal orbits to re-enter at nearly any zenith angle. The conditions for escape are 1.) that a particle is produced with a pitch angle less than 90° so that it travels up the field and 2.) that the particle is produced in a direction above the horizon ($\alpha < 90^\circ$). A particle directed toward the south at a small downward angle can satisfy condition #1, but the diameter of its orbit is so large that it dives deep in the atmosphere preventing escape. The portion of the particle distribution satisfying both conditions is shown as the shaded portion in Figure 8b. Particles produced in the direction $\phi=0^\circ$ (northward) must have horizon angles $(90^\circ - \alpha) > \delta$ while particles produced with $90^\circ < \phi < 270^\circ$ (any direction toward the south) merely require $(90^\circ - \alpha) > 0$.

Model #2 applies to cases in which the detector half angle ξ is small and when the smoothing effects of large dip angle δ or violation of adiabatic invariance do not apply. In that case albedo particles observed by the detector can arise (due to the pitch angle restraints given in Equation IV-5.) only from an upward cone in Figure 8b. of half angle $(\xi + \delta)$ tilted to the south at an angle δ .

In each of the two models the angular distribution of secondary particles shown in Figure 8b. was numerically averaged over the limiting solid angle (e.g. the shaded portion for model #1 or the tilted cone for model #2) and expressed as a fraction of the downward flux at 0° zenith angle. These fractions, when multiplied by the equilibrium

secondary spectrum (curve labelled "large depth" in Figure 3) give the albedo spectra predicted by each model. Columns 4 and 5 of Table III list the fraction obtained for each model for the range of cut off rigidities covered in this work. Also shown in Table III are the scaling factors (also used for direct secondaries) which allow for the effects of solar modulation and geomagnetic cutoff (see Chapter III).

Examination of the information summarized in Table III reveals that the albedo flux at a particular energy can vary by no more than a factor of two between extremes of solar modulation and latitude. Most of this variation is due to the spectral dependent factor calculated at solar minimum and maximum conditions shown in columns 6 and 7 of Table III, respectively. There is essentially no latitude variation in the escape factors primarily because the dip angle, shown in column 3, changes so little over the whole latitude range.

It is possible that albedo observations could differ by an additional factor of two depending upon which of the two escape models applied to the observations. (In particular, was the intensity restricted to the vertical or averaged over a wide range of zenith angles?) However, it will be shown that the observations reported here agree more closely with the prediction of model #1. Whereas, the observations were obtained under conditions, neglecting smoothing effects, better represented by model #2. Since the observations are also the most intense albedo fluxes reported, it appears that the smoothing effect of non-adiabatic motion of the albedo particles dominates requiring application of model #1 to all observations obtained at rigidities near the cutoff.

One must, however, avoid taking the absolute intensity predictions of the models too seriously. The model intensity is strongly sensitive to the angular distribution of the emitted secondary particles and the precise conditions for escape which can only be estimated at the present time. The confidence level used here will be $\pm 50\%$ which is estimated from the wide intensity range given by the two models.

A comparison of the intensities at 200 MeV predicted by each model with the observed fluxes is shown in Figure 7. Solid lines indicate the intensity and solar cycle variation obtained from each model. The two models essentially provide upper and lower limits on the observed fluxes. Model #1 appears to provide a better approximation to the observed flux level.

D. Discussion

A comparison of the predictions of the two models with observations of re-entrant albedo at middle latitudes is presented in Figure 9. The spectrum obtained from equations derived by Ray (1967) using a model similar to the one outlined above is also shown. All spectra refer to zero depth. The work by Teegarden (1967) and Ray (1967) was scaled upwards by 7%, and the POGO (Bingham et al., 1968) and Ormes and Webber (1968) observations were scale downward by 35% and 2%, respectively, to match the level of solar modulation during Flight 974-N which was selected as a typical flight.

One notes that the flat spectra observed in Figure 6 are predicted by both Ray's model and the one presented above, however, the adjustments for solar cycle and geomagnetic variation fail to resolve the observed differences in intensity. The outstanding difference between the results reported here and previous measurements is the relatively large intensity observed above 200 MeV which gives the flat energy spectra. Two independent measures of the intensity in this interval, however give the same large flux. The intensity in the interval 200-260 MeV is measured in three separate categories of particles stopping in the hodoscope (RANGE 7, 8, 9). The required signature of these events (one tube fired in each tray up to the last plus pulse heights in the interval occupied by stopping protons) is so restrictive it is difficult to see how they could arise from events that were not protons of the specified energy. The background contribution from relativistic protons obtained from the accelerator calibrations amounts to only 20% of the quoted flux. The atmospheric secondary contribution amounts to only

23%. The quoted fluxes already contain corrections for both effects.

An independent measure of the albedo intensity involves a comparison of the integral fluxes of penetrating protons ($E \geq 260$ MeV) measured at Churchill and Minneapolis. Figure 10 shows a regression curve of the fluxes of these particles at Churchill (solid circles) and Minneapolis (open circles) against Deep River Neutron Monitor (Steljes, 1972) over the period 1965-69. One notes that the regression curves are quite well defined and appear to join near solar maximum. This observation suggests that at this time the albedo intensity below the cutoff energy at Minneapolis, 720 MeV, has essentially the same intensity as the primary flux over the same energy interval. As an example consider the fluxes obtained during 1967. It will be shown in Chapter V that the cutoff was depressed during both Sioux Falls flights. It is more proper therefore to use the flux obtained from the regression curve which passes through the fluxes obtained during periods of normal cutoff. For conditions applying to Flight 1208-N (Deep River Neutron Monitor = 6572) the fluxes at Churchill and Minneapolis were, respectively

$$J_{\text{Church}}(>260\text{MeV}) = 1654 \pm 52 \text{ P/M}^2 \text{ sec. ster.}$$

$$J_{\text{Msp}}(>260\text{MeV}) = 1470 \pm 60 \text{ P/M}^2 \text{ sec. ster.}$$

Since $J_{\text{Church}}(>260) = J_{\text{prim}}(260 \leq E \leq 720 \text{ MeV}) + J_{\text{prim}}(E > 720 \text{ MeV})$ and $J_{\text{Msp}}(>260) = J_{\text{albedo}}(260 \leq E \leq 720 \text{ MeV}) + J_{\text{prim}}(E > 720 \text{ MeV})$ the difference between the integral fluxes then gives the difference between the primary and albedo flux between the instrumental and geomagnetic cutoff.

$$\begin{aligned} J_{\text{Church}}(>260) - J_{\text{Msp}}(>260) &= J_{\text{prim}} - J_{\text{albedo}}(260 \leq E \leq 720 \text{ MeV}) \\ &= 184 \pm 75 \text{ P/M}^2 \text{ sec. ster.} \end{aligned}$$

The primary intensity in this interval obtained from the hodoscope is

$$J_{\text{prim}}(260 \leq E \leq 720 \text{ MeV}) = 426 \pm 17 \text{ P/M}^2 \text{ sec ster.}$$

while that obtained for a similar period by Lezniak and Webber (1971) is

$$J_{\text{prim}}(260 \leq E \leq 720 \text{ MeV}) = 417 \pm 22 \text{ P/M}^2 \text{ sec ster.}$$

Even using the lower primary intensity reported by Lezniak and Webber gives an albedo intensity of

$$J_{\text{albedo}}(260 \leq E \leq 720 \text{ MeV}) = 233 \pm 78 \text{ P/M}^2 \text{ sec ster.}$$

which also gives a differential albedo intensity of

$$j(260-720 \text{ MeV}) = 0.51 \pm .17 \text{ P/M}^2 \text{ sec. ster. MeV.}$$

This result is in full agreement with both the observations of Flight 974-N and the model #1 calculations in that region.

The origin of the flat spectrum obtained in this interval can be seen from consideration of the secondary particle model discussed in Appendix A. It is assumed as previously noted that the shape of the albedo spectrum is identical to that obtained from the secondary propagation model in the limit of large depths. The secondary proton intensity U at a depth x and energy E is given by

$$U(E, x) = \frac{1}{\frac{dE}{dx}(E)} [Q(E) - Q(Ex)] \quad (\text{IV-6.})$$

(The reader is referred to Appendix A for further definition of terms and symbols.) For particles whose range is less than the nuclear mean free path, 100 gms/cm^2) the source function $Q(E)$

$$Q(E) \approx \text{const.} \times E^{-(0.6 \text{ to } 0.9)} \quad (E \leq 300 \text{ MeV}) \quad (\text{IV-7.})$$

This is obtained from the integral of the differential source function $q(E)$ shown in Equation A-2. At large depths the observed energy is substantially less than the primary energy so that the first term in the brackets in Equation IV-6. dominates and can be replaced with Equation IV-7. The ionization loss rate for particles in the same energy band is given by

$$\frac{dE}{dx} = 243.6 E^{-0.78} \text{ MeV}/(\text{gm}/\text{cm}^2) \quad (\text{IV-8.})$$

Application of both approximations to Equation IV-6. gives

$$\begin{aligned} U(E,x) &\approx \text{const} \times E^{+0.78} x E^{-(0.6 \text{ to } 0.9)} \\ &\approx \text{const} \times E^{(+0.1 \text{ to } -0.1)} \end{aligned} \quad (\text{IV-9.})$$

which approximates the secondary proton intensity in the limit of large depths and low energies. This form is evident in many of the secondary particle spectra shown in Figure 3. The steepening at higher energies is a result of the nuclear absorption weighting factor in Equation A-2.

In trying to resolve the disparity among the balloon measurements one is first tempted to blame an over-correction for secondary protons in the other experiments since previous assumptions of the constancy of the secondary flux appear to be doubtful. While this may be the case for the data given by Ormes and Webber (1968) the detailed analysis given by Teegarden (1967) leaves little doubt that there is an unresolvable difference in flux levels. Teegarden obtained the energy spectrum of atmospheric secondary protons at Churchill in 1964 and 65 by comparing balloon and satellite measurements of the proton intensity. The fluxes fully agree with the predictions of the model discussed in Chapter III. However, his total flux in the 20-80 MeV interval of 0.7

protons/ M^2 sec. ster. MeV at 5 gms/ cm^2 measured at Sioux Falls in 1964 matches the intensity of direct secondary particles alone. Arguing that the variation of the secondary intensity due to latitude and solar cycle effects is less than 13%, Teegarden derived an upper limit of 0.18 p/ m^2 sec. ster. MeV at 95 MeV. Briefly, to agree with the measurements obtained here his flux observed at Sioux Falls would have to be 80% albedo when it actually appears to be 100% secondary on the basis of both his measurements and the model obtained in Chapter III.

Perhaps the most favorable agreement with the present albedo determination is the POGO (Bingham et al., 1968) albedo spectrum which does not have the disadvantage of any secondary particle correction. In fact, prior to application of the 30% downward adjustment for solar cycle effects the two spectra were in full agreement below 150 MeV. A possible problem at higher energies is that the energy measurement on POGO relied on pulse height measurements on penetrating particles which can easily be confused by small fluctuations in counter output.

To summarize, it is not possible to explain the wide disparity in the albedo measurements by either solar cycle effects, strong latitude variations, or highly anisotropic fluxes. Observational difficulties most likely are involved. It has been argued here on both theoretical and experimental grounds that the present observations of flat reasonably intense energy spectra in the region 100-300 MeV are a valid representation of the re-entrant albedo component. The flat spectral form is a natural outcome of secondary proton propagation in the large depth limit. Though not as well determined as the spectral shape, the general flux level obtained from model calculations confirms the observations. Two independent measurements of the re-entrant albedo flux levels near 200-300 MeV having low background contamination both give the same flat spectra.

V. QUIET TIME GEOMAGNETIC CUTOFFS

A. Introduction

In the early days of cosmic ray research, Compton (1933) and others (Clay, 1927) correctly interpreted the variation with latitude of the sea level intensity as proof that cosmic rays consisted of charged particles acted upon by the geomagnetic field. Around the same time, Störmer (1931) developed the theory of charged particle motion in a pure dipole field which even today provides a rough quantitative and certainly qualitative description of cut-off effects. The Störmer cutoff rigidity P_{st} is given by,

$$P_{st} = \frac{M}{r_e^2} \left(\frac{1 - \sqrt{1 + \sin \psi \cos \phi \cos^3 \lambda}}{\sin \psi \cos \phi \cos \lambda} \right)^2 \quad (V-1.)$$

$$= 59.6 \text{ GV.} \frac{\cos^4 \lambda}{(1 + \sqrt{1 + \sin \psi \cos \phi \cos \lambda})^2} \quad (V-2.)$$

where λ is the geomagnetic latitude and where ψ and ϕ are, respectively, the zenith angle and azimuth, as measured from the west, of the particle trajectory at the surface of the earth. Here, M and r_e are, respectively the magnetic moment and radius of the earth. These equations apply to positive particles. For negative particles ϕ must be increased by 180° . For particles arriving in the meridian plane ($\phi = 90^\circ$) and, in particular, vertically, Equation V-2 reduces to,

$$P_{\text{vert.}} = \frac{M}{4r_e^2} \cos^4 \lambda = 14.9 \cos^4 \lambda \text{ GV.} \quad (V-3.)$$

This basic equation describes a strong dependence on latitude which has proved to be characteristic of cutoff phenomena. The east-west effect is a consequence of equation V-2 where the cutoff rigidity for positive particles coming from the west ($\phi=0^\circ$) is lower than that for particles coming from the east ($\phi=180^\circ$) at the same latitude and zenith angle.

A complication in applying Störmer theory arises from the fact that some trajectories, which would be otherwise allowed, intersect the earth before passing into space. These penumbral effects were first considered by Lemaitre and Vallarta (1933) who found that they were absent at rigidities greater than 1.6 times the Störmer cutoff.

Around 1956-58, high altitude balloon experiments and extensive neutron monitor surveys made evident discrepancies between observations and the predictions of Störmer theory. Observed cutoffs were 30-50% lower than predicted over North America and 15-25% higher over Europe even when an eccentric dipole calculation was employed (Waddington, 1956; Fowler and Waddington, 1956; Fowler et al., 1957; Aly and Waddington, 1957; McDonald, 1957; Quenby and Webber, 1959; Rose et al., 1956; Kodama and Miyazaki, 1957; Skorka, 1958; Katz et al., 1958). Surveys of the cosmic ray equator (the latitude at which the neutron monitor registers a minimum counting rate) by a number of investigators notably Meyer and Simpson (1958) showed that its location did not coincide with the geomagnetic equator. Rothwell and Quenby (1958) found that the cosmic ray equator corresponded closely to the latitude where the geomagnetic field is horizontal i.e. the dip equator.

These results put pressure on the theorists to explain the discrepancies and stimulated the consideration of second order effects due to external currents and non-dipole terms in the multipole expansion of the earth's field.

A theory that adequately describes the effects of the earth's internal field is needed before any model employing external current systems can be invoked. Since the electronic computer had not achieved its present popularity when the problem of computing orbits in a perturbed dipole field was first considered, a number of approximate theories were developed which, as it turned out, were reasonably successful in removing the problems occurring in the low and mid-latitude observations. It was not until many years later that balloon and satellite observations of the diurnal variation of high latitude cutoffs and of cutoff depression during geomagnetic storms required external sources for their explanation.

Quenby and Webber (1959) obtained approximate solutions for the cut-off rigidity in two regions: latitudes greater than 40° and latitudes less than 20° . They determined the cutoff in the intervening latitude interval by averaging the results from the two approximations. For latitudes greater than 40° they assert that the higher order terms in the field expansion act only near earth and serve to define an effective latitude of arrival $\bar{\lambda}$ which differs only slightly from the geomagnetic latitude λ . For latitudes less than 20° , the effect of the high order terms is approximated by a change in the earth's magnetic moment M in Equation V-3. A

modification of this theory by Quenby and Wenk (1962) uses a new definition of $\bar{\lambda}$ obtained, for latitudes greater than 40° , by tracing the field lines calculated by Hultqvist (1958) from the earth's surface to a radius where only the dipole component is significant.

Detailed calculations of particle orbits offer a technique for obtaining cutoffs limited only by the accuracy with which the magnetic fields are known and by the availability of computer time. The trajectories of negatively charged particles are traced back from a point on earth by numerical integration of the equations of motion. Orbits which intersect the earth are considered forbidden while those which reach several earth radii are considered allowed. Orbits at each location are calculated for a range of rigidities near cutoff to determine the structure of the penumbral bands. In an early application of this technique, Kellogg and Schwartz (1959) carried out orbit calculations in a third order field expansion and showed that internal sources could account for the position of the cosmic ray equator. More recently, Shea, Smart and McCracken (1965), have invoked a sixth order expansion of the geomagnetic field (Finch and Leaton, 1957), to calculate a virtually exact set of cutoffs based upon the assumption that the earth's field is produced by internal sources alone. In applying these calculations to the problem of explaining cosmic ray cut-off anomalies, these authors conclude that, for ground based measurements, discrepancies are reduced to about the 8% level but not completely eliminated. (Shea et al., 1965; Shea and Smart, 1967)

Up to this point, the theories presented have assumed that the geomagnetic field is completely of internal origin, however the observation of radically depressed cutoffs during the main phase of geomagnetic storms (Anderson et al., 1959; Freier, Ney, and Winckler, 1959; Winckler, Bhavsar, and Peterson, 1961) proved that on occasion the cutoff is affected by external currents. It had long been assumed that the main phase of a geomagnetic storm (wherein the equatorial field is depressed about 100γ) was due to a ring current acting in the equatorial plane (Schmidt 1924). Chapman and Bartels (1940) introduced a measure of magnetic activity D_{st} , which is the longitude independent component of the geomagnetic field disturbance, as an indicator of ring current intensity. These early direct measurements of cutoffs during solar disturbances were facilitated by the presence of solar protons whose large flux overwhelmed the contribution of atmospheric secondary and re-entrant albedo particles allowing measurements over short times using small geometric factors (Earl, 1962; Freier, 1962), and whose steep energy spectrum allowed interpretations of time variations and differences in the response of integral particle detectors at high and low latitudes in terms of relatively small changes in cutoff rigidity (Winckler, Bhavsar, and Peterson, 1961). At this time the practice of representing cutoffs in terms of an exponential transmission function was introduced (Earl, 1962; Freier, 1962).

To explain these observations several calculations were presented which invoked an external ring current as suggested by Singer

(1957), (Störmer, 1955; Ray, 1956). This current is due to particles trapped in the radiation belts because: 1) spiraling of the particles has a diamagnetic effect and 2) large scale drift of the particles caused by the field gradient and curvature of the field lines results in a ring current.

Kellogg and Winckler (1961) found that cutoff reductions of a factor of two at intermediate latitudes during geomagnetically disturbed times occurring with only 100 γ field depressions at the equator were easily explained by their model. Since the cutoff value scales directly as M' , the magnetic moment of the ring current, and the equatorial surface field scales as M'/R^3 , a value of the current loop radius $R \approx 8$ earth radii is sufficient to account for the effect. Prompted by the existence of the permanent radiation belts, Kellogg and Winckler proposed a quiet time ring current to explain the weaker distant field of the earth as observed by Smith et al. (1960), and to explain the fact that cut-offs tended to be somewhat lower than predicted by fields of internal origin. Their estimated quiet time ring current was located at eight earth radii and had a magnetic moment half that of the earth.

A ring current was also considered by Sauer (1963) who employed various ring currents to supplement a sixth order field expansion tracing trajectories using the guiding center approximation to fit measured cutoffs about 45° . His best fit employs a ring current at seven earth radii having a dipole moment equal to that of the earth.

Even after the detailed orbit calculations of Shea, Smart and McCracken (1965) had apparently removed most of the discrepancies which had motivated earlier ring current models, direct measurements of the cutoff from balloons and satellites compiled by Bingham et al. (1968) indicated that the observed cutoffs ran from 7% to 25% below the detailed orbit values above $\lambda = 45^\circ$. An examination of the latitude variation of the discrepancy then lead the authors to estimate a ring current of magnetic moment $0.08 M_e$ at five earth radii in addition to the effects due to the limited nature and assymetry of the magnetosphere.

It was not until the discovery of substantial depressions of the high latitude cutoff (Stone, 1964) and its concomitant diurnal variation (Jokipii, L'Heureux, and Meyer, 1967) that external sources were truly required to explain the quiet time cutoffs. In his satellite observation of low energy protons in the polar cap regions, Stone (1964) found that cutoff latitudes were displaced several degrees toward the equator. Several years later Jokipii et al. (1967) reported balloon observations of a diurnal variation in the intensity of low energy electrons which was characterized by fairly sharp step-like transitions from a significant re-entrant albedo flux during the day to a much lower primary flux at night. By this time greater understanding of the interaction of the solar wind with the earth's magnetic field had evolved the concept of a bounded magnetosphere in which the earth's field is confined to a distance of 10 earth radii on the sunward side and is drawn out into a long

magnetotail in the antisolar direction. Field lines at high northern latitudes are connected to the Southern Hemisphere during the day restricting low rigidity observations to albedo particles while on the night side at the same latitude the field lines connect only to the tail allowing access to low rigidity primary particles. Further observations of the diurnal cutoff including those made with the present detector have been reported by Webber (1968), Israel and Vogt (1969), Rockstroh and Webber (1969), Hovestadt and Meyer (1970), Luhmann (1971), and Luhmann and Earl (1973).

Incorporation of the external fields of the magnetosphere into the detailed orbit calculations by Gall et al. (1968) and Smart et al. (1969) using the magnetospheric model of Williams and Mead (1965) has resulted in a reproduction of the qualitative picture discussed above. However, cutoffs observed at high latitudes appear to be systematically depressed below those refined calculations (Fanselow and Stone, 1972) and exhibit a high degree of day to day variability (Fanselow and Stone, 1972; Luhmann and Earl, 1973). These observations have again raised the problem of additional external sources of magnetic perturbations.

Before closing this review, a short mention of the expected cutoff variations due to the secular field variation of the earth is in order. In considering this problem Shea and Smart (1970a) compared cutoff calculations using a variety of field models at several locations. Specifically, application of the Finch and Leaton (1957) time

derivatives to the problem yields as much as a 5% increase in cutoff value over a 10 year period for several locations in North America.

In this thesis we will analyze the results of an extensive survey of cutoff phenomena at intermediate latitudes ($1.0 \leq P_c \leq 2.0\text{GV}$). The main objectives are 1) to verify the detailed orbit calculations 2) to determine the magnitude of the diurnal variation, 3) to detect any evidence of the day to day variability which characterizes the high latitude observations. Although there have been several recent direct determinations of quiet time cutoff (Webber and Ormes, 1965; Bingham et al., 1968; Ormes and Webber, 1968), none has involved such an extensive series of balloon flights nor employed a detector as well suited to the task as the hodoscope.

The method used here involves a determination of the cutoff transmission function obtained by taking the ratio of the differential rigidity spectrum of helium nuclei obtained over the Upper Mid-West to that obtained at high latitudes. Helium spectra are used because:

- 1.) Helium nuclei stopping in the detector have rigidities (720-1680MV) comparable to mid-latitude cutoff rigidities.
- 2.) There is essentially no secondary or re-entrant albedo helium which might mask cutoff phenomena.

The advantages offered by the hodoscope are the following:

- 1.) Since the rigidity measurement depends only on the amount of material penetrated not on an electronic calibration it is easier to identify small changes in cutoff.

- 2.) Absolute cutoff determinations depend only on the precision with which the range-rigidity relation is known.
- 3.) The lack of significant range straggling (Rossi, 1952) limits the instrumental smearing of the cutoff to the effects of the 100MV rigidity windows.
- 4.) Compared to satellite observations temporal variations are much easier to separate from spatial variations because of minimal balloon drift.

To implement the last point many balloon flights were conducted at the time of wind turn-around in early September. Flights lasting 36 hours were achieved. Nevertheless, because of balloon drift and separation of launch locations, the latitude variation of the cutoff was clearly evident. Long duration flights made at varied levels of geomagnetic activity made it possible to demonstrate the expected cutoff depression during highly active periods as well as significant day to day variations in the cutoff level not correlated with such activity. It was also demonstrated in the long duration flights that any significant diurnal variation was overwhelmed by the day to day variation.

To provide a systematic basis for the analysis, the data were organized by comparison with the detailed orbit cutoff using internal sources (Shea et al., 1968). To facilitate these comparisons, a convenient means of determining the predicted cutoff at any latitude and longitude in the U.S. was necessary. Recognizing that interpolation on the $5^{\circ} \times 15^{\circ}$ grid supplied is rather difficult, Smart and Shea (1967) propose an empirical relation ($P_c = 15.96L^{-2.005}GV$) between

P_c and the McIlwain L parameter (McIlwain, 1961), however, this still requires a rather complicated procedure for determining L. Instead the cutoff was approximated by the polynomial,

$$P_{\text{calc}} = \exp \left(\sum_{j=0} \sum_{\substack{i=0 \\ j+i \leq 3}} A_{ij} x^i y^j \right) \quad (\text{V-4.})$$

where: $x = \log [(longitude - 90^\circ W)/15^\circ]$ (V-5.)

$y = \log [(latitude - 47.5^\circ N)/5^\circ]$ (V-6.)

and where the coefficients A_{ij} , which are listed in Table V were obtained from a least squares fit to the grid. A Hewlett Packard 9100B calculator program was used to evaluate all cutoffs including those shown as curves of constant rigidity in Figure 13. At the grid points the polynomial yields cutoffs within 1% of the nominal values over the range from $35^\circ N$ to $60^\circ N$ and from $60^\circ W$ to $120^\circ W$.

B. Empirical Determination of Geomagnetic Cutoffs

Before launching into a detailed description of the method of cutoff determination some theoretical aspects of the cutoff phenomenon require clarification. It is a consequence of Liouville's theorem that the cosmic ray intensity at a given rigidity and direction is either equal to the free-space intensity or zero. No regions of partial transmission can exist. The existence of the penumbral structure introduces some degree of complication in defining exactly what is meant by the cutoff rigidity. This situation is illustrated in Figure 11. The lower portion displays the penumbral structure for Sioux Falls, South Dakota as determined from detailed orbit calculations (personal communication M. A. Shea). Shea et al. (1965) define P_s as the rigidity below which no particle can reach earth, P_m as the rigidity above which all orbits are allowed, and the effective cutoff rigidity P_c which is defined as an average cutoff integrated over the penumbral region.

$$P_c = P_m - \int_{P_s}^{P_m} [dP] \text{ allowed} \quad (V-7.)$$

These characteristic rigidities are indicated by arrows in Figure 11.

In observing a penumbral region, a detector with finite resolution will smear out the penumbral bands and a smooth cut-off transition will appear to take place. In the top portion of Figure 11, the solid curve is a schematic representation of the transmission as it would be observed with a detector having a window width of 100 MV - a typical interval defined by the hodoscope (see Table I). The sloping

dashed curve is an empirical fit to an exponential form which was first used by Earl (1962) in discussing the "sharpness" of the observed cutoff,

$$J_{\text{observed}}(P) = J_{\text{prim}} \exp - \left[\frac{P_0 - P}{\Delta P} \right] \quad P < P_0 \quad (\text{V-8.})$$

where P_0 is an empirical cutoff rigidity defined as the point at which the exponential transmission function reaches 1.0 and ΔP is the "e-folding" parameter describing the slope of the exponential relationship which characterizes the sharpness of the cutoff.

From the stated definitions one might tend to identify P_0 with P_m and $(P_0 - \Delta P)$ with P_c . It is evident from Figure 11, however, that P_0 most closely corresponds (within 0.02 GV) to P_c because the upper penumbral band has little or no effect on the location of the cutoff edge upon which the empirical determination is based. In the comparisons that will be made here it will be assumed that the relationship between P_0 and P_c established in Figure 11 can be scaled to other latitudes according to,

$$P_0 = P_c + .02 \text{ GV} \frac{P_c}{1.69 \text{ GV}} = 1.012 P_c \quad (\text{V-9.})$$

This semi-empirical relationship between P_0 and P_c which embodies the 100 MV rigidity window of the hodoscope provides a method for comparing cutoffs on an absolute basis.

As a means of illustrating the methods by which the cutoff was determined, reference is made to the helium rigidity spectrum obtained

for Flight 1038-W presented in Figure 12. The semi-log format allows one to interpret the cutoff in terms of the empirical exponential form just discussed. The dashed line reproduces the primary helium spectrum obtained from the Churchill flights made earlier that summer. In rare cases it is necessary to scale the primary spectrum slightly owing to changes in the solar modulation level as measured by the Deep River Neutron Monitor. The solid line which is a fit to the data below cutoff intersects the primary spectrum at the rigidity P_0 , which in this case is 1.36 GV. The points at which lines of maximum and minimum slope consistent with the indicated errors intersect the error limits of the primary spectrum then define the errors in P_0 (± 0.04 GV. in the example). The slope of the solid line relative to the primary spectrum defines ΔP , the "e-folding" rigidity ($\Delta P = .095$ GV in the example).

In addition to the graphical determination of P_0 , an attempt was made to approximate P_c as defined by Shea et al. (1965) (Equation V-7.) using the following method. In the presence of a cutoff having a complex penumbral structure, the integral flux J_{obs} observed below some rigidity P_{max} (which must be located above the penumbral region) may be ideally represented as the integral of the primary flux j_{prim} which is cutoff sharply below the effective cutoff rigidity P_{cx} ,

$$J_{\text{obs}} = \int_{P_{\text{min}}}^{P_{\text{max}}} j_{\text{observed}}(P) dP + \Delta J = \int_{P_{\text{cx}}}^{P_{\text{max}}} j_{\text{prim}}(P) dP \quad (\text{V-10.})$$

where j_{observed} is the observed rigidity spectrum, and P_{min} is the minimum rigidity observed by the hododcope. The small correction

factor ΔJ is the flux below P_{\min} obtained by extrapolating the observed exponential cutoff behavior to zero rigidity. In practice the value of P_{cx} is obtained by adjustment of the lower limit of the integral on the right of Equation V-10. so that the integral equals the total helium flux observed below P_{\max} . The errors in P_{cx} are determined from a combination of the statistical errors in j_{observed} and the indeterminacy of j_{prim} . In the example of Flight 1038-W $P_{\text{cx}} = 1.278 \pm .010$.

An extension of this method was used in one case to determine the cutoff when it fell above the RANGE 10 rigidity limit. In that case an upper limit to the cutoff was obtained by using the RANGE 10 integral helium flux and letting $P_{\max} \rightarrow \infty$.

C. Narrative Description of Cutoff Variations.

1.) Flight 1038-W. We begin a description of the cutoff determinations from the Minneapolis/Sioux Falls flight series by consideration of Flight 1038-W the results of which demonstrated the effectiveness of the hodoscope in determining cutoff rigidities. The flight trajectory is shown in Figure 14. The balloon was launched shortly before sunrise from South St. Paul, Minnesota and reached a ceiling altitude of 8 gms/cm^2 in about two hours. During ascent and the subsequent 9 hours at ceiling it drifted very slowly westward nearly parallel to a line of constant cutoff rigidity. At cutdown, shortly before sunset, it had drifted only 28 MV in cutoff rigidity. Although many other attempts have been made in this series no other flight has even approached the degree of cutoff stability obtained on this occasion.

The helium rigidity spectrum obtained from the entire ceiling portion of the flight is presented in Figure 12. A summary of cutoff determinations for all mid-latitude flights is contained in Table IV. The apparent cutoff P_o is $1.36 \pm .04$ GV and the sharpness parameter ΔP is .095 GV. The detailed orbit cutoff P_c obtained from Equation V-4. for this flight is also 1.36 GV. Basing a comparison of the observed cutoff P_o and the calculated cutoff P_c on Equation V-9. gives agreement well within the 3% experimental uncertainty. An empirical estimate of P_{cx} obtained by applying Equation V-6. however, gives only $1.278 \pm .010$ GV nearly 6% below the expected value.

2.) Flight 1056-W. The second flight in this series was launched just after sunrise on August 27, 1966 finally reaching a

ceiling altitude of 8 gms/cm^2 after 3 1/2 hours when a serious ballasting problem was finally resolved by the balloonist. The flight trajectories for both Flights 1056-W and 1057-W are given in Figure 15. While not as slow moving as Flight 1038-W, during the 6 hours at ceiling as Flight 1056-W drifted south along the Mississippi River a total change of .040 GV in cutoff occurred. Due to the ballasting problem, the planned 24 hour flight had to be terminated instead at sunset of the first day.

The helium rigidity spectrum obtained from this flight is shown in Figure 16. The observed values of P_o and P_{cx} , $1.38 \pm .04 \text{ GV}$ and $1.302 \pm .012 \text{ GV}$, respectively, at least indicate the expected .03 GV increase owing to the slightly lower latitudes encountered in this flight. Again nearly perfect agreement between the observed value of P_o and calculated P_c (1.380 GV) is obtained while the observed P_{cx} falls about 6% below the expected value. The slightly larger sharpness parameter, $\Delta P = .117 \text{ GV}$, is evidence for the .012 GV RMS smearing expected from the latitude drift.

3.) Flight 1057-W. The third flight of the series, Flight 1057-W, was launched at sundown on August 29, 1966 reaching and maintaining a ceiling altitude of 10 gms/cm^2 for 21 1/2 hours. After reaching ceiling over Prescott, Wisconsin the balloon slowly drifted west nearly parallel to the 1.41 GV line of constant cutoff with an RMS departure of .023 GV. In the two day period between the cutdown of Flight 1056-W and the launch of Flight 1057-W a series of solar flares occurred in McMath plage region 8461. During Flight 1057-W cutoff rigidities were strongly affected by geomagnetic

disturbances related to these flares. Consequently further discussion of cutoffs during this flight lies outside of the present discussion of quiet time cutoffs and will be deferred to a later chapter.

4.) Flights 974-N and 975-N. In 1967 the launch location was shifted to Sioux Falls, South Dakota and two modifications were made to the hodoscope. An additional 39 gms/cm^2 of lead absorber was distributed evenly throughout the hodoscope to enable it to measure the expected increased cutoffs. The digital carrier frequency was also increased by a factor of four so that the trigger rate was no longer limited by the read-out time. The improved statistics that resulted from this change allowed construction of rigidity spectra for each five hour interval of flight time. The slow north-eastward drifts facilitated measurements of the latitude variations of the cutoff.

Flight 974-N was launched just after sunrise September 14, 1967 reaching a ceiling of 3.3 gms/cm^2 three hours later over Marshall, Minnesota. The flight trajectory is shown in Figure 17. During the first five hours at ceiling it remained close to Marshall and then started a fairly rapid northward drift past Redwood Falls reaching Wilmar after five more hours.

The helium rigidity spectra for the four segments of this flight are shown in Figure 18. The empirical cutoffs P_0 for the first two five hour intervals $1.35 \pm .05 \text{ GV}$ and $1.21 \pm .08 \text{ GV}$, respectively, show the expected 8% cutoff decrease due to the north-eastward drift. However, the absolute cutoff level appears to be depressed 18% below that predicted by the detailed orbit calculations.

($P_c = 1.547$ and 1.428 GV for these two intervals.)

The trend continues in the next two flight segments. At sundown of the first day the trajectory turned eastward drifting nearly parallel to the 1.34 GV line of constant cutoff passing just north of Minneapolis at the end of this ten hour period. The observed cutoff P_o for this period is $1.13 \pm .04$ GV much lower than expected for the Minneapolis area. The D_{st} index for this period $+6.6$ indicates no evidence of a ring current that might cause such a depression. After sunrise on the second day, the balloon again headed on a northeastward course toward Lake Superior being cutdown that afternoon after 27 hours at ceiling when it got too near the lake. Although the expected cutoff for this final portion of the flight is .15 GV below that of the previous section it remained essentially the same ($P_o = 1.12$ GV $\pm .05$). We will return to this indication of an increased cutoff during the day in a later discussion section.

The flight trajectory and helium spectra for Flight 975-N are given in Figures 19 and 20, respectively. The balloon was launched just before sunset September 21, 1967 and reached a ceiling of 4.0 gms/cm² two hours later over Sioux City, Iowa. Most of the night and following morning portion of the flight were spent in a slow meandering drift northward over Sioux Falls picking up speed in the afternoon and being cutdown by the timer after 21 hours at ceiling near Fairfax, Minnesota. We note again, in Figure 20, the corresponding decrease in cutoff as the balloon drifted northward and the generally lower cutoffs than expected from the detailed orbit calculations. Depressed cutoffs in this case are not so surprising

because the Dst index averaged -18 during the flight indicating a respectable ring current. We shall see in a later section that a D_{st} index of -100 corresponded to a factor of two cutoff reduction during Flight 1057-W.

5.) Flights 1078-W and 1079-W. For the two flights in 1968 the launch location was moved back to South St. Paul and the hodoscope was restored to its standard configuration. The flight trajectories and helium rigidity spectra for these two flights are given in Figures 21 and 22, respectively. Flight 1078-W was launched just before sunrise September 5, 1968 reaching a ceiling altitude of 5 gms/cm² over Deer Lake, Wisconsin 2 1/2 hours later. Only 4 1/2 hours of ceiling data had been accumulated when its rapid approach toward Lake Superior and the Canadian border beyond forced a premature shutdown. The single cutoff determination over Spooner, Wisconsin gives $P_o = 1.29 \pm .08$ GV slightly larger than the calculated cutoff of $P_c = 1.19 \pm .03$ GV but within errors.

Although it appeared that the high altitude winds had already switched to their eastward direction for the rest of the winter, we decided to make one more attempt at a 36 hour balloon flight. Flight 1079-W was launched just before sunrise September 10, 1968 drifting south this time to a ceiling altitude of 4.6 gms/cm² over Rochester, Minnesota. Upon reaching ceiling the balloon drifted towards the west and south slowing down at night over northwest Iowa and taking a hooked path over northeast Nebraska the following day. A total of 32 hours of ceiling data were obtained.

The progressive increase in cutoff as the balloon drifted to lower latitudes is quite apparent in Figure 22. In fact it was impossible to determine the cutoff from the differential measurements once the balloon drifted into Nebraska. For this reason an upper limit to the cutoff for these portions was obtained from application of Equation V-10 to the RANGE 10 integral helium flux. Any reduction of this flux should be due only to the increased cutoff. The primary RANGE 10 flux was determined from the early sections of the flight when no cutoff effects were present and the rigidity spectrum in the region of the cutoff was assumed to be flat. It is apparent from the Churchill spectrum in Figure 22 that the latter assumption is likely to be valid well past 1.6 GV. Note also that as in both Flights 974-N and 975-N the cutoff was observed to be depressed below its nominal value; about 10% in this case. The fact that a depression was not observed five days earlier in Flight 1078-W is an indication that this is not a long term effect.

Now that the assorted cutoff effects that we wish to consider have been enumerated on a flight by flight basis, in the following section we will summarize these results and draw some conclusions by comparing the results of all of the flights.

D. Discussion

The cutoff observations reported here appear to be characterized more by day to day variability of a depressed cutoff as observed by Fanselow and Stone (1972) than by either the steady depression discussed by Bingham et al. (1968) or the diurnal effects predicted by Shea and Smart (1970b). Quiet time cutoffs range from the full internal value observed on three independent occasions to a maximum depression of 35% with a 20% depression being most typical. At most, the data concerning any diurnal effect is inconclusive being masked by the day to day variability.

Detailed comparisons of the measured cutoff rigidities with those predicted by Shea et al. (1968) are shown in Figures 23 and 24. In Figure 23 the empirical cutoff, P_o , is plotted vs. the calculated cutoff, P_c , derived from the polynomial of Equation V-4. The horizontal rigidity interval on each point is the root mean square cutoff excursion that occurred during that portion of the flight. The letters associated with each point indicate day (D) and night (N) observations. The solid diagonal line indicates the empirical relation between P_o and P_c expressed by Equation V-9. All but three cutoff observations fall an average of 21% below the internal cutoffs and there is considerable dispersion.

In Figure 24 a similar comparison of P_{cx} as obtained from Equation V-10 is plotted vs. the calculated value, P_c . The diagonal line indicates the expected one to one relationship. The depression and dispersion of measured cutoffs are again evident.

Although the 19% depression observed by Bingham et al. (1968) (dashed line in Figure 23) appears to characterize the data on an average basis, observations of significantly different cutoffs on a number of occasions and a tendency of individual flights to follow tracks of constant fractional cutoff depression suggest that the dispersion in observed cutoffs apparent in Figure 23 is due to external current systems varying on a time scale of a few days rather than experimental indeterminacy or diurnal effects. Bingham et al. (1968) ascribed the bulk of the cutoff depression to the magnetospheric boundary plus a small ring current ($.08M_e$). When a realistic magnetospheric boundary is incorporated into the detailed orbit calculations (Smart et al., 1969; Shea and Smart, 1970b), the result at the latitudes considered here is a 9% cutoff reduction at local noon increasing to a 19% reduction peaked at local midnight. If the observed depression is caused by the magnetospheric boundary one expects a rather prominent diurnal variation which is not observed.

In examining the track followed by the observations from Flight 975-N (open squares in Figure 23) one notes that a single line parallel to but below the expected track (solid line) passes through all points with no evidence of the expected 10% depression of night time cutoffs. The track followed by the observations of Flight 974-N (open circles) has nearly the same character except that the last day point (lower left) lies above the average track. Of the three long duration flights only 1079-W (solid triangles) shows a consistent night time depression; amounting interestingly to the expected 10%. The Flight 1078-W/1079-W series also gives a measure of the time scale of the variability. Only

five days separate these flights in which the cutoff tracks differed by at least 16% while during the 32 hours that Flight 1079-W was at ceiling the variation was 15% most of which can be ascribed to a diurnal variation.

A clear example of the depressed cutoff can be seen by the comparison of the cutoff observed during Flight 1038-W over Minneapolis ($P_0 = 1.36 \pm 0.04$ GV) to that obtained from the 0200-1200 U.T. segment of Flight 974-N which passed only .02 GV north of Minneapolis ($P_0 = 1.13 \pm 0.04$ GV). Reference to the two rigidity spectra shown in Figure 27 demonstrates that to obtain the same cutoff for both observations would require statistical variations of at least three standard deviations for each of three data points - all in the same direction. Although this segment of Flight 974-N occurred during the night, it has already been shown that the diurnal variation is considerably less than the $20 \pm 3\%$ observed difference in cutoff levels.

Fanselow and Stone (1972) also observed a general depression of cutoff level at high latitudes coupled with variability from day to day. Direct comparison of the observations summarized in Figure 23 with their results, however, does reveal some differences. Rather than the $3-5^\circ$ average depression observed at high latitudes only 1.6° is observed here. Similarly, the $1-2^\circ$ variability apparent at high latitudes shows up as only a $\pm 1^\circ$ variation at intermediate latitudes. Neither of these observations is surprising since cutoff perturbations are expected to be more prominent near the poles.

Two effects could be responsible for the variability and general depression of the cutoff: short term changes in the magnetospheric

boundary or a fluctuating ring current. The absence of a prominent diurnal depression owing to the assymetry and the lack of correlation with interplanetary activity as measured by K_p (Fanselow and Stone, 1972) both appear to rule out a changing magnetospheric boundary. Contrary to the findings of Fanselow and Stone (1972), however, a significant correlation of depressed cutoffs does exist for the quiet time data (correlation coefficient = -0.57) suggesting that a ring current could account for the depression.

While the exact configuration of the external current systems responsible for the depressed cutoffs is undoubtedly very complex, the ring current model of Kellogg and Winckler (1961) provides a convenient means of estimating the location of an equivalent ring current by comparing the cutoff depression with equatorial D_{st} . Their model predicts that the cutoff P' varies as:

$$P' = \frac{P}{1 + \left(\frac{R'}{R_E}\right)^3 \left(\frac{D_{st} - D_{sto}}{2 B_{eq}}\right)} \quad (V-11.)$$

where P is the cutoff existing with no ring current. The perturbation term in V-11. will be recognized as the ratio of the magnetic moment of the ring current M' to that of the earth:

$$\frac{M'}{M_E} = \left(\frac{R'}{R_E}\right)^3 \left(\frac{D_{st} - D_{sto}}{2 B_{eq}}\right) \quad (V-12.)$$

where R'/R_E is the radius of the ring current in earth radii and B_{eq} is the equatorial surface field strength (32000 γ). Since there may be some question concerning the zero point of the D_{st} scale, D_{sto} denotes the value of D_{st} when there is no ring current. Providing Equation V-11

applies, a plot of P/P' vs. D_{st} for a particular geomagnetic disturbance should yield a straight line whose slope is governed by the parameter R' which characterizes the radial position of the ring current.

In Figure 25 this type of plot is used to compare the cutoff fluctuations observed during so called "quiet times" with the strongly depressed cutoffs occurring during large geomagnetic disturbances. The solid line labelled Q is a least squares fit to the quiet time data which includes all flights except 1057-W which occurred during a disturbed period. The line labelled D characterizes the cutoff disturbance during that flight. Further discussion of these observations is contained in a succeeding chapter. Additional data obtained by Earl (1962), Freier (1962), Hoffman and Winckler (1963), and Biswas et al. (1962) is included in Figure 25 to further define the cutoff behavior during disturbed periods.

Several factors indicate an offset of $10-20\gamma$ in the D_{st} scale. The disturbed (D) and quiet time (Q) cutoff relations in Figure 25 intercept the zero ring current condition ($P_c/P_o = 1.0$) at 15γ and 19γ , respectively. The histogram of hourly D_{st} values for the first six months of 1967 shown in Figure 26 also indicates a peak at 10γ and a rather sharp edge above 16γ . Assuming that this last observation corresponds to zero ring current conditions, in addition to the other two determinations, results in the estimated offset of $D_{sto} = 17 \pm 5\gamma$. The remaining diagonal lines in Figure 25 indicate the relation predicted by Equation V-11 for ring currents of various radii assuming this offset in D_{st} . Strictly speaking one should use the ring current radii shown in parentheses which have been corrected for the earth's inductive effect on D_{st} (see Appendix B).

We can now apply the ring current model to the observations shown in Figure 25. The model's placement of the ring current causing the disturbance during Flight 1057-W at the outer limits of the magnetosphere ($10-12 R_E$) would seem to suggest that the storm time geomagnetic disturbance is associated with activity at the magnetospheric boundary rather than in the radiation belts. While not as clear cut as the Flight 1057-W observations, the additional disturbed time observations of Earl (1962), Freier (1962), Hoffman and Winckler (1963), and Biswas et al. (1962) shown in Figure 25 also indicate that the disturbed time cutoff fluctuations appear to arise from currents located at the outer reaches of the magnetosphere. A more extensive examination of the disturbed time cutoff in Chapter VI, however, will reveal that substantially lowered cutoffs can be achieved with very little D_{st} response when the field lines at lower latitudes are swept into the tail of the magnetosphere during the magnetic storm. On the other hand, the quiet time variations suggest a ring current with a magnetic moment 0.1 to $0.2 M_E$ acting at a radius of 6 to $9 R_E$ - well within the magnetosphere. These numbers should not be considered as precise ring current parameters, but they do serve as a guide to the feasibility of the ring current explanation of the variability. Although cutoff depression cannot be treated strictly in terms of a ring current model, the comparison offered by the ring current analysis in Figure 25 emphasizes the difference between the quiet-time cutoff variations and the storm time cutoff depression.

It is reasonable to ask whether a quiet time ring current of the magnitude and location proposed is consistent with observed particle

intensities in the radiation belts. From observations of low energy protons and electrons ($200 \text{ eV} \leq E \leq 50 \text{ keV}$) in the radiation belts, Frank (1967) obtained a quiet time ring current peaked at $7 R_E$ having a magnetic moment $\sim 0.08 M_E$. The value, $D_{st} = 12\gamma$, that results from this current can be identified with the D_{st} offset discussed earlier. During magnetic storms, substantial increases in the deduced ring current intensity were able to completely account for observed variations of equatorial D_{st} , thus resolving a long standing problem of the ring current hypothesis. It appears that the ring current proposed here is certainly plausible both in magnitude and location.

Concerning the day to day variability no explanation for its ultimate source is offered here. But if the currents responsible for the $\pm 15\gamma$ variation in D_{st} evident in Figure 26 are indeed located at $6 R_E$ or beyond, then the mid-latitude cutoff must fluctuate $\pm 5\%$ or more on a random basis during "quiet times".

Considering now the "sharpness" of the cutoff we take the rigidity spectrum from Flight 1038-W as our best measure of the sharpness since that flight had particularly good charge resolution and, as noted earlier, drifted less than a total of 28 MV in cutoff from launch to impact. Since the nature of the penumbral structure is so different from the empirical exponential form of Equation V-8, it is extremely difficult to separate the effects due to the hodoscopes 100 MV window size from those due to the width of the penumbral region. Because of this problem we are limited to a method of analysis which compares the sharpness of cutoffs as already smoothed by the 100 MV resolution to the flight observations. A measure of the expected width of the

cutoff owing to the penumbral bands as resolved by the hodoscope's rigidity intervals can be obtained from the slope of the empirical transmission function shown in Figure 11. Since one expects no major change in the character of the penumbral bands over the limited rigidity interval separating Minneapolis and Sioux Falls, scaling ΔP using the assumption that the ratio $\Delta P/P_0$ is a constant appears to be fairly reasonable. Under this assumption the ΔP of 65 MV at Sioux Falls becomes 55 MV at Minneapolis. Before drawing a comparison of this value with the 95 MV observed during Flight 1038-W consideration is due for the effects of an 8 MV RMS widening owing to the drift of the balloon and a $\pm 5\%$ smearing owing to the average 16° zenith angle of the observed particles. The latter effect was calculated assuming that the Störmer relation for non-vertical cutoffs (Equation V-2) applies. Application of these effects to the empirical cutoff spectrum suitably scaled for the latitude difference then gives a cutoff function which intercepts all data points in the spectrum (dotted curve shown in Figure 12) even to the extent that it steepens at lower rigidities giving a better fit than the straight line cutoff shown in that figure. Since application of the same treatment to a perfectly sharp cutoff results in a transmission function having $\Delta P=40\text{MV}$, the width of the cutoff observed in Flight 1038-W is primarily due to the penumbral structure.

There has been considerable discussion in the literature concerning the sharpness of the cutoff. Bingham et al. (1968) labeled their observation of a ≈ 150 MV band covering the 10% - 90% transmission function in their balloon results as clearly "not sharp." This is to

be compared with 150 MV obtained from Flight 1038-W after removal of zenith angle smearing and balloon drift effects. Earl (1962) describes the cutoff observed during a cutoff depression due to a solar event as being "quasi-sharp" with a $\Delta P = 48-55$ MV. when the cutoff was running about half its quiet time value. Freier (1962) reports a similar unsharp cutoff with $\Delta P = 65$ MV determined from emulsion observations of the same event. Not wishing to deal in relative terms we simply conclude here that the observed cutoff is consistent with the penumbral band structure obtained by Shea et al. (1965).

VI. AUGUST 28, 1966 FLARE-INTERPLANETARY AND GEOMAGNETIC DISTURBANCE - FLIGHT 1057-W.

A. Introduction

At 1521 U.T. on August 28, 1966, an importance 3 solar flare occurred at solar coordinates $N21^{\circ} E04^{\circ}$. During the major event that followed Flight 1057-W was launched from South St. Paul, Minnesota at 0022 U.T., August 30, 1966, reaching a ceiling of 10 mb. and maintaining that altitude until cutdown at 2340 U.T. No solar energetic particles were detected, but the intensity of galactic cosmic rays underwent variations due to interplanetary and geomagnetic effects. The geomagnetic cutoff was depressed and a large Forbush decrease occurred during the flight. The process of separating the geomagnetic and interplanetary effects is not too difficult, but enough detail is required that both topics will be discussed concurrently.

Most of the phenomena observed during Flight 1057-W follow the classic pattern presented by Winckler, Bhavsar, and Peterson (1961). A brief review of the picture that has emerged follows. A short time after a large optical flare on the sun, particles, predominantly protons, of cosmic ray energies are seen at earth. Typical delay times run from a few tens of minutes to several hours depending on particle energy and location of the flare relative to the magnetic field line connecting the earth and the sun. The onset of geomagnetic effects occurs after a period of one to two days heralded by a sudden commencement (S.C.) which marks the arrival of the enhanced solar wind plasma generated by the flare. Earth based magnetometers detect at first an increase in the geomagnetic field lasting typically one to several

hours, the initial or positive phase, followed by a general decrease of the geomagnetic field which may last several days, the main phase. The equatorial surface field depression is typically 100γ .

During the main phase, geomagnetic cutoffs are often reduced below 30% of their quiet time values (Winckler et al., 1961) considerably less than expected from simple scaling of the equatorial field depression. This effect was first observed by Freier, Ney, and Winckler (1959) using emulsions for energy determination plus ion chambers and Geiger counters for time resolution. Further confirmation was provided by Winckler et al. (1961), Earl (1962), and Freier (1962).

The main phase field depression has been attributed to diamagnetic effects of a hot plasma (Dessler and Parker, 1959) or energetic electrons trapped in the radiation belts (Singer, 1957) which reduce the distant magnetic fields resulting in lower cutoff rigidities (Kellogg and Winckler, 1961). Both phenomena can be described in terms of ring currents which account for the symmetric field depression observed at the equator (negative D_{st} values). More recently, particle observations throughout the magnetosphere have shown that an enhanced ring current consisting primarily of protons in the 3-50 keV interval trapped at $3.0-5.5 R_E$ produces the observed main phase field depression (Frank, 1967). These observations favor the Dessler-Parker model of the main phase in which hydro-magnetic waves generated at the magnetospheric boundary by the interplanetary disturbance dissipate energy in the radiation belts rapidly heating the ambient plasma.

Although the main phase ring current has been observed, its role in the explanation of cutoff reduction as proposed by Kellogg and

Winckler (1961) (see section V-D.) has been criticized by Akasofu and Lin (1963). They assert that the intensity of a ring current reaches an upper limit when the energy density of the trapped particles approaches the energy density of the trapping field. Equation V-11 remains valid but is restricted to cases when $M' \lesssim M_e$. Frank (1967) has observed particle intensities in only moderate excess of this saturation level during magnetic storms.

Earlier, Rothwell (1959) had proposed that cutoff reduction would occur when the magnetic storm swept away the outer portions of the magnetosphere. The nature of the interaction between the solar wind and the magnetosphere is, however, such that the surface currents flowing on the magnetopause which act to cancel the field outside the magnetosphere effectively increase the field within the cavity (Chapman and Ferraro, 1931). This effect was related to the cutoff rigidity by Akasofu, Lin, and Van Allen (1963) as a symmetric compression of the geomagnetic field which acts to increase the cutoff slightly rather than reducing it during periods of enhanced solar wind flow.

According to Akasofu, Lin, and Van Allen (1963), a combination of anisotropic magnetospheric compression and a ring current, however, can account for the cutoff reductions that are observed. The effect of this combination is to lower significantly the minimum latitude where the field lines are connected to the tail of the magnetosphere effectively reducing the cutoff to zero. A compression of the magnetosphere from $10R_E$ to $8R_E$ on the sunward side acting with a ring current at $3R_E$ producing $D_{st} = 150\gamma$ reduces the minimum latitude for .17GV particles from 69° to 60° (geomagnetic). The cutoff at 60° is reduced to one sixth

its quiet time value. Although the cutoff reduction in this model still scales with the ring current (therefore with D_{st}), Equation V-11 no longer applies since the compression which forces the boundary latitude toward the equator produces effectively no change in the equatorial field strength.

In addition to the geomagnetic effects outlined above, a marked decrease in the galactic cosmic ray intensity observed by ground based detectors, neutron monitors, ion chambers, and meson telescopes, accompanies the magnetic storm. This effect, a Forbush decrease, begins at the time of the sudden commencement and lasts several days (Forbush, 1937). The mechanism of the Forbush decrease, although not fully understood, is certainly analogous to the mechanism of the 11-year solar modulation of galactic cosmic rays. The latter process is treated rather extensively in Rygg (1970). The convection of galactic cosmic rays out of the solar cavity is balanced by their inward diffusion and deceleration in the disordered magnetic field carried by the solar wind plasma. The enhanced velocity and magnetic disorder of the solar flare plasma cloud apparently upsets this balance until a new equilibrium is reached.

An obvious aim in studying the Forbush decrease is to draw comparisons between it and long-term modulation effects. A goal of many modulation studies is to determine the rigidity dependence of the modulation. To compare changes in cosmic ray intensity at different rigidities a regression plot relating rates measured by detectors with different thresholds is often employed. By plotting the intensity measured by one detector vs. that measured by the other detector over

the same time period, one can compare the fractional changes in intensity occurring at one rigidity relative to those that occur at another. The slope of such a plot is a measure of the relative rigidity dependence of the modulation. To obtain the long term stability and statistics that are necessary for such a regression analysis, integral detectors having different effective rigidities owing to different thresholds or rigidity response functions (neutron monitors, Geiger tube monitors, ion chambers, meson telescopes) are often used.

Several studies of the Forbush decrease comparing integral fluxes from various detectors have been performed. McCracken (1960) and Kane (1966) in comparing the rates of neutron monitors at several latitudes found a somewhat weaker rigidity dependence than the 11-year variation. Kane et al. (1965) compared ion chamber results from space probes with neutron monitors and ascribed the dispersion of their results to Forbush decreases but did not specifically analyze their data to demonstrate the effect. Balasubrahmanyam and Venkatesan (1970) found no evidence of any differing rigidity dependence between short and long-term variations in their comparison of the IMP and OGO Geiger tube monitors with neutron monitors. Lockwood and Webber (1969) and Lockwood et al. (1970) found a considerably weaker rigidity dependence for several Forbush decreases observed by the Pioneer 8 detector ($E \geq 60\text{MeV}$) and the Mt. Washington neutron monitor. The only reported analysis of spectral dependence is that of McDonald and Webber (1960) who found that the rigidity dependence appeared to agree with the 11-year modulation.

There are several complications involved in assuring that integral measurements yield a valid comparison. One should use the same or

very similar detectors in measuring each effect because integral measurement techniques usually employed involve non-linear spectral functions that make it difficult to compare measurements. The Forbush decrease is correlated with directly produced solar radiation (protons, electrons and x-rays) and depressed geomagnetic cutoffs. Both of these effects can add low energy particles to the flux imitating a weaker rigidity dependence than is actually present. While most studies consider these effects, differential spectral measurements such as those presented here are really required to assure that they are properly treated.

B. Observations During the August 28, 1966 Disturbance

The geomagnetic and interplanetary disturbances following the August 28 flare were more complex than outlined in the preceding section. Although the disturbed period lasted until September 9, the discussion in this section will concentrate on a short review of the conditions existing during the period spanned by Flights 1056-W and 1057-W - August 27-31. Due to the complex nature of the event, the intent of this discussion is to give a background for the hodoscope results rather than to attempt an interpretation.

A summary of observations for the period August 27-31 is shown in Figure 28. The launch (x) and ceiling portions (solid line) of Flights 1056-W and 1057-W are shown on the top line followed by the fluxes of penetrating protons on line 2. The brackets at the left indicate the size of the experimental error. Line 3 of Figure 28 is a plot of the Deep River Neutron Monitor intensity (Steljes, 1966). On lines 4 and 5 magnetic conditions at earth and in nearby space are shown in plots of equatorial D_{st} (Sugiura and Poros, 1971) and K_p index. The sudden commencements on August 29 and 30 are shown as vertical dashed lines. Optical flare observations also indicated as dashed lines are shown along with observations of x-rays and type IV radio emission on succeeding lines. The remaining three lines summarize the observations of solar protons (Kinsey and McDonald, 1968) and energetic storm particle fluxes of electrons and protons (Lin and Anderson, 1967).

The observations from Flight 1056-W launched one day before the flare provide a good baseline for quiet time conditions. During this flight the K_p index remained below 1^+ and both D_{st} and the neutron

monitor were very stable. No statistically significant variations in the penetrating proton flux were observed.

Dodson and Hedeman (1968) have published a detailed discussion of the optical observations for this flare which are briefly summarized below. The solar flare causing the initial disturbance occurred in McMath Plage 8459 at 15:21:46 U.T. on August 28 and was immediately followed at 15:22:35 U.T. by flare emission from McMath Plage 8461 trailing region 8459 15° to the east. In all, nine distinct regions of flare emission were observed in the two plages with the second plage providing most of the H_{α} emission for the flare. The optical flare peaked near 1531 U.T. and had considerably diminished in intensity by 1630 U.T. in most regions. One region in the trailing plage, however, continued to show flare emission until at least 2000 U.T. Type IV radio emission (often associated with the release of relativistic electrons) began at 1527 U.T. (intensity 3^{+}) and lasted until approximately 1640 U.T. Bursts of type III radio emission and type V continuum associated with a rapidly expanding (700 km/sec.) blast wave seen propagating across the solar surface were also reported. A burst of solar x-rays began at 1525 U.T. peaked at 1530 U.T. and diminished to zero around 1545 U.T. (Arnoldy et al., 1968). Prompt 40keV electrons arrived at 1 A. U. at 1531 U. T. (Lin and Anderson, 1967). Solar protons ($E > 15\text{MeV}$) were detected near earth at 1700 ± 15 U.T. (Kinsey and McDonald, 1968) peaking at 1825 U.T. slowly diminishing over the next few days.

The data of Lin and Anderson (1967) presented in Figure 28 reveal that the energetic storm electrons arrived at the time of the sudden commencement at 1314 U.T. on August 29 (22 hours after the flare). The

positive phase of the first magnetic disturbance appeared as a sharp jump in D_{st} and a strong increase in K_p . The 40 keV electrons also showed a sharp increase at this time. The energetic storm protons, which also appeared at this time, however, were more slow to respond. The positive phase of the storm lasted until 2100 U.T. when the main phase began. During the main phase of this storm the magnetic field attained a maximum depression of -67γ from 0200 to 0300 U.T. August 30 about the time Flight 1057-W reached ceiling.

A second sudden commencement occurred at 1112 U.T., August 30 producing a second positive phase and further enhanced K_p activity. Although there is a slight indication in the neutron monitor data of a decrease at the beginning of the first main phase (0000 U.T., August 30), a clear cut Forbush decrease began at the second sudden commencement. A significant decrease in the Flight 1057-W penetrating proton flux took place before the Forbush decrease began, but it will be shown later that this variation was associated with the temporary restoration of the geomagnetic cutoff rather than with the Forbush effect.

There are two possible causes of the second sudden commencement:

- 1) a second solar flare of importance 2B in plage region 8461 at 2021 U.T. August 29 or
- 2) a second plasma stream being ejected by the trailing flare from the August 28 event. Neither possibility is ruled out by the observations. Since the first sudden commencement occurred only 22 hours after the flare, the observation of the second only 14 hours after the second flare seems fairly reasonable. However, a 44 hour delay after the first flare is not too unreasonable either. The increase of the $>15\text{MeV}$ particles which seems to be associated with the

second flare could just as easily be part of the flux of energetic storm particles when compared with the >500 keV protons.

In the following sections, observations of geomagnetic cutoff variations and of cosmic ray intensity variations during the Forbush decrease associated with the second sudden commencement will be presented and discussed. At the beginning of Flight 1057-W, the cutoff was depressed below 40% of its quiet time value observed three days earlier during Flight 1056-W. The cutoff was restored to the approximate quiet time level during the positive phase of the second storm returning to its depressed state as the main phase developed near the end of the flight. The cutoff depression in the early and late portions of the flight made it possible to determine the low energy proton spectral intensity both before and after the Forbush decrease appeared in the neutron monitor record. The rigidity dependence of the Forbush modulation from 0.5 through 2GV. is thus available for study.

C. Geomagnetic Cutoff Variations During Flight 1057-W

1.) Analysis Procedure. In subsequent analysis of the data from Flight 1057-W it will be shown that the cutoff was depressed at times below 0.5 GV. To show this, the method used earlier of determining the cutoff from the spectra helium nuclei in the interval 0.9-1.55 GV is extended to lower rigidities using proton and electron observations. Cutoffs in the rigidity interval 0.50-0.80 GV can be identified from the proton spectra by determining whether the observed fluxes are primary particles or are due only to re-entrant albedo. Similarly the electron component in the 15-65 MV and 45-150 MV rigidity intervals studied for this flight by Luhmann and Earl (1973) can be used to set limits on the cutoff in the corresponding rigidity intervals by distinguishing between primary and albedo flux levels.

Liouville's theorem predicts that the position of the cutoff will be marked by a fairly sharp transition from the albedo flux level below cutoff to the primary flux level above cutoff. To identify this transition each observed proton spectrum must be compared with idealized primary and albedo spectra based on previous work. If the cutoff is greater than 0.8 GV only albedo particles will be observed. If the cutoff is below 0.5 GV the observed flux should match the primary intensity. The cutoff observations discussed in Chapter V imply that the transition region is no wider than 0.1 GV. Although the statistical accuracy of the data is limited, it is more than sufficient to make the distinction of a factor of 2 or 3 in flux level required to distinguish primary and albedo spectra.

Since the modulation level was changing throughout the flight, it

was necessary to adjust the intensity of the reference spectra (without changing their shape) to match the corresponding modulation level. Empirical relationships between the spectral intensity of both primaries and re-entrant albedo particles to the Deep River neutron intensity have been established through many years of observations with the hodoscope over a wide range of solar modulation levels. Below 0.7 GV the primary spectrum has maintained the form:

$$J = AT \quad (VI-1.)$$

throughout the entire increasing phase of solar activity 1965-1969 (Rygg and Earl, 1971). Here, A is a quantity independent of energy which embodies all the time dependence and relates the spectral intensity $J(T)$ (in energy units) to kinetic energy T . The magnitude of A is obtained for each flight interval from the long term relation between A and Deep River Neutron Monitor obtained by Rygg and Earl (1971). The reference spectra for re-entrant albedo are obtained from the long term solar variation discussed in Chapter IV (dashed curve in Figure 7).

The rigidity dependence of the modulation during a Forbush decrease may differ to some extent from the rigidity dependence of the long term (eleven-year) modulation affecting the intensity of the low energy primary and albedo protons. The magnitude of this effect is such that it is unlikely that this difference would cause any ambiguity between primary and albedo flux levels.

Low energy cosmic ray electrons may be used to probe even lower cutoff rigidities than are available with protons at balloon altitudes. Electrons incident on the top of the atmosphere lose only 3 or 4 MeV

in reaching balloon altitudes while protons of 50 or 60 MeV (310-340 MV) are completely stopped in that distance. Determining the cutoff from the electron data proceeds in a manner similar to that described for protons. In this case the albedo exceeds the primary intensity by more than a factor of 3. Luhmann and Earl (1973) have shown that the electron fluxes obtained by the hodoscope during Flight 1057-W in two broad low rigidity intervals (15-65 MV and 45-150 MV) remained at the albedo level throughout the flight placing a lower limit of 150 MV on the cutoff.

2.) Cutoff Determinations. The proton and helium spectra for five 4 hour intervals of Flight 1057-W are shown in Figures 29 and 30, respectively. Most of the variability in flux apparent in those figures can be attributed to temporal changes in geomagnetic cutoff. Geomagnetic latitude along the flight trajectory remained essentially constant. The expected quiet time cutoff was 1.410 GV and varied by no more than +.014, -.049 GV. The proton spectra were individually corrected for secondaries and ionization loss using the average neutron monitor rate during each interval. The resulting spectra are plotted as a function of rigidity in Figure 29. Dashed lines indicate the primary and albedo reference spectra obtained for each segment of the flight on the basis of the long term modulation as discussed in the previous section. Helium rigidity spectra that will be used to determine the cutoff in the manner discussed in Chapter V are presented for the five flight intervals in Figure 30. Assumed primary spectra shown as dashed lines were obtained from the long term modulation of this component determined by Rygg and Earl (1971).

Segment 1 of Flight 1057-W (0216-0620 U.T.) occurred during the main phase of the first magnetic storm. The proton spectrum for this interval (panel 1 of Figure 29) lies somewhat below the primary spectrum predicted from the long term modulation. However, the spectrum does follow the $J=AT$ form and is well above the expected albedo spectrum. It appears, therefore, that the proton spectrum during this segment consisted of primaries down to the lowest rigidity implying that the cutoff remained below 0.5 GV. The helium spectrum for this interval, shown in panel 1 of Figure 30 appears to be completely primary over the full rigidity range observed showing that the cutoff was below 1.0 GV. Fortunately the cutoff depression during this early portion of the flight allows a measurement of the low energy primary proton spectrum at a time before the Forbush decrease was apparent in the neutron monitor rate.

Segment 2 of Flight 1057-W (0620-1020 U.T.) occurred near the end of the first magnetic storm. The proton spectrum shown in panel 2 of Figure 29 appears to be purely albedo at low rigidities with a rather prominent transition toward the primary spectrum indicating a cutoff near 0.80 ± 0.03 GV. This interpretation is consistent with the helium spectrum for this period (panel 2 of Figure 30) which appears to be completely primary indicating a cutoff below 1.0 GV.

Segment 3 of the flight (1020-1420 U.T.) occupies the last hour of the first main phase and the first 3 hours of the positive phase of the second storm. The proton spectrum for this segment (panel 3 of Figure 29) lies near or below the albedo level for all rigidities. The two fluxes lying somewhat below the albedo level are probably nothing more than statistical deviations, but they also could be due to a slight

oversubtraction of atmospheric secondaries at low rigidities. The helium spectrum for this portion of the flight (panel 3 of Figure 30) reveals a depression of 2.2 standard deviations (2.2σ) of the RANGE 4 flux and a 1σ depression of the RANGE 5 flux. This spectrum is consistent with a cutoff at 1.22 ± 0.04 GV.

Segment 4 of the flight (1420-1920 U.T.) occupies the last 4 hours of the positive phase and the first hour of the main phase of the second storm. The proton spectrum for this interval (panel 4 of Figure 29) lies right at the albedo level. The helium spectrum (panel 4 of Figure 30) exhibits the effect of a cutoff at 1.34 ± 0.04 GV.

Segment 5 of the flight (1920-2340 U.T.) covers the second and more strongly depressed main phase of the storm period. The proton spectrum for this segment (panel 5 of Figure 29) is clearly primary down to 0.55 GV, but the flux in the lowest rigidity interval from 0.50 to 0.55 GV is statistically consistent with either primary or albedo levels. Consequently, the proton observations place an upper limit of 0.55 GV on the cutoff. The helium spectrum for this segment is consistent with a pure primary spectrum indicating that the cutoff is somewhere below 1.0 GV.

During this interval (segment 5), the maximum depression associated with the Forbush decrease that occurred during the flight was observed. As in segment 1, the reduced cutoff allowed a measurement of the low energy proton intensity spectrum to be made fortunately in this case at a time of large short term modulation. The fact that the proton spectrum falls only slightly below the reference spectra expected from the neutron intensity during this deeply modulated period is important in

the discussion (in a later section) of the rigidity dependence of the modulation during the Forbush decrease.

Considering briefly both sections 1 and 5 of the flight when the cutoff was reduced below 0.5 GV, one further observation concerning the low energy primary protons is in order. There was no significant contribution of solar particles during either period. Solar particles have a characteristic spectrum of the form

$$J \propto T^{-\gamma} \quad (2.5 \leq \gamma \leq 5) \quad \text{VI-2.}$$

Excess fluxes at low rigidities predicted by this form are not apparent in the proton spectra for either segment 1 or 5 of the flight (see Figure 29 panels 1 and 5). Furthermore a power law extrapolation of the solar particle spectrum determined by Kinsey and McDonald (1968) for this period of the event gives $0.02 \text{ p/M}^2 \text{ sec. ster. MV}$ at 0.5 GV. far below even the expected albedo flux.

Further evidence confirming the pattern of cutoff variations discussed above is shown in Figure 31, which presents hourly RANGE 10 ($E \geq 260 \text{ MeV}$) proton fluxes plotted against Deep River Neutron Monitor. The progression in time is indicated by the arrows. The topmost solid line ($P_c \leq 0.74 \text{ GV.}$) is the regression curve for primary particles obtained from Churchill flights over the last half solar cycle (Rygg, 1970). The lower solid line ($P_c = 1.36 \text{ GV.}$) is the regression curve for albedo ($0.74 \leq P \leq 1.36 \text{ GV.}$) plus primary ($P \geq 1.36 \text{ GV.}$) protons obtained from the Minneapolis flight series (Rygg, 1970). Regression curves calculated for intermediate cutoff rigidities from the known primary and albedo spectra are also shown. Solid circles indicate the primary fluxes measured at Churchill in 1966 (1.) and 1967 (2.). The cross

indicates the flux measured at Minneapolis just before the event during Flight 1056-W. Early in Flight 1057-W and again towards the end, the flux was close to the Churchill curve confirming the depressed cutoff deduced above from the proton spectra. In the middle of the flight the flux fluctuated about the normal Minneapolis curve confirming the near normal cutoffs deduced above. At times the flux was even lower than the normal regression curve, indicating cutoffs above normal.

3.) Discussion. Figure 32 shows a time history of the cutoffs deduced above. The solid points indicate the cutoffs determined from the proton and helium spectra. Lower limits on the cutoff of 0.15 GV during the first and last periods of the light were obtained from the observations of low rigidity electrons in the manner described earlier. The one hour bars are cutoffs determined from the family of regression curves shown in Figure 31 by selecting the cutoff required to explain the observed flux. A bracket at the left indicates the typical error on these points.

As expected, the variation of the cutoff is well correlated with equatorial D_{st} (Sugiura and Hendricks, 1967) which is included in the upper part of Figure 32 for comparison. The nature of this correlation is also indicated in Figure 25 where a single line D intersects all but one point obtained from Flight 1057-W (solid circles). The depression of cutoff and negative D_{st} that are apparent in Figure 32 before the sudden commencement occurred during the main phase of the first storm which began on the 29th. Note that during the positive phase of the second storm (1100-1800 U.T.) the cutoff was restored at times to its full quiet time level and possibly above. Also note that the cutoff was depressed below 40% of its quiet time value during both main phases.

Examples of the disturbed time cutoff variation obtained from observations of other storm events (Earl, 1962; Freier, 1962; Hoffman and Wincker, 1963; Biswas et al., 1962) which are shown in Figure 25 exhibit cutoff - D_{st} correlations similar in nature to that observed during Flight 1057-W. That is, the observations from a single event are generally consistent with the relationship expected from a ring current of variable strength acting at a fixed radius. The strength of the cutoff- D_{st} relationships (or the value of the nominal ring current radius), however, varies widely. Most of the events, nevertheless, show larger cutoff reductions for a given D_{st} depression than is observed during quiet times (line Q). The observations from Flight 1057-W and the July 20-21, 1961 storm reported by Hoffman and Winckler (1963) are the most extreme examples of this behavior. Cutoff reductions exceeding a factor of 2.5 occurred with depression of only -40γ . The July 18-19, 1961 event (points numbered 2.) also observed by Hoffman and Winckler shows a much weaker cutoff response. In general when it was possible to observe cutoff variations over a period of several hours, the cutoff did appear to track the D_{st} variations. In addition to the case of Flight 1057-W discussed earlier, this correlation is particularly evident for the observations of Earl (1962) and Freier (1962). The two cutoff determinations obtained by Earl lie right on the line corresponding to a ring current parameter of 8 (9.15) to 9(10.3) R_E . The cutoffs obtained by Freier are not as clearly correlated with D_{st} but do show a clustering along a track similar to that shown by Earl's results. The cutoff appeared to be depressed somewhat even before the equatorial field was depressed. Some complication may arise here since Freier's cutoff variations for this event were inferred

from changes in ion chamber rates calibrated by emulsion observations at various points in the event rather than direct observation of changes in the rigidity spectrum.

Before considering any models that might explain the cutoff behavior presented above, it should prove helpful to review the experimental situation. Cutoff depressions amounting to less than 40% of the quiet time value have been observed over the Upper Mid-West on several occasions. The depression appears to be linearly correlated with equatorial D_{st} throughout individual events. However the strength of the relationship between cutoff depression and D_{st} varies widely from event to event. In two of the events discussed the cutoff depressions 40% of normal corresponded to D_{st} of only -40γ . The observations of Flight 1057-W provide an estimate of the time scale involved. In that event the cutoff was restored from half its normal value to its full value in a period of 1-2 hours when a second positive phase occurred. A similarly rapid cutoff depression accompanies the ensuing main phase.

Briefly, the model that is adopted to explain the observations obtained during 1057-W must have the following characteristics: 1.) Relatively minor D_{st} depressions were associated with substantial depressions of the geomagnetic cutoff. 2.) The full cutoff was rapidly restored during the positive phase. 3.) Similarly, the cutoff was depressed rapidly during the main phase. In addition to explaining these characteristics peculiar to this event, the model must also be consistent with established magnetospheric properties and explain the broad variety of tracks shown by other events in Figure 25.

The basic ring current model of Kellogg and Winckler (1961) can produce almost any combination of cutoff and D_{st} depression by appropriate selection of the intensity and radius of the ring current. In relation to the disturbed time cutoff variation, however, it fails to satisfy a number of other constraints. A diamagnetic ring current having a magnetic moment varying from 0 to $1.8 M_E$ located at 11.3 (12.9) R_E quite successfully reproduces the track traced by Flight 1057-W in Figure 25. However if the ring were circular it would extend $2-5 R_E$ beyond the limits of the magnetosphere on the sunward side. Presumably an assymmetric ring current producing the observed D_{st} and cutoff variation could be contained wholly within the magnetosphere by allowing it to bulge outward in the antisolar direction, but it would still be confined to the outer reaches of the magnetosphere. The magnetic field at this distance, however cannot contain a ring current plasma of the required intensity. Parker and Stewart (1967) have argued that if the energy density of the ring current plasma exceeds $\sim 20\%$ that of the ambient field, the plasma can no longer be contained. Appendix C. shows that the energy of the required ring current, if it were confined beyond $13R_E$ in a dipole field, would amount to half the total energy available in the magnetic field beyond that distance. For a magnetospheric shell between 13 and $15 R_E$ this factor is nearly the same. It is also shown in Appendix C. that applying the Parker-Stewart condition throughout the magnetosphere requires that the magnetic moment of any ring current cannot exceed $0.6 M_E$; one third that needed here. Akasofu and Lin (1963) obtained a similar relation ($M_R \lesssim M_E$) using a different approach. Furthermore, the ring current producing the main phase field depression has been identified by Frank (1967) and Cahill (1966) to

exist from 3 to 7 R_E - well within the magnetosphere. It is unlikely that the simple ring current model could overcome these objections.

Akasofu, Lin, and Van Allen (1963) have incorporated the effects of anisotropic magnetospheric compression into the ring current model. This approach may provide a more successful account of the observations. As discussed by Akasofu et al., the compression acting with a ring current extends to lower latitudes the regions around the polar caps whose field lines connect to the magnetotail. The geomagnetic cutoff in these regions is essentially zero and the cutoff in neighboring regions is substantially reduced. The qualitative effect is illustrated for three cases in Figure 33 which contains schematic views of the magnetosphere in the noon-midnight meridian plane. In case A there is no solar plasma and the earth's field is a pure dipole. Low rigidity particles have access to only two points on earth - the North and South Poles. Case B depicts the magnetospheric model of Williams and Mead (1965) in which the solar wind is blowing from the left in its quiet time state so that the magnetopause occurs at a subsolar radius of $10 R_E$. One observes that the field lines emerging at latitudes above 82° on the sunlit side now open into the magnetotail. Case C illustrates a calculation made by Akasofu et al. to depict disturbed times wherein enhanced solar wind momentum flux compresses the magnetosphere to $8 R_E$ at the subsolar point and a ring current at $3 R_E$ produces a D_{st} of -150γ . The polar cap region now extends down to 77° on the sunlit side and cutoffs are lowered nearby. The cutoff - D_{st} relation calculated for 30 MeV protons by Akasofu et al. (1963) for this model gives a track in Figure 25 that essentially duplicates the effects of a ring current at $9(10.3) R_E$.

Since Akasofu et al. calculated the perturbed cutoff for only one case (30 MeV protons, a ring current at $3 R_E$, and a magnetospheric compression to $8 R_E$), effects produced at different rigidities, by different ring currents and compressions can only be assumed at the present time. The qualitative effects, however, can be seen by comparing the effects with and without the compression. Both the degree of compression and the radial location of the ring current govern the slope and position of the cutoff tracks in Figure 25. Noting that the 100 MeV protons considered here have only twice the rigidity of the 30 MeV protons considered by Akasofu et al., it should be possible to explain the cutoff depression observed during Flight 1057-W by moving the ring current to a slightly larger radius (to decrease the surface field depression, $D_{st} = 2M_R/R^3$) or by moderately increasing the field compression (to decrease the cutoff for a given ring current). The wide range of tracks produced by assuming different magnetospheric compressions also may explain the large event to event variations seen in Figure 25 for the disturbed time cutoffs.

Several effects associated with this model are already established. Roederer (1969) has reported compression of the magnetosphere down to $7 R_E$ during strong magnetic storms. Ness and Williams (1966) observed a movement of the polar cap regions toward lower latitudes during magnetic storms. As previously discussed, a ring current of the proper magnitude and location also exists during magnetic storms (Frank, 1967).

The Akasofu et al. model, however, lacks one attractive feature allowed by the simple ring current model that could explain the rapid cutoff restoration coinciding with the positive phase in the middle of

Flight 1057W. Obayashi (1959) has shown that symmetric compression of the magnetosphere acts to increase geomagnetic cutoffs. It has long been accepted (Chapman and Ferraro, 1931) that the D_{st} increase during the positive phase is caused by magnetospheric compression. Akasofu et al. argue, however, that the solar-wind magnetospheric interaction is better characterized by anisotropic compression that acts to reduce cutoffs in the manner described earlier. Undoubtedly, the positive D_{st} excursion observed during the positive phase is due, at least in part, to such compression. In any case, the equatorial field must increase with the compression as the eastward current sheet flowing on the magnetopause to produce the compression intensifies and moves inward. However, if the ring current remains, anisotropic compression should reduce the cutoffs even further during the positive phase. Removing the ring current during the second positive phase of the August 28 storm would produce the observed restoration of the cutoff to near normal levels and preserve the Akasofu et al. model.

Although not yet correlated with increased cutoffs or the positive phase, dumping of the radiation belts during severe magnetic storms has been observed. Craven (1966) found that the fluxes of ≥ 40 keV electrons at $L \approx 5$ were substantially reduced from their pre-storm level for a 3 hour period during a large magnetic storm. The flux was regenerated on a time scale of several hours presumably as further plasma heating occurred. Craven also observed that the artificial belt at $L=3.0$ produced by Russian nuclear tests in 1962 was completely dumped by the magnetic storm of June 6, 1963. Frank (1967) reported only a marked increase in radiation belt proton intensities associated with magnetic

storms, although his time resolution was such that dumping on the time scale noted by Craven could have occurred.

The picture of the cutoff behavior during Flight 1057-W that has emerged from this discussion is as follows. The cutoff depression observed at the beginning of the flight is due to the ring current and magnetospheric compression associated with the main phase of the first magnetic storm. The cutoff was restored to its normal level during the positive phase of the second storm when the radiation belts were dumped near the time of the second sudden commencement. The second cutoff reduction occurred as the ring current again built up toward the end of the flight establishing the main phase of the second storm. In short it is proposed that the two main phase disturbances are quite independent of each other the effects of the first being completely erased during the second positive phase.

Before closing this discussion section it should be noted that the present state of the Akasofu et al. model assumes low rigidity approximations that may not directly apply to the higher rigidity mid-latitude results discussed here. It was singled out, however, because it had features which were able to explain the observations without strongly conflicting with other constraints. An adequate test of the model at higher rigidities requires machine calculations of particle orbits in a complex magnetospheric field configuration for a variety of conditions. An investigation of this nature appears justified by this analysis but is beyond the scope of this work.

D. Forbush Decrease of August 30, 1966

In the preceding section the position of the geomagnetic cutoff was defined throughout Flight 1057-W. The possibility of a significant contribution of solar particles to the low energy proton flux was also ruled out. Thus having established the cutoff and solar particle behavior during this event, the remainder of this chapter will be devoted to comparing the short term modulation of the observed primary fluxes with the long term modulation effects observed with the hodoscope over the period 1965-1969 (Rygg, 1970; Rygg and Earl, 1971). Low rigidity protons were observed during times of cutoff depression both before and after the Forbush decrease appeared in the neutron monitor record so that it is possible to study the long term and short term effects down to rigidities of 0.5 GV. Differential spectral measurements of protons and helium nuclei provide coverage up to 1.5 GV. while the integral penetrating proton and helium fluxes extend this coverage up to effective rigidities of 2.9 GV. and 4.1 GV. respectively.

Before proceeding with the analysis it should be noted that the time limitations intrinsic to balloon work allowed study of only a 21 hour portion of the event whereas the Forbush modulation associated with the series of events starting on August 28 lasted until September 9. Over this short but most interesting period, however, the moderate geometric factor and high bit rate of the hodoscope allowed better coverage of the flux variations at these rigidities than has been available previously.

Beginning at the lowest rigidities we consider the low energy primary proton spectra which, because of the changing cutoff, are available

only during segments 1 and 5 of the flight. Given that the data are of limited statistical accuracy, it is clear that the proton spectra for these two segments (panels 1 and 5 of Figure 29) follow the $J=AT$ form quite closely -- at least to the extent that they are neither considerably steeper nor flatter than that form. That this form appears to persist during a period when the overall intensity has changed by 40% strongly suggests that the mechanism maintaining the $J=AT$ form of the spectrum, presumably adiabatic deceleration, is operative on a time scale of several hours or less. Rygg and Earl (1971) argued that the problem of long term cosmic ray modulation could be considered in two limiting cases. At high rigidities the convective transport of cosmic rays out of the solar cavity is balanced by inward diffusion driven by the intensity gradient that is established (Parker, 1963). At low rigidities the cosmic rays which are essentially trapped in the solar cavity diffuse only slowly through an expanding medium which, consequently, is constantly adiabatically decelerating them. The $J=AT$ spectral form is a direct consequence of this low rigidity limit independent of the rigidity dependence of the diffusion. It is argued here, therefore, that the spectral shape alone indicates that the Forbush modulation shows a strong resemblance to the eleven-year modulation in this low rigidity limit.

For the long term modulation the intensity at all rigidities is governed by the effect of diffusion and convection on the higher rigidity particles. In the models discussed by Rygg (1970) and O'Gallagher (1972), it is deceleration of higher rigidity particles rather than diffusion that is the primary source of low rigidity particles observed

near the earth. The intensity at low rigidities thus depends in some way on that at higher rigidities. In the idealized model presented by O'Gallagher (1972), the intensity at low rigidities varies directly as the intensity at some critical rigidity that separates purely diffusive and decelerative regimes. In this picture the rigidity dependence of the diffusion governs only the intensity above this critical rigidity below which the spectrum maintains a $J=AT$ form. Thus to the extent that such models describe long term and short term modulation, the regression analyses that follow will determine primarily the relative rigidity dependence of the Forbush decrease and the eleven-year modulation in the high energy or diffusion-convection limit.

An accurate measurement of the Forbush modulation requires knowledge of the spectrum immediately before the Forbush decrease. For rigidities above the nominal cutoff at Minneapolis, 1.36 GV., this is provided by Flight 1056-W made one day before the flare. Segment 1 of Flight 1057-W could provide the pre-decrease spectrum if there was complete assurance that the cutoff remained below the instrumental cutoff, 0.5 GV., during the entire segment. The nature of the proton spectrum for this segment, shown in Figure 29, and the cutoff behavior inferred from the penetrating protons in Figures 31 and 32, however, allows the possibility that the cutoff may have exceeded this level during part of the segment. Study of the neutron monitor record for August, 1966 shown in Figure 34 suggests that Flight 1178-N, made from Ft. Churchill August 6 offers the best prospect for establishing the pre-decrease flux level at low rigidities. The arrows show the periods covered by each of the three flights made that month. Since the modulation at neutron monitor energies remained constant within $\pm 0.6\%$

during the entire period separating Flight 1178-N and the Forbush decrease, using the protons from that flight to establish the flux level prior to the decrease should be a fairly sound procedure.

If there is any difference in the rigidity dependence of the two modulations it should appear most strongly in the low rigidity protons. Figure 35 is a regression plot against Deep River Neutron Monitor for the parameter A in Equation VI-1. which describes the modulation of low energy protons ($E \lesssim 250\text{MeV}$) over the long term (Rygg and Earl, 1971). The solid and open circles are, respectively, the hodoscope (Rygg, 1970) and satellite observations (Hsieh, 1970; Hsieh et al., 1971). The crossed circles represent measurements obtained during the first (0215-0620 U.T.) and fifth (1920-2340 U.T.) segments of Flight 1057-W. The point designated 0. indicates the flux level obtained from Flight 1178-N which should represent conditions existing before the Forbush decrease occurred.

Depending upon the interpretation of the observations of segment 1, the Forbush modulation may match either the long term form or the much flatter form obtained by Lockwood et al. (1970). If the low intensity observed during segment 1. results from effects of the geomagnetic cutoff as discussed earlier, then that point can be ignored and one can conclude that the Forbush modulation was as strong or possibly stronger than the eleven-year modulation. The weaker modulation implied by the observations of Lockwood et al. (1970) which is represented by the dashed line does not fit the observations.

On the other hand, if the flux measured during segment 1. does represent the primary spectrum at that time, then the low energy intensity must have experienced a substantial decrease some time before

segment 1. The modulation acting between segments 1 and 5 would then appear to be completely consistent with the form reported by Lockwood et al. represented by the dotted line in Figure 35. The modulation acting between segments 0. and 1. must also be associated with the Forbush decrease since departures from the regression curve of this magnitude (30%) during quiet times were not observed during the entire period 1965-1969. If the Forbush effect produced the modulation observed during segment 1, then it would appear that the Forbush decrease affected the low rigidity particles several hours before there was any effect at neutron monitor rigidities. Since the first sudden commencement occurred many hours before segment 1. it would not be unusual to see Forbush modulation at this time. However, a time delay of several hours between the effects at low and high rigidities has not been seen before.

At higher rigidities, complications of the changing cutoff and poor statistics exhibited by the regression curve of penetrating protons ($E \geq 260\text{MeV}$) shown in Figure 31 do not allow one to determine whether the Forbush modulation more closely follows the eleven-year form (solid line labelled 0.74) or the flatter form obtained by Lockwood et al. (dashed curve). The nature of this problem is similar to that obtained for the low rigidity protons. The average flux level for the first four hours of the flight (corresponding to segment 1.) appears to be slightly depressed below the predecrease level represented by Flight 1178-N (solid circle designated 1.). The flux levels observed during the last four hours of the flight (corresponding to segment 5) are clearly consistent with the flux predicted by the long term modulation.

The solid circle (numbered 2.) which is nearby provides a reference level for the flux obtained the following summer (1967) at Churchill. If one assumes that the Lockwood et al. relationship should extend from the level of Flight 1178-N (dashed line in Figure 31), then the fluxes observed late in Flight 1057-W fail to agree with that form. However, moving the dashed line down to agree with the flux level of segment 1 also produces agreement with segment 5.

These observations imply a situation similar to that obtained for the lowest rigidity protons. The intensity observed at the beginning of the flight was depressed below the level expected on the basis of the neutron monitor rate and the measured pre-decrease level. Later after the Forbush decrease had appeared in the neutron monitor rate, the fluxes matched those expected from the long term variation. A regression curve connecting the two points matches the flat variation obtained by Lockwood et al. for other Forbush decreases. Again it appears that the Forbush modulation of lower rigidity particles occurred at an earlier time than it did for higher rigidity particles.

A similar effect appears to apply to the helium intensity shown in Figure 36. The lower portion is a regression curve of the differential helium flux in the interval 200-250 MeV/nucleon. Since this interval falls above even the quiet time cutoff, the complications of the cutoff variation are removed. The fluxes for segments 1-3 observed before there was a significant depression of the neutron monitor rate fall right on the regression curve obtained from the eleven-year variation (solid line) (Rygg, 1970). The cross indicating the predecrease level obtained from Flight 1056-W also falls on the curve. During segment

4. the intensity falls somewhat below the quiet time curve while that observed in segment 5 falls right at the level expected from the eleven-year variation. Since these measurements were made at a higher rigidity (1.5 GV.), it is not surprising that the long term relation appears to give a better fit than the less steep form obtained by Lockwood et al. (dashed line). With such poor statistics that flatter form is not ruled out, however.

The upper portion of Figure 36 shows the regression curve obtained for the penetrating helium nuclei ($E > 260$ MeV/nucleon). The solid line represents the long term variation obtained by Rygg (1970). Again the flux level early in the flight appears slightly depressed below the pre-decrease level (cross) obtained from Flight 1056-W. The low fluxes observed during segments 2-4 provide yet another indication that the Forbush decrease affected the lower rigidity particles more strongly early in the event than later on. The statistics and the form of the variation favor neither the long term variation nor the short term variation (dashed line) obtained by Lockwood et al.

Summarizing the observations, the following properties appear common to most of the regression curves presented above. 1.) Early in Flight 1057-W before there was any significant depression of the neutron monitor rate, the flux already appeared depressed below the pre-decrease level established in earlier flights. For protons below 260 MeV it is possible that cutoff effects may have complicated this observation. 2.) Late in the flight (segment 5.) all fluxes fell on the regression curves representing the eleven-year variation. At no time did the flux exceed the level predicted by the eleven-year variation. 3.) Comparing the results from segment 5. with the pre-decrease

flux levels indicates that the eleven-year variation may describe the early stages of the August 30, 1966 decrease as well. 4.) Alternatively, comparing the results of segment 5. with those from segment 1. indicates that the flatter modulation form obtained by Lockwood et al. (1970) may describe the rigidity dependence of the Forbush decrease after an initial decrease that does not appear at neutron monitor rigidities. This initial decrease may be interpreted as a time delay effect in which the Forbush decrease first becomes apparent at low rigidities progressing up in rigidity at later times. Since this event may have involved two separate magnetic storms, it is possible that the first, which occurred before the flight, may have (through a strong rigidity dependence) affected only the low rigidity particles while the second (having a weak rigidity dependence) had a greater effect at high rigidities. Such a situation, however, seems quite contrived.

Although not discussed by Lockwood et al., the pre-decrease effect proposed in point 4.) may be present in their data. In superimposing their long-term variation on the Forbush variations one notes that, for the September 30 and October 29, 1968 events especially, half of the flatness of the variation is due to exceptionally low fluxes at high neutron monitor rates in addition to the relatively high fluxes at low neutron monitor rates. Since there is no time identification of their data it is not possible to determine whether the low fluxes occurred early or late in the event.

Although an effect of this type can be produced by changing the geomagnetic cutoff at the neutron monitor station, it does not appear to be of sufficient magnitude to explain the observations reported

here. When the cutoff is reduced by the magnetic storm, the additional primary particles that are admitted can produce anomalously high neutron monitor rates masking the early stages of the Forbush decrease. Since the Forbush decrease and geomagnetic storm are both associated with solar events, one should use a high latitude neutron monitor for the basic comparison to avoid confusion owing to cutoff variations. When this technique was applied to the hodoscope observations using the Alert Neutron Monitor (Steljes, 1966) the result was to provide a little better agreement with the long term modulation during segment 5. However, the results for segment 1. show only a minor improvement. The depression is not removed.

Thus the regression analyses described above provide no conclusive demonstration that the rigidity dependence of the modulation acting during the early stages of the August 30, 1966 Forbush decrease was weaker than the eleven-year modulation. Instead, there is some evidence that the Forbush modulation shows an unusual temporal behavior in which low rigidity particles appear to exhibit modulation before it is evident at high energies. Possible confusion concerning the behavior of the geomagnetic cutoff and statistical considerations, however, do not allow an unequivocal statement that such evolutionary effects were present. Nevertheless, the low energy proton data do conclusively exhibit the $J=AT$ form that is characteristic of low energy proton spectra throughout the solar cycle.

VII. SUMMARY AND CONCLUSION

Differential measurements of the proton and helium intensities in the 100 - 260 MeV/nucleon interval and integral fluxes above 260 MeV/nucleon were obtained from seven balloon flights over the Upper Mid-West area. The main conclusions obtained from the analysis of these data will be summarized below with respect to atmospheric secondary and re-entrant albedo protons, geomagnetic cutoff rigidities, and short term modulation effects.

i.) Atmospheric secondaries and re-entrant albedo. The atmospheric secondary protons at Churchill and Minneapolis are observed to be modulated as predicted by the model derived in earlier work (Rygg, 1970). Poor statistics do not allow verification of the slightly lower secondary intensity at Minneapolis predicted by the model. The re-entrant proton albedo energy spectra are observed to be flat in the 100 - 200 MeV interval and are more intense than previously reported levels. Model calculations of the albedo intensity presented here and those reported by Ray (1967), however, predict flat spectra with intensities of the same order as the observations. The flat spectra are a direct consequence of the generation and propagation of secondary particles in large thicknesses of matter. The accuracy of the flux determination is insufficient to demonstrate the effect of solar modulation on the albedo intensity. A factor of ten disparity among the albedo observations reported by several observers cannot be explained even when effects due to geomagnetic cutoff variation, direct atmospheric secondaries, and solar modulation are considered.

ii.) Geomagnetic cutoffs. The geomagnetic cutoffs observed in fairly

quiet times over the Upper Mid-West area are variable on a day to day basis and appear to fall an average of 23% below those predicted on the basis of the internal field alone. The observed variations are well correlated with equatorial D_{st} . The strength of the cutoff - D_{st} relationship essentially identifies currents in the radiation belts as the source of the day to day variation. No strong day/night cutoff variations were detected at mid-latitudes. Although variations of detectable magnitude may have been present, they were masked by the high degree of day to day variability. The slight unsharpness of the cutoff observed on the flights having the best resolution and smallest latitude drift can be fully accounted for in terms of the response of the detector to the penumbral bands obtained from the calculations of Shea et al. (1965). The cutoff disturbance observed during the geomagnetically disturbed period following the August 28, 1966 solar flare shows a much different character than the day to day variations observed during quiet times. The cutoff reduction of a factor of 2.5 or greater correlated with an equatorial field depression of only 40γ appears to rule out a pure ring current source for the cutoff depression. A combination of anisotropic magnetospheric compression and a ring current suggested by Akasofu et al. (1963), however, may account for the depression observed here. The wide variation in the character of cutoff - D_{st} relationships obtained in other events is also explained by this model. Rapid restoration of the cutoff observed during the positive phase of a second magnetic storm that occurred during the flight requires in this model that the ring current providing the previous main phase be dumped at the onset of the positive phase. The geomagnetic

effects of the subsequent main phase are in this picture completely independent of the first storm.

iii.) Short term modulation (Forbush decrease). The observations of the Forbush decrease associated with the August 28, 1966 flare show an unusual premature decrease in the low rigidity fluxes observed early in the event. This decrease may be the result of a time dependent geomagnetic cutoff that partially excludes the low rigidity particles. If the decrease has a geomagnetic origin then the rigidity dependence of the Forbush modulation, at least in the early stages, is indistinguishable from the eleven year modulation. This result clearly conflicts with the observation of quite a weak rigidity dependence obtained by Lockwood and Webber (1969) and Lockwood et al. (1970). Fluxes in all rigidity intervals obtained during the most deeply modulated portion of the flight fall right on the regression curves obtained from the eleven-year modulation. However, if the premature decrease is associated with the Forbush modulation, then flat regression curves of the form observed by Lockwood and Webber (1969) and Lockwood et al. (1970) do result. In this picture, the Forbush decrease becomes evident first at the lowest rigidities propagating upward in rigidity over a period of several hours. Flat regression curves are obtained because 1.) the flux at low rigidities is reduced below the quiet time level before appreciable modulation appears at neutron monitor rigidities. 2.) By the time the decrease appears in the neutron monitor intensity no further response of the low rigidity flux occurs. Owing therefore to the possible complications of the changing cutoff, the rigidity dependence of the Forbush modulation cannot be clearly established here. It does

appear, however, that the low rigidity flux may at times fall below the expected intensity but does not exceed the intensity predicted by the long term variation.

APPENDIX A

ATMOSPHERIC SECONDARY PROTONS

REVISION FOR BEHAVIOR AT LARGE DEPTHS

The original version of this calculation (Rygg, 1970) was directed towards a determination of the atmospheric secondary corrections to be applied at small depths and low energies. In that spirit the range-energy relation and source spectra that were employed were not intended for use above 4-500 MeV. Two modifications of the original presentation described below serve to extend the application of the model to depths of a few hundred grams and energies up to 1000 MeV while retaining essentially the same form at small depths.

Equation A1 presents the general result obtained in the earlier treatment (Rygg, 1970; Rygg and Earl, 1971) relating the intensity, U , of protons of energy, E , observed at depth, x , to the intensity at the top of the atmosphere, U_0 , of primary energy E .

$$U(E, x) = \frac{1}{\frac{dE}{dx}} [Q(E) - Q(E_x)] + \frac{E}{E_x} e^{-x/\lambda} U_0(E_x) \quad (A-1.)$$

The first term gives the secondary contribution in terms of the integral source spectrum, $Q(E)$, modified for the effects of nuclear interactions.

$$Q(E) = \int_E^{\infty} q(E') \exp \frac{R(E) - R(E')}{\lambda} dE' \quad (A-2.)$$

$R(E)$ is the range in air of a particle of energy E . The differential source function, $q(E)$, is related to $N(E)$ the spectrum of secondary protons, deuterons, and tritons produced in nuclear emulsions by cosmic rays at 50 gms/cm² (Powell et al., 1959).

$$q(E') = 0.85 \theta(E') N(E') \sum_Z \frac{J_{\text{prim}}^{(Z)}}{\lambda_Z} \quad (A-3.)$$

The factor 0.85 relates the intensity observed in emulsions to that in air (Fichtel et al. 1964) and $\theta(E')$ is the fraction of secondaries emitted in the forward direction ($0.5 \leq \theta(E') \leq 1.0$). The summation relates the number of secondaries produced by each primary species (protons, helium, etc.) to the flux of that species, $J_{\text{prim}}(Z)$. The dependence on the shape of the primary spectrum is introduced in $J(Z)$ at this point as a normalization factor obtained from an integral of the multiplicity over the primary spectrum. This factor is required to account for the effects of solar modulation and geomagnetic cutoff.

The modifications introduced now are merely changes in $N(E)$ and the range energy relation to be applied. Investigation of the behavior of $N(E)$ at high energies revealed that the spectral dependence, $E^{-2.8}$, given by Powell et al. (1959) did not fit the data on which it was based (Camerini et al. , 1950) nor did it account for the reservations expressed by those authors concerning the cutoff above 800 MeV. A more realistic behavior, $E^{-1.64}$, fits both the Camerini et al. data up to the 800 MeV cutoff and the internucleon cascade calculations of Metropolis et al. (1958) beyond. Although of minor importance above 30 MeV a flatter spectrum, $E^{-0.54}$, was used in the low energy regime to account for the less prevalent spectrum of nuclear evaporation particles produced in air compared to emulsion (Metropolis, 1958). The resulting fit to the secondary spectrum, $N(E)$, is then given by the following.

$$N(E) = \left[\left(\frac{E^{0.543}}{.0445} \right)^2 + \left(\frac{E^{1.636}}{6.64} \right)^2 \right]^{-\frac{1}{2}} \quad (\text{A-4.})$$

The range-energy relations applied in the present model involve sixth degree polynomials in $\log E - \log R$ which were fit to the tables of Barkas and Berger (1964) over the energy interval 10 MeV to 10 GeV.

The secondary proton spectra at various indicated depths resulting from the modified calculations as shown in Figure 3 differ by not more than 5% from the earlier calculations at depths up to 30 gms/cm² and energies below 200 MeV. The only significant changes in secondary intensity are at depths greater than 40 gms/cm² and energies above 250 MeV where much flatter energy spectra are obtained. The spectrum at 300 gms/cm² is essentially the equilibrium spectrum obtained in the limit of large depths and is used in section IV.C. as the basis for the calculation of the intensity and energy spectrum of the re-entrant proton albedo.

APPENDIX B

INDUCTIVE EFFECT OF THE EARTH ON OBSERVED D_{st} VALUES

Parker (1967) has shown that the conductivity of the earth produces an inductive effect which acts to increase observed equatorial D_{st} values 50% above the portion that arises from external currents. Thus Equation V-11 is more correctly written

$$P' = \frac{P}{1 + 1.5 \left(\frac{R'}{R_E} \right)^3 \left(\frac{D_{st} - D_{sto}}{2 B_{eq}} \right)} \quad (B-1.)$$

where D_{st} means observed value. The factor of 1.5 can be incorporated into the ring current analysis of Figure 25 by multiplying all ring current radii R' by $(1.5)^{1/3}$. The resulting radii given in parentheses in that figure are then more properly treated as the correct ring current radii. To reduce confusion concerning which radius is being discussed in the text, the convention adopted in Figure 25 of first giving the nominal radius obtained from Equation V-11 followed by the corrected value obtained from Equation B1 will be used.

APPENDIX C

ENERGY DENSITY IN THE EARTH'S FIELD AND LIMITATIONS ON RING CURRENT STRENGTH

The problem of applying the Kellogg and Winckler (1961) ring current model to cases of substantial cutoff reduction is complicated by the ability of the earth's field to contain the diamagnetic plasma that forms the ring. Parker (1967) has argued that the energy density of the plasma must remain small compared to the energy density of the magnetic field that contains it. Since the surface field perturbation (D_{st}) produced by such a current is related only to the total energy of the ring current plasma (Dessler and Parker, 1959; Sckopke, 1966), calculation of the total energy in the earth's field in some radial interval will yield an upper limit to the surface field perturbation that can arise from a ring current in that interval.

The surface field perturbation produced by ring current plasma of energy E_{plasma} is given by (Dessler and Parker, 1959; Sckopke, 1966) :

$$D_{st} = - 0.77 \times 10^{-20} \left(\frac{\gamma}{\text{erg}} \right) E_{\text{plasma}} \quad (\text{C-1.})$$

Alternatively, the plasma energy can be obtained by inverting the relation

$$E_{\text{plasma}} = - 1.3 \times 10^{20} \left(\frac{\text{erg}}{\gamma} \right) D_{st} \quad (\text{C-2.})$$

The energy density of the earth's dipole field at a geocentric distance r and co-latitude θ is

$$\frac{B^2}{8\pi} (r, \theta) = \frac{(.312 \text{ gauss})^2 (2 \cos^2 \theta + \sin^2 \theta)}{8\pi (r/R_E)^6} \quad (\text{C-3.})$$

The total magnetic energy in a spherical shell of radius r and thickness dr is

$$\begin{aligned} dE_{\text{field}} &= r^2 dr \int \frac{B^2(\theta, r)}{8\pi} d\Omega \\ &= 4\pi r^2 dr \int_0^{\pi} \frac{2 \cdot (.312g)^2 (2\cos^2\theta + \sin^2\theta) \sin^2\theta d\theta}{8\pi (r/R_E)^6} \end{aligned} \quad (\text{C-4.})$$

$$= (1.2 \times 10^{25} \text{ ergs}) \frac{d\rho}{\rho} \quad (\text{C-5.})$$

where $\rho = \left(\frac{r}{R_E}\right)$.

The total energy in the earth's field beyond $13R_E$ (in the dipole approximation) obtained from Equation C-5 is 17.3×10^{20} ergs. This is to be compared with the plasma energy required to produce the 40 γ field depression observed during segment 1 of Flight 1057-W obtained from Equation C-2 which is 9.2×10^{20} ergs. In a limited magnetosphere, the field near the surface is of order 2 \times its dipole value (Williams and Mead, 1965) so that the magnetic energy contained in a magnetospheric shell from $13R_E$ to $15R_E$ has four times the energy obtained from Equation C-5 or 19.1×10^{20} ergs. Thus, the plasma energy density is half that of the field which is supposed to contain it. This exceeds by more than a factor of two the condition for stability of such a situation obtained by Parker and Stewart (1967):

$$E_{\text{plasma}} \lesssim 1/5 E_{\text{field}} \quad (\text{C-6.})$$

Since the cutoff depression in the Kellogg and Winckler (1961) ring current model is directly proportional to the magnetic moment of the ring current, it will be informative to determine the total magnetic moment of a ring current that meets the Parker-Stewart condition

throughout the magnetosphere. The surface field disturbance arising from a ring current shell of thickness $d\rho$ and radius ρ can be obtained from Equations C-1, C-5, and C-6 as the following:

$$d(D_{st}) = \frac{9.2 \times 10^4}{5} (\gamma) \frac{d\rho}{\rho^4} \quad (C-7.)$$

The magnetic moment of such a shell is

$$dM = - \frac{R_E^3 \rho^3}{2} d(D_{st}) \quad (C-8.)$$

The total magnetic moment for shells extending from the surface to $10R_E$ is

$$M_{max} = (9.2 \times 10^3 \gamma) R_E^3 \int_1^{10} \frac{d\rho}{\rho} = 0.6 M_E \quad (C-9.)$$

Thus the magnetic moment of any ring current is restricted by the Parker-Stewart condition to the case

$$M_{ring} \lesssim 0.6 M_E \quad (C-10.)$$

Akasofu and Lin (1963) obtained a similar limit ($M_{ring} \lesssim M_E$) from consideration of a number of specific ring current models. It should be noted that Equation C-10 applies to a pure dipole field; the limit might increase somewhat if the compression of the outer field were considered.

REFERENCES

- Akasofu, S. -I., and W. C. Lin, The magnetic moment of model ring current belts and the cutoff rigidity of solar protons, *J. Geophys. Res.*, **68**, 973, 1963.
- Akasofu, S. -I., W. C. Lin, and J. A. Van Allen, The anomalous entry of low-rigidity solar cosmic rays into the geomagnetic field, *J. Geophys. Res.*, **68**, 5327, 1963.
- Aly, H. H., and C. J. Waddington, The flux of primary cosmic ray α -particles over Sardinia, *Nuovo Cim., Ser. X*, **5**, 1679, 1957.
- Anderson, K. A., R. Arnoldy, R. Hoffman, L. Peterson, and J. R. Winckler, Observations of low-energy solar cosmic rays from the flare of 22 August 1958, *J. Geophys. Res.*, **64**, 1133, 1959.
- Arnoldy, R. L., S. R. Kane, and J. R. Winckler, The observation of 10-50 keV solar flare x-rays by the OGO satellites and their correlation with solar radio and energetic particle emission, *IAU Symp, No. 35*, Springer-Verlag, New York, 490, 1968.
- Balasubrahmanyam, V. K., and D. Venkatesan, Spectral variations in short term (Forbush) decreases and in long term changes in cosmic-ray intensity, *Acta Physica Academiae Scientiarum Hungaricae*, **29**, Suppl. 2, 327, 1970.
- Bingham, R. G., D. M. Sawyer, J. F. Ormes, and W. R. Webber, Direct measurements of geomagnetic cutoffs for cosmic-ray particles in the latitude range 45° to 70° using balloons and satellites, *Can. J. Phys.*, **46**, S1078, 1968.
- Biswas, S., P. S. Freier, and W. Stein, Solar protons and α particles from the September 3, 1960, flares, *J. Geophys. Res.*, **67**, 13, 1962.
- Cahill, L. J., Inflation of the inner magnetosphere during a magnetic storm, *J. Geophys. Res.*, **71**, 4505, 1966.
- Chapman, S., and V. C. A. Ferraro, A new theory of magnetic storms, *Terrest. Magnetism Atmospheric Elec.*, **36**, 77, 1931.
- Chapman, S., and J. Bartels, *Geomagnetism*, Oxford University Press, New York, 1940.
- Clay, J., Penetrating radiation, *Proc. Roy. Acad. Sci. Amsterdam*, **30**, 1115, 1927.
- Compton, A. H., A geographic study of cosmic rays, *Phys. Rev.*, **43**, 387, 1933.
- Craven, J. D., Temporal variations of electron intensities at low altitudes in the outer radiation zone as observed with satellite Injun 3, *J. Geophys. Res.*, **71**, 5643, 1966.

- Dessler, A. J., and E. N. Parker, Hydromagnetic theory of geomagnetic storms, *J. Geophys. Res.*, 64, 2239, 1959.
- Dodson, H. W., and E. R. Hedeman, The proton flare of August 28, 1966, *Solar Phys.*, 4, 229, 1968.
- Earl, J. A., Cloud-chamber observations of solar cosmic rays over Minneapolis on September 4, 1960, *J. Geophys. Res.*, 67, 2107, 1962.
- Fanselow, J. L., and E. C. Stone, Geomagnetic cutoffs for cosmic ray protons for seven energy intervals between 1.2 and 39 MeV, *J. Geophys. Res.*, 77, 3999, 1972.
- Finch, H. F., and B. R. Leaton, The earth's main magnetic field — epoch 1955.0, *Mon. Not. Geophys. Suppl.*, 7, 314, 1957.
- Forbush, S. E., On the effects in cosmic-ray intensity observed during the recent magnetic storm, *Phys. Rev.*, 51, 1108, 1937.
- Fowler, P. H., and C. J. Waddington, The energy distribution of cosmic ray particles over northern Italy, *Phil. Mag.*, 1, 637, 1956.
- Fowler, P. H., C. J. Waddington, P. S. Freier, J. Naugle, and E. P. Ney, The low energy end of the cosmic ray spectrum of alpha-particles, *Phil. Mag.*, 2, 157, 1957.
- Frank, L. A., On the extraterrestrial ring current during geomagnetic storms, *J. Geophys. Res.*, 72, 3753, 1967.
- Freier, P. S., E. P. Ney, and J. R. Winckler, Balloon observation of solar cosmic rays on March 26, 1958, *J. Geophys. Res.*, 64, 685, 1959.
- Freier, P. S., The measurement of the cutoff rigidity at Minneapolis, using solar protons and α -particles from July 10, 1959, flare, *J. Geophys. Res.*, 67, 2617, 1962.
- Freier, P. S., and C. J. Waddington, Singly and doubly charged particles in the primary cosmic radiation, *J. Geophys. Res.*, 73, 4261, 1968.
- Gall, Ruth, Jaime Jimenez, and Lucilla Comarcho, Arrival of low-energy cosmic rays via the magnetospheric tail, *J. Geophys. Res.*, 73, 1593, 1968.
- Hoffman, D. J., J. R. Winckler, Simultaneous balloon observations at Fort Churchill and Minneapolis during the solar cosmic ray events of July, 1961, *Space Research III.*, North Holland, Amsterdam, 662, 1963.
- Hovestadt, D., and P. Meyer, The geomagnetic cutoff at Ft. Churchill and the primary cosmic ray electron spectrum from 10 MeV to 12 GeV in 1968, *Acta Physica Academiae Scientiarum Hungaricae*, 29, Suppl. 2, 525, 1970.

- Hsieh, K. C., Study of solar modulation of low-energy cosmic rays using differential spectra of protons, ^3He , and ^4He at $E \leq 100$ MeV per nucleon during the quiet time in 1965 and 1967, *Astrophys. J.*, 159, 61, 1970.
- Hsieh, K. C., G. M. Mason, and J. A. Simpson, Cosmic-ray H^2 from satellite measurements from 1965 to 1969, *Astrophys. J.*, 166, 221, 1971.
- Hultqvist, B., The geomagnetic field lines in higher approximation, *Ark. Geofs.*, 3, 63, 1958.
- Israel, M. H., and R. E. Vogt, Characteristics of the diurnally varying electron flux near the polar cap, *J. Geophys. Res.*, 74, 4714, 1969.
- Jokipii, J. R., J. L'Heureux, and P. Meyer, Diurnal intensity variation of low-energy electrons observed near the polar cap, *J. Geophys. Res.*, 72, 4375, 1967.
- Kane, R. P., Comparison of spectral characteristics of long-term and short-term changes in cosmic ray intensity, *Nuovo Cim.*, 45, B. N. 2, 132, 1966.
- Kane, S. R., J. R. Winckler, and R. L. Arnoldy, Response of ion chambers in free space to the long-term cosmic ray variation from 1960 to 65, *J. Geophys. Res.*, 70, 4107, 1965.
- Katz, L., P. Meyer, and J. A. Simpson, Further experiments concerning the geomagnetic field effective for cosmic rays, *Nuovo Cim. Suppl.* 8, 277, 1958.
- Kellogg, P. J., and M. Schwartz, Theoretical study of the cosmic ray equator, *Nuovo Cim.* 8, 761, 1959.
- Kellogg, P. J., and J. R. Winckler, Cosmic ray evidence for a ring current, *J. Geophys. Res.*, 66, 3991, 1961.
- Kinsey, J. H., and F. B. McDonald, Observations of the solar proton event of August 28, 1966, *IAU Symp. No. 35*, Springer-Verlag, New York, 536, 1968.
- Kodama, M., and Y. Miyazaki, Geomagnetic latitude effect of the cosmic-ray nucleon and meson components at sea level from Japan to the Antarctic, *Rep. of Ionospheric Res. in Japan*, 11, 99, 1957.
- Lemaitre, G. E., and M. S. Vallarta, On Compton's latitude effect of cosmic rays, *Phys. Rev.*, 43, 87, 1933.
- Lezniak, J. A., and W. R. Webber, The solar modulation of cosmic ray protons, helium nuclei, and electrons a comparison of experiment with theory, *J. Geophys. Res.*, 76, 1605, 1971.

- Lin, R. P., and K. A. Anderson, Electrons >40 keV and protons >500 keV of solar origin, *Solar Phys.*, 1, 446, 1967.
- Lockwood, J. A., and W. R. Webber, Cosmic ray intensity variations on January 26-27, 1968, *J. Geophys. Res.*, 74, 5599, 1969.
- Lockwood, J. A., J. Lezniak, P. and W. R. Webber, Rigidity dependence for Forbush decreases in 1968 compared with that for the 11-year variation, *J. Geophys. Res.*, 75, 6885, 1970.
- Luhmann, J. M., *A Study of the Solar Modulation of Low Energy Cosmic Ray Electrons Between 1965 and 1970*, M. S. Thesis, University of Maryland Tech. Rept. 71-127, 1971.
- Luhmann, J. M., and J. A. Earl, Solar and geomagnetic modulation of low energy secondary cosmic ray electrons, *J. Geophys. Res.*, in press, 1973.
- McCracken, K. G., Energy dependence of transient changes in the primary cosmic-ray spectrum, *Phys. Rev.*, 117, 1570, 1960.
- McDonald, F. B., Study of geomagnetic cutoff energies and temporal variation of the primary cosmic radiation, *Phys. Rev.*, 107, 1386, 1957.
- McDonald, F. B., and W. R. Webber, Changes in the low rigidity primary cosmic radiation during the large Forbush decrease of May 12, 1959, *J. Geophys. Res.*, 65, 767, 1960.
- McIlwain, C. E., Coordinates for mapping the distribution of magnetically trapped particles, *J. Geophys. Res.*, 66, 3681, 1961.
- Metropolis, N., R. Bivins, M. Storm, J. M. Miller, and G. Friedlander, Monte Carlo calculations on intranuclear cascades, II High energy studies and pion processes, *Phys. Rev.*, 110, 204, 1958.
- Meyer, P., and J. A. Simpson, New changes in the low energy particle cutoff and spectrum of the primary cosmic radiation, *Nuovo Cim. Supl.* 8, 233, 1958.
- Meyer, Peter, Cosmic rays in the galaxy, *Ann. Rev. Astron. Ap.*, 7, 1, 1969.
- Ness, N. F., and D. J. Williams, Correlated magnetic tail and radiation belt observations, *J. Geophys. Res.*, 71, 322, 1966.
- Obayashi, T., Entry of high energy particles into the polar ionosphere, *Rept. Ionosphere and Space Res. Japan*, 13, 201, 1959.
- O'Gallagher, J. J., Idealized model for the radial gradient of modulated cosmic rays, *J. Geophys. Res.*, 77, 513, 1972.

- Ormes, J. F., and W. R. Webber, Proton and helium nuclei cosmic-ray spectra and modulations between 100 and 2000 MeV/nucleon, *J. Geophys. Res.*, 73, 4231, 1968.
- Parker, E. N., *Interplanetary Dynamical processes*, John Wiley and Sons, New York, 1963.
- Parker, E. N., Disturbance of the geomagnetic field by the solar wind, *Physics of Geomagnetic Phenomena*, Academic Press, New York, 1153, 1967.
- Parker, E. N., and H. A. Stewart, Nonlinear inflation of a magnetic dipole, *J. Geophys. Res.*, 72, 5287, 1967.
- Quenby, J. J., and W. R. Webber, Cosmic ray cutoff rigidities and the earth's magnetic field, *Phil. Mag.*, 4, 90, 1959.
- Quenby, J. J., and G. J. Wenk, Cosmic ray threshold rigidities and the earth's magnetic field, *Phil. Mag.*, 7, 1457, 1962.
- Ray, E. C., Effects of a ring current on cosmic radiation, *Phys. Rev.*, 101, 1142, 1956.
- Ray, E. C., An improved cosmic-ray re-entrant albedo calculation, *J. Geophys. Res.*, 72, 4839, 1967.
- Rockstroh, J., and W. R. Webber, A measurement of the spectrum of cosmic ray electrons between 20 MeV and 3 BeV in 1968-- further evidence for extensive time variations of this component, *J. Geophys. Res.*, 74, 5041, 1969.
- Roederer, J. G., Quantitative models of the magnetosphere, *Rev. Geophys.*, 7, 77, 1969.
- Rose, D. C., K. B. Fenton, J. Katzman, and J. A. Simpson, Latitude effect of the cosmic ray nucleon and meson components at sea level from Arctic to the Antarctic, *Can. J. Phys.*, 34, 963, 1956.
- Rossi, B., *High Energy Particles*, Prentice Hall, Inc., Englewood Cliffs, N. J., 1952.
- Rothwell, P., and J. Quenby, Cosmic rays in the earth's magnetic field, *Nuovo Cim., Supl.* 8, 249, 1958.
- Rothwell, P., Magnetic cutoff rigidities of charged particles in the earth's field at times of magnetic storms, *J. Geophys. Res.*, 64, 2026, 1959.
- Rygg, T. A., *Cosmic Ray Proton and Helium Measurements over Half a Solar Cycle 1965-1969*, M. S. Thesis, University of Maryland Tech. Rept. 70-111, 1970.

- Rygg, T. A., and J. A. Earl, Balloon measurements of cosmic ray protons and helium nuclei over half a solar cycle 1965-1969, *J. Geophys. Res.*, 76, 7445, 1971.
- Sauer, H. H., A new method of computing cosmic ray cutoff rigidity for several geomagnetic field models, *J. Geophys. Res.*, 68, 957, 1963.
- Schmidt, A. Das Erdmagnetische Aussenfeld, *Z. Geophysik*, 1, 1, 1924-25.
- Sckopke, N., A general relation between the energy of trapped particles and the disturbance field near earth, *J. Geophys. Res.*, 71, 3125, 1966.
- Shea, M., D. F. Smart, and K. G. McCracken, A study of vertical cutoff rigidities using sixth degree simulations of the geomagnetic field, *J. Geophys. Res.*, 70, 4117, 1965.
- Shea, M. A., and D. F. Smart, World wide trajectory-derived vertical cutoff rigidities and their application to experimental measurements, *J. Geophys. Res.*, 72, 2021, 1967.
- Shea, M. A., D. F. Smart, and John R. McCall, A five degree by fifteen degree world grid of trajectory-determined vertical cutoff rigidities, *Can. J. Phys.*, 46, S1098, 1968.
- Shea, M. A., and D. F. Smart, Secular variations in cosmic ray cutoff rigidities, *J. Geophys. Res.*, 75, 3921, 1970a.
- Shea, M. A., and D. F. Smart, On the application of trajectory derived cutoff rigidities to cosmic-ray intensity variations, *Acta Physica Academiae Scientiarum Hungaricae*, 29, Suppl. 2, 533, 1970b.
- Singer, S. F., A new model of magnetic storms and aurorae, *Trans. AGU*, 38, 175, 1957.
- Skorka, S., Breiteneffekt der nukleonen-mesonenkomponente der ultrastrahlung in meereshöhe im Indischen und Atlantischen Ozean, *Z. Phys.*, 151, 630, 1958.
- Smart, D. F., and M. A. Shea, A study of the effectiveness of the McIlwain coordinates in estimating cosmic ray vertical cutoff rigidities, *J. Geophys. Res.*, 72, 3447, 1967.
- Smart, D. F., M. A. Shea, and R. Gall, The daily variation of trajectory-derived high-latitude cutoff rigidities in a model magnetosphere, *J. Geophys. Res.*, 74, 4731, 1969.
- Smith, E. J., P. J. Coleman, D. L. Judge, and C. P. Sonett, Characteristics of the extraterrestrial current system: Explorer VI and Pioneer V, *J. Geophys. Res.*, 65, 1858, 1960.
- Steljes, J. F., *Cosmic Ray N. M.-64 Neutron Monitor Data IV*, Atom. Eng. Can. Ltd. Rept. #2663, Chalk River, Ontario, 1966.

- Steljes, J. F., *Cosmic Ray N. M.-64 Neutron Monitor Data XX*, Atom. Eng. Can. Ltd. Rept. # 4148, Chalk River, Ontario, 1972.
- Stone, E. C., Local time dependence of non-Störmer cutoff for 1.5 MeV protons in quiet geomagnetic field, *J. Geophys. Res.*, 69, 3577, 1964.
- Störmer, C., *Über die probleme des polar lichtetes*, *Ergebn. kosm. Phys.*, Leipzig, 1, 22, 1931.
- Störmer, C., *The Polar Aurora*, Oxford University Press, London, 1955.
- Sugiura, M. and S. Hendricks, *Provisional Hourly Values of Equatorial D_{st} for 1961, 1962, and 1963*, Tech. Note NASA TN D-4047, Nat. Aero. Sp. Adm., Washington, D. C., 1967.
- Sugiura, M. and D. J. Poros, *Hourly Values of Equatorial D_{st} for the Years 1957 to 1970*, Tech. Rept. No. X-645-71-278, Goddard Space Flight Center, Greenbelt, Md. 1971.
- Teegarden, B. J., Atmospheric secondary and re-entrant albedo protons, *J. Geophys. Res.*, 72, 4857, 1967.
- Waddington, C. J., Observations on the multiply charged particles of the cosmic radiation, *Phil. Mag.*, 1, 105, 1956.
- Webber, W. R., and J. F. Ormes, Cerenkov scintillation counter measurements relating to the isotopic composition of helium nuclei in the primary cosmic radiation, *Phys. Rev.*, 138, B416, 1965.
- Webber, W. R., Diurnal variation of the intensity and energy spectrum of low-energy electrons incident at Fort Churchill, Canada, *J. Geophys. Res.*, 73, 4905, 1968.
- Williams, D. J., and G. M. Mead, Nightside magnetosphere configuration as obtained from trapped electrons at 1100 kilometers, *J. Geophys. Res.*, 70, 3017, 1965.
- Winckler, J. R., P. D. Bhavsar, and L. Peterson, The time variations of solar cosmic rays during July 1959 at Minneapolis, *J. Geophys. Res.*, 66, 995, 1961.
- Barkas, W. H., and M. J. Berger, *Tables of Energy Losses and Ranges of Heavy Charged Particles*, National Aeronautics and Space Administration, SP-3013, Washington, D. C., 1964.
- Camerini, U., P. H. Fowler, W. O. Lock, and H. Muirhead, Nuclear transmutations produced by cosmic ray particles of great energy. Part IV. The distribution in energy, and the secondary interactions of the particles emitted from stars, *Phil. Mag.*, 41, 413, 1950.

Fichtel, C. E., D. E. Guss, G. R. Stevenson, and C. J. Waddington, Cosmic-ray hydrogen and helium nuclei during a solar quiet time, *Phys. Rev.*, 133, B818, 1964.

Powell, C. F., P. H. Fowler, D. H. Perkins, *The Study of Elementary Particles by the Photographic Method*, Pergamon Press, New York, 1959.

TABLE I - IONIZATION DEPTHS IN THE DETECTOR

POSITION	STANDARD CONFIGURATION				MODIFIED CONFIGURATION-SIOUX FALLS 1967			
	DEPTH (gms/cm ² Pb Equiv.)	P or He ENERGY* (MeV/NUCLEON)	P RIGIDITY (MV)	He RIGIDITY (MV)	DEPTH (gms/cm ² Pb Equiv.)	P or He ENERGY* (MeV/NUCLEON)	P RIGIDITY (MV)	He RIGIDITY (MV)
Tray 4 (Center)	8.27	66.4	359	718	8.27	66.1	358	716
Calorimeter Plate 1	18.05	106.3	459	916	18.05	105.8	458	914
Tray 5 (Center)	20.42	114.5	477	953	20.42	114.0	476	951
Tray 6	29.62	143.2	538	1073	37.22	163.7	578	1152
Tray 7	41.96	176.7	602	1201	57.16	212.0	665	1326
Tray 8	51.16	199.1	643	1282	73.96	247.6	725	1445
Tray 9	63.50	226.8	691	1376	93.90	286.0	786	1566
Tray 10	76.52	253.8	735	1465	114.52	322.3	842	1676

* Includes effect of inclined trajectories.

TABLE II - SUMMARY OF FLIGHT DATA

Flight	Location	Launch Date	Time*	Ceiling	End of Data	Altitude (millibars)	CEILING DATA		Exposure (m ² sec-ster)	Deep River Neutron Monitor
							Total No. [†] of Triggering Events	Total No. ^{††} of Clean Triggers		
1036	Churchill	8/2/65	1234	1430	1730	6.3	7,765	3,260	1.02	6999
1037	Churchill	8/7/65	1130	1320	1730	6.5	16,477	8,005	2.53	7014
1038	Minneapolis	9/8/65	1210	1350	2251	8.0	38,612	17,037	6.66	7042
1171	Churchill	7/26/66	0941	1230	0220	6.5	55,066	24,495	8.16	6872
					7/27/71					
1178	Churchill	8/6/68	0928	1200	2200	6.3	17,942	7,412	2.56	6874
1056	Minneapolis	8/27/66	1200	1540	2140	8.2	32,962	13,358	5.32	6887
1057	Minneapolis	8/30/66	0022	0215	2340	9.0	116,386	48,767	19.74	6840-6600
1208	Churchill	7/31/67	1007	1300	0046	3.4	128,501	50,569	21.72	6572
					8/1/67					
974	Sioux Falls	9/14/67	1334	1620	1905	3.3	215,727	73,325	34.69	6614
					9/15/67					
975	Sioux Falls	9/21/67	2356	0215	2332	4.0	168,429	55,247	27.56	6536
				9/22/67	9/22/67					
1236	Churchill	7/18/68	0120	0530	1818	2.5	128,415	41,852	22.92	6414
1244	Churchill	7/23/68	2007	0030	1321	2.0	135,876	43,641	23.31	6462
				7/24/68						
1078	Minneapolis	9/5/68	1204	1440	1805	5.0	34,731	11,773	6.79	6324
1079	Minneapolis	9/10/68	1137	1430	2251	4.6	307,443	94,903	59.17	6416
1273	Churchill	7/11/69	2048	2246	1604	4.7	165,002	52,358	34.41	6174
				7/12/69						
1274	Churchill	7/18/69	0500	0730	0141	4.7	147,265	46,941	30.25	6225
				7/19/69						
1293	Churchill	7/7/70	0658	0925	1900	4.1	96,026	29,828	20.19	6183
1297	Churchill	7/18/70	2040	0125	1723	3.1	156,386	47,434	33.01	6287
				7/19/70	7/19/70					
1308	Churchill	7/18/71	0645	1005	0130	3.5	129,062	45,755	19.45	6844
				7/19/71						
1316	Churchill	7/21/71	1013	1302	0210	3.0	107,967	37,627	16.78	6749
				7/22/71						

* All times are Universal Time.

[†] This includes only the events received without bit errors.

^{††} Clean triggers are defined as events in which one and only one tube was fired in trays 1-4. The analysis was limited to this class of events.

TABLE III
RE-ENTRANT ALBEDO SCALE FACTORS[†]

P_c (GV)	ENERGY (MeV)	MAGNETIC FIELD ZENITH ANGLE- δ	ESCAPE FACTOR (Fraction of Vertical Flux)		SPECTRAL DEPENDENT FACTOR ^{††}	
			MODEL #1	MODEL #2	SOLAR MIN. (DRNM=7030)	SOLAR MAX. (DRNM=6210)
<.02 (Churchill)	-	-	-	-	1.183	0.754
1.0	435	16.1°	0.279	0.141	1.126	0.738
1.36 (Minneapolis)	720	17.8°	0.277	0.152	1.067	0.714
1.5	834	18.4°	0.277	0.155	1.045	0.704
2.0	1275	20.3°	0.275	0.165	0.978	0.671
2.5	1737	22.1°	0.274	0.175	0.926	0.644

[†]The product of the escape factor and the spectral dependent factor times the equilibrium secondary proton spectrum gives the albedo spectrum.

^{††}Includes the effects of solar modulation and geomagnetic cutoff. Normalized to 1.00 for Churchill flux when Deep River Neutron Monitor = 6700.

TABLE IV

TABULATION OF OBSERVED CUTOFF RIGIDITIES

Flight	Interval	Observed P_m (GV)	Observed P_c (GV)	Latitude (geographic)	Longitude	Calculated P_c^\dagger (GV)	ΔP (GV)	Dst
1038-W	- -	1.36 \pm .04	1.278 \pm .010	45.08°N	93.57°W	1.351 \pm .010	0.095	+ 9
1056-W	- -	1.37 \pm .04	1.302 \pm .020	44.72°N	92.5° W	1.380 \pm .012	0.117	+20
974-N	1620-2100Z	1.35 \pm .05	1.227 \pm .040	44.26°N	96.0° W	1.547 \pm .014	0.240	-10
"	2100-0200Z	1.21 \pm .08	1.072 \pm .034	44.9° N	95.5° W	1.428 \pm .035	0.180	- 4
"	0200-1200Z	1.13 \pm .04	0.980 \pm .035	45.22°N	94.0° W	1.340 \pm .008	0.230	+ 6.6
"	1400-1900Z	1.12 \pm .05	0.957 \pm .053	45.92°N	92.0° W	1.195 \pm .047	0.180	+ 7.2
975-N	0215-0700Z	1.63 \pm .10	1.389 \pm .044	42.5° N	96.2° W	1.869 \pm .015 - .057	0.310	-36.8
"	0700-1100Z	1.60 \pm .12	1.386 \pm .049	43.03°N	96.8° W	1.790 \pm .046	0.250	-18.3
"	1100-1800Z	1.39 \pm .05	1.244 \pm .022	43.8° N	96.5° W	1.641 \pm .010	0.175	-13.7
"	1800-2330Z	1.15 \pm .04	1.121 \pm .039	44.46°N	96.1° W	1.516 \pm .049	0.110	-19.6
1078-W	- -	1.29 \pm .08	1.123 \pm .033	45.86°N	91.5° W	1.193 \pm .034	0.160	+ 4
1079-W	1430-1900Z	1.34 \pm .03	1.326 \pm .019	44.18°N	93.5° W	1.490 \pm .016	0.073	-12.2
"	1900-0000Z	1.44 \pm .06	1.366 \pm .022	44.0° N	95.0° W	1.561 \pm .068 - .022	0.133	- 4.6
"	0000-0800Z	1.44 \pm .05	1.391 \pm .016	43.19°N	96.0° W	1.734 \pm .036	0.088	-15.4
"	0800-1400Z	1.49 \pm .10	<<1.71	42.60°N	96.6° W	1.843 \pm .017	0.085	- 8.2
"	1400-1900Z	1.51 \pm .05	$P_c < 1.69$	42.14°N	97.5° W	1.987 \pm .020	- -	- 3.8
"	1900-2245Z	1.51 \pm .05	$P_c < 1.71$	42.6° N	98.0° W	1.915 \pm .029	- -	+ 1.0

[†]Calculated from Shea et al. (1968).

TABLE V
 COEFFICIENTS, A_{ij} , FOR FITTING
 SHEA ET AL. (1968) CUTOFF GRID

i	0	1	2	3
j				
0	-.040990	.234729	.096071	-.021990
1	-.604536	.010975	.017878	- -
2	-.043847	.004013	- -	- -
3	.000177	- -	- -	- -

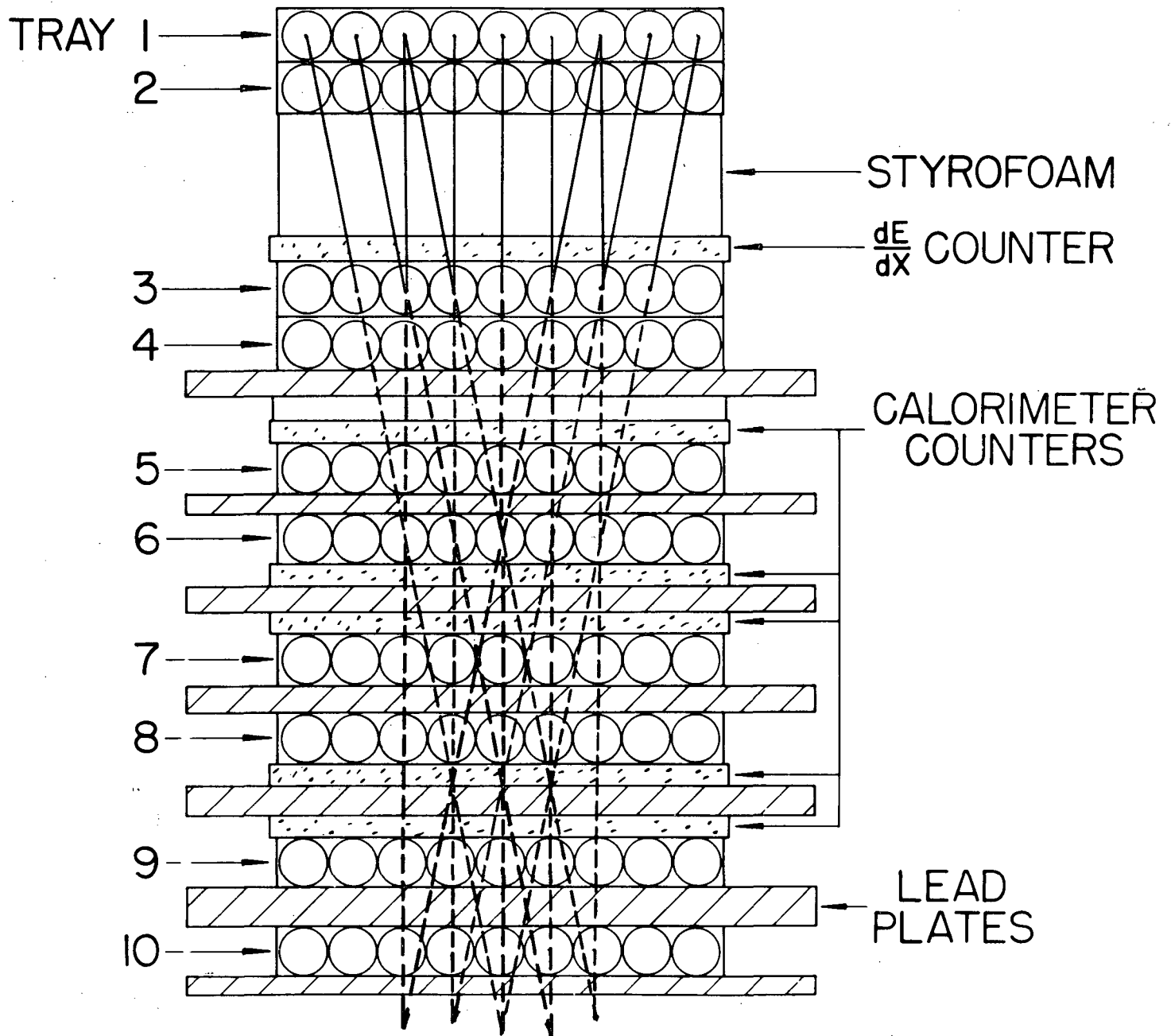


Figure 1. Schematic diagram of the hodoscope identifying its major components and indicating some triggering trajectories. For clarity, end views of all Geiger tubes are shown, but the axes of tubes in odd trays are actually perpendicular to those in even trays.

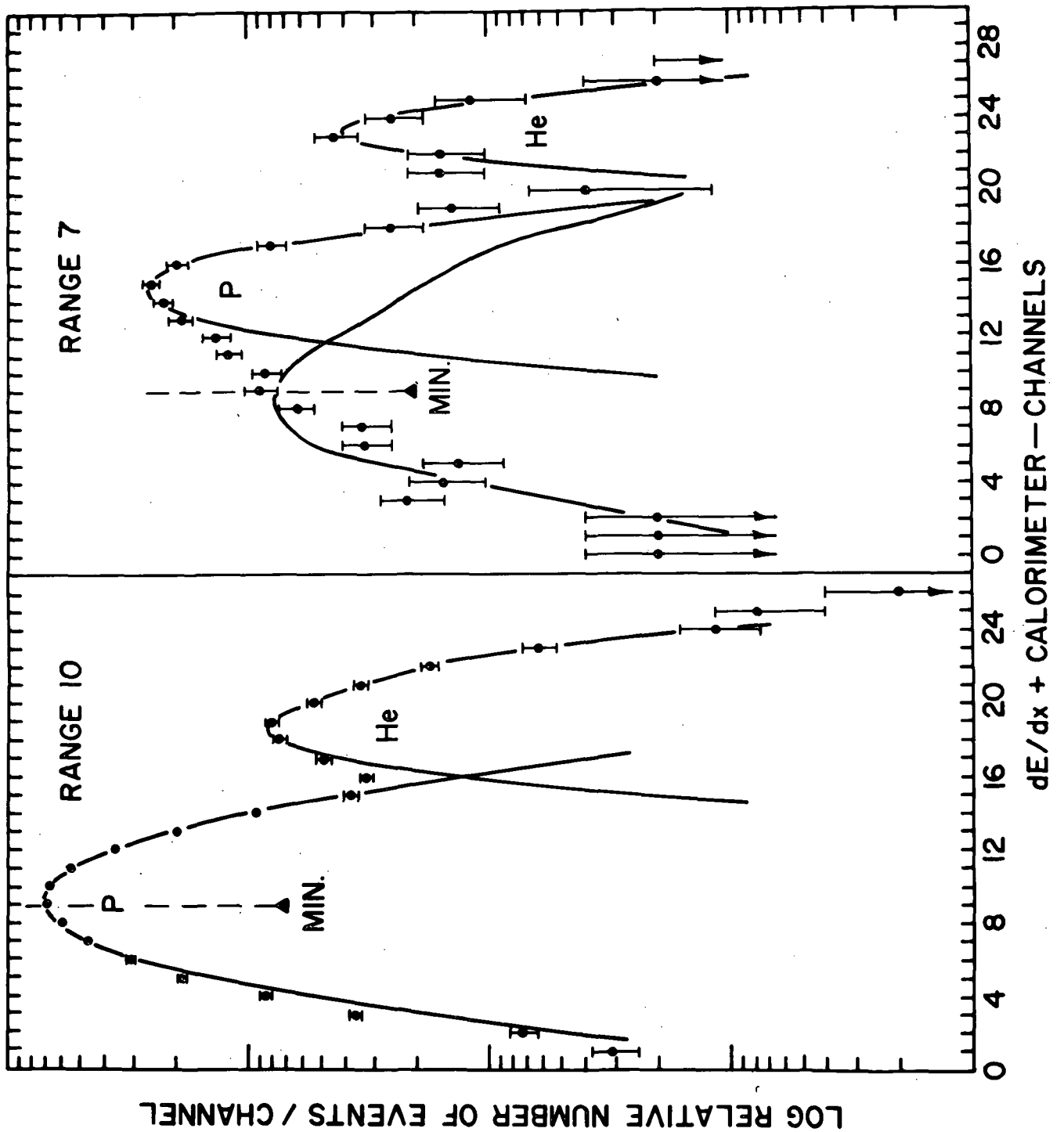


Figure 2. Sample pulse height distributions for events with RANGE=10 (penetrating particles) and RANGE=7 (stopping in the fourth lead plate of Figure 1). The curves are those predicted by folding detector resolution into expected scintillator response.

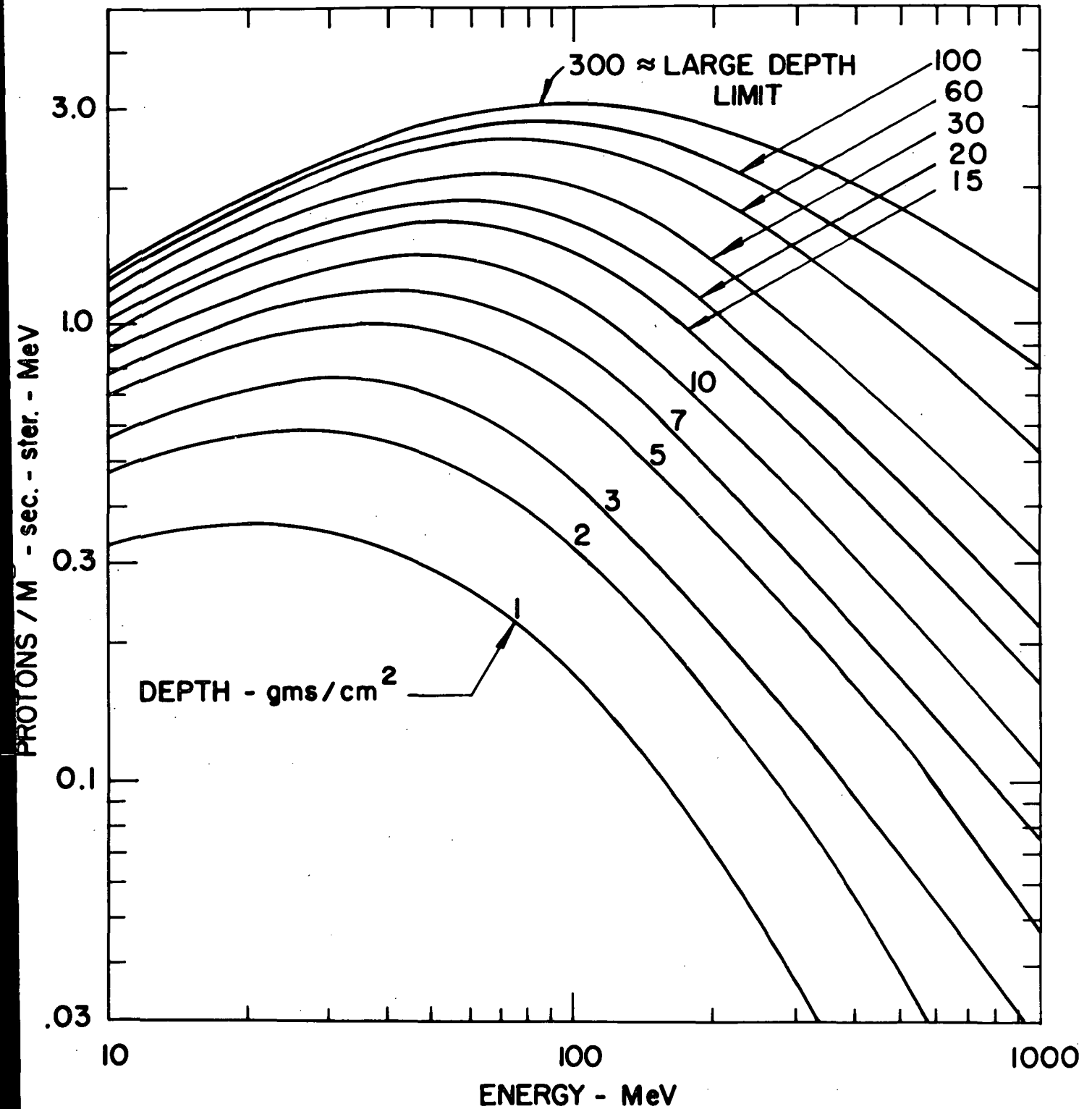


Figure 3. Calculated secondary proton spectra expected at various depths for Deep River neutron rate of 6700.

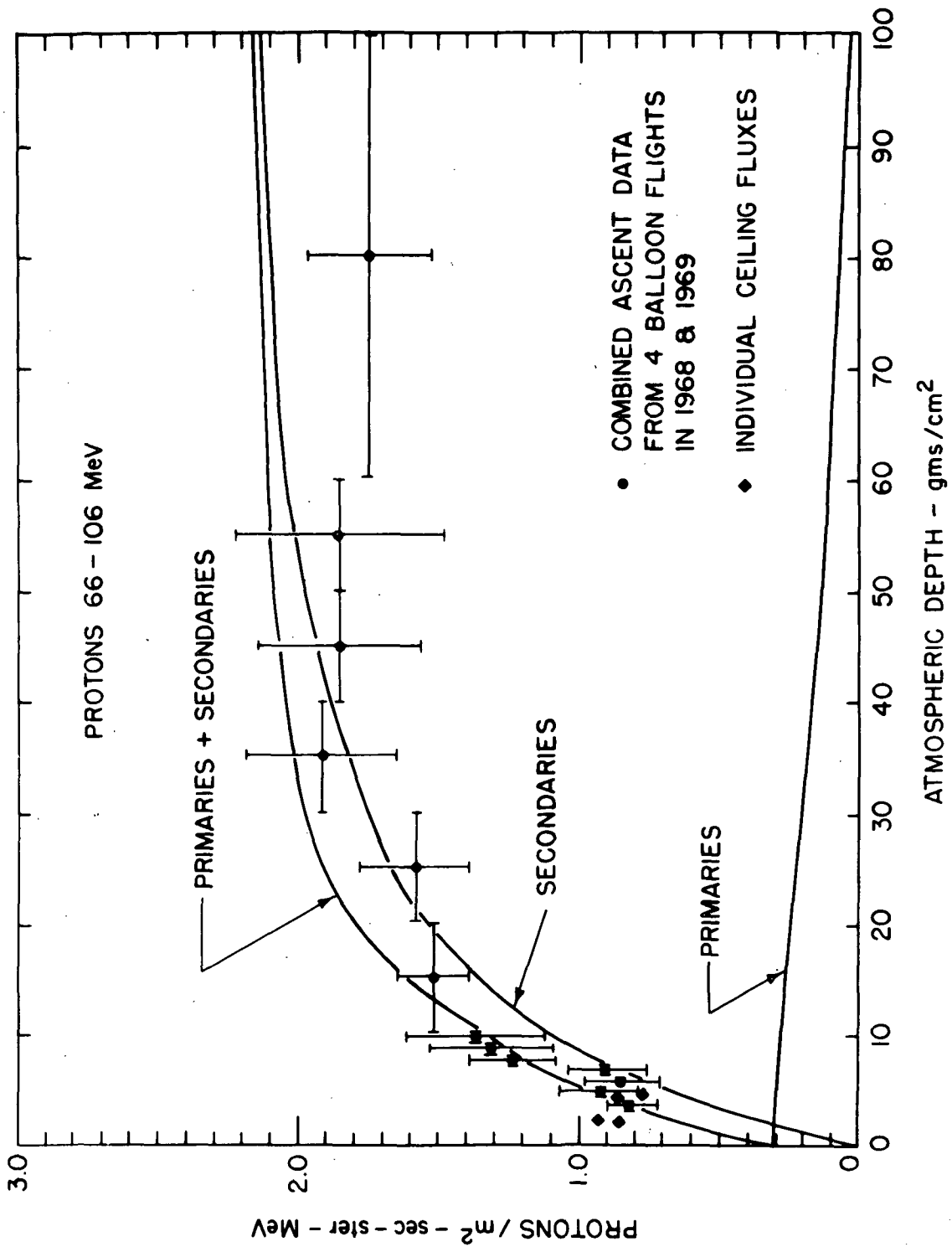


Figure 4. Observations of low energy protons deep in the atmosphere are well represented by the calculated secondaries. Note that the intensity reaches an equilibrium beyond 30 gms/cm².

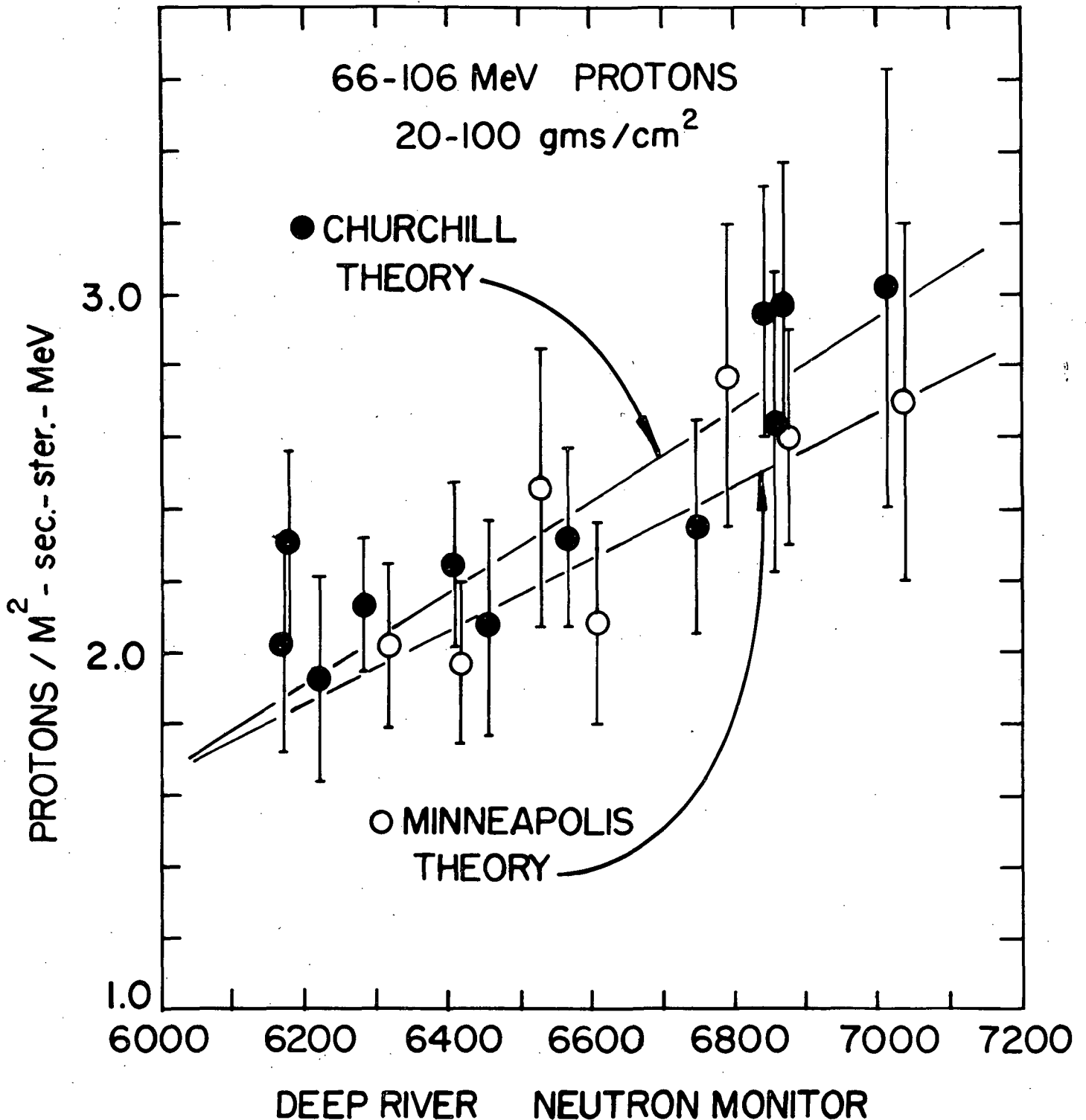


Figure 5. Regression curves₂ of RANGE 4 proton flux averaged over the depth interval 20-100 gms/cm² for individual flights made from Churchill (solid circles) and Minneapolis (open circles) for 3/4 of a solar cycle. Referring to Figure 4 one note that protons in this interval are at an equilibrium level which measures the intensity of atmospheric secondary production. Solid lines show the predicted solar cycle variation of secondary protons at the two locations.

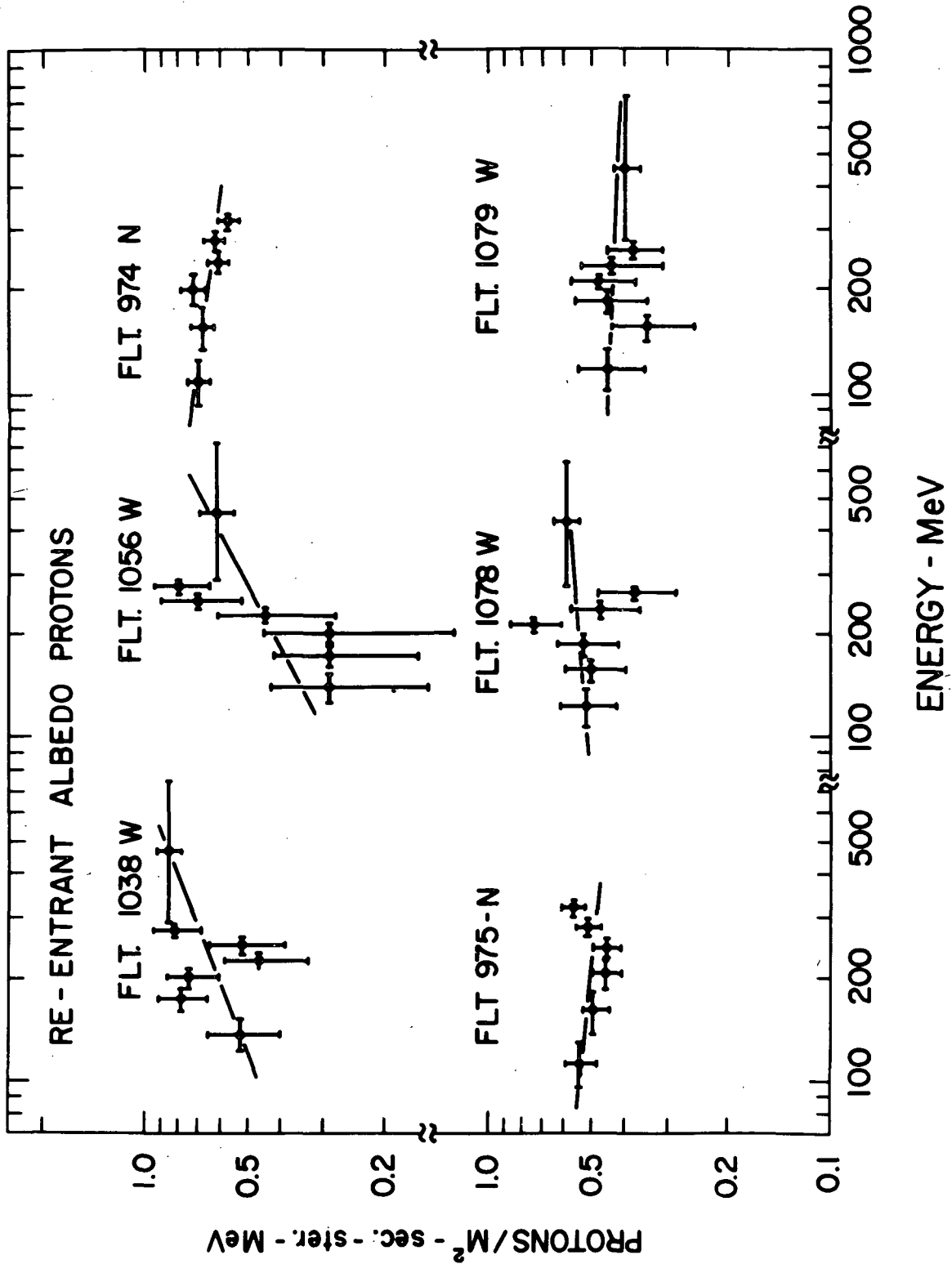


Figure 6. Energy spectra of re-entrant albedo protons corrected to the top of the atmosphere for 6 balloon flights made over the Upper Mid-West area.

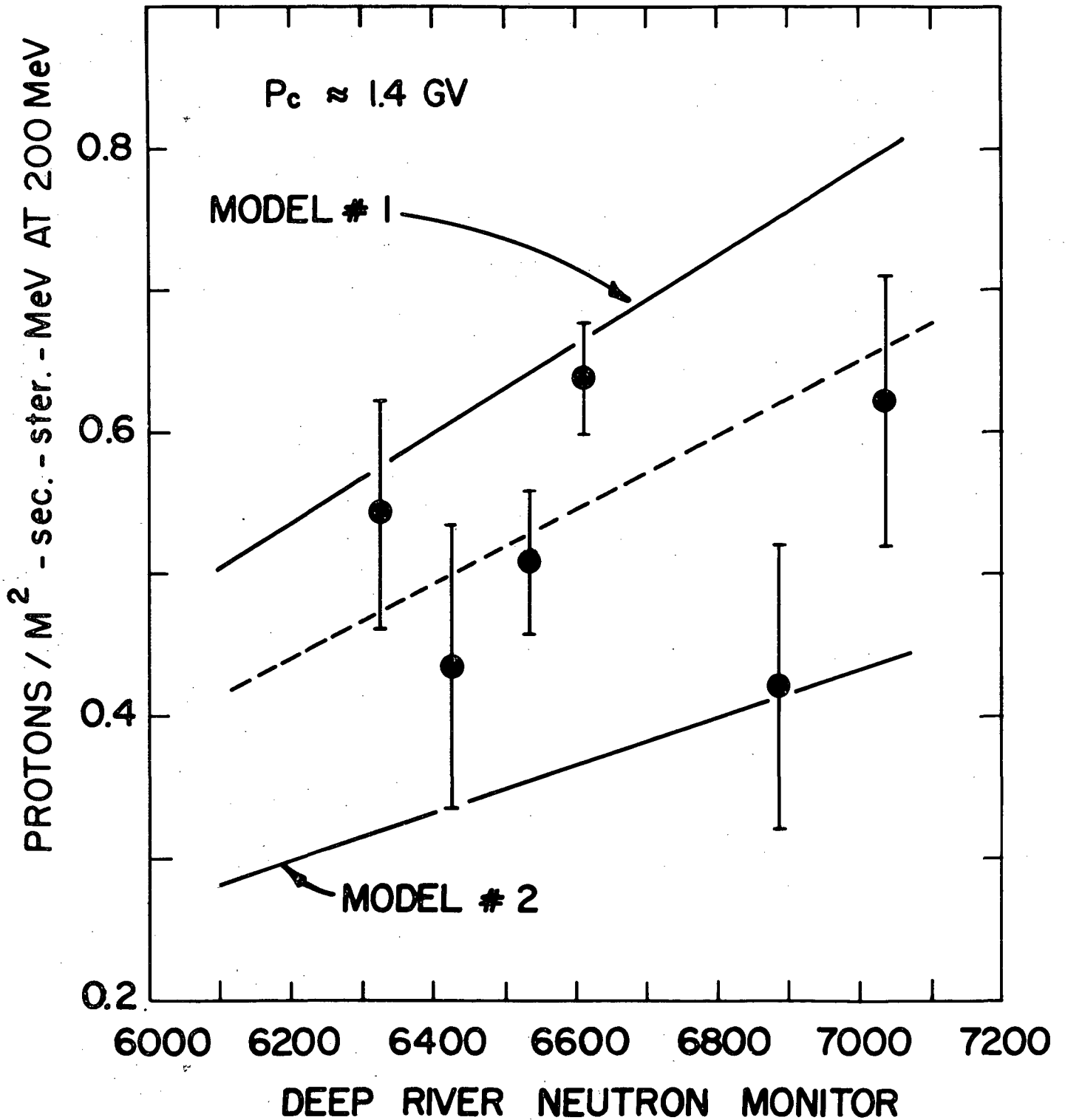


Figure 7. Regression curve of re-entrant albedo proton intensity at 200 MeV spanning most of the solar cycle variation. Solid lines indicate the intensity and solar cycle variation predicted by two models discussed in the text. The dashed line is an attempt to fit the data with a line having the predicted solar variation.

Figure 8a. Schematic representation of albedo particle orbits for particles generated at angles 20° to the horizon in four principal directions. The local magnetic field \vec{B} is shown with a dip angle δ .

Figure 8b. Angular distribution of atmospheric secondary protons assuming isotropic illumination of energetic primaries over the upper hemisphere. As viewed in the meridian plane, the shaded portion represents those particles that can escape and re-enter the atmosphere in the opposite hemisphere. Dashed lines indicate a cone of half angle $\xi + \delta$ tilted to the south at an angle δ . Assuming purely adiabatic motion, particles escaping in this cone can re-enter the atmosphere at the conjugate point with zenith angles $\leq \xi$.

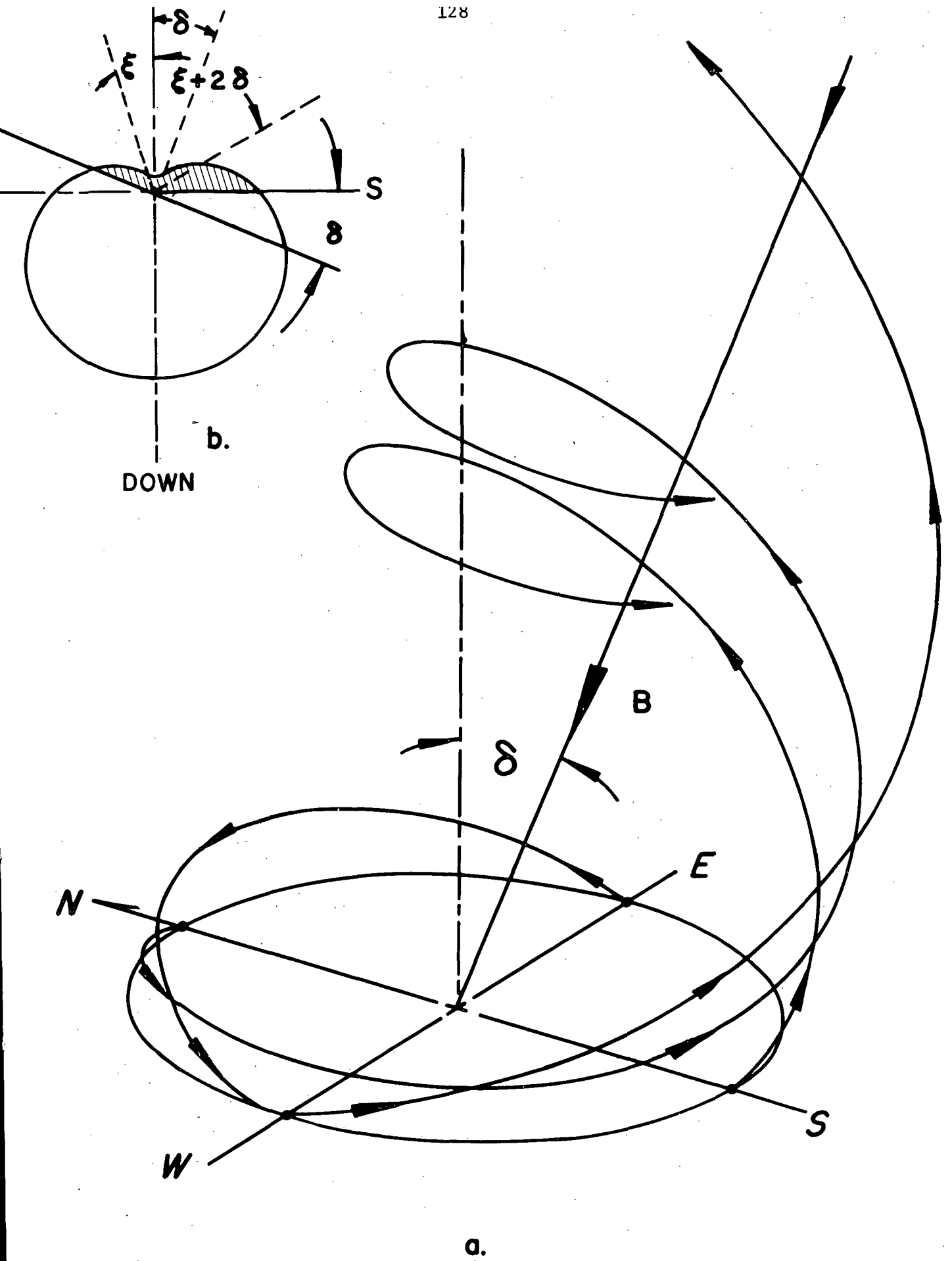


Figure 8.

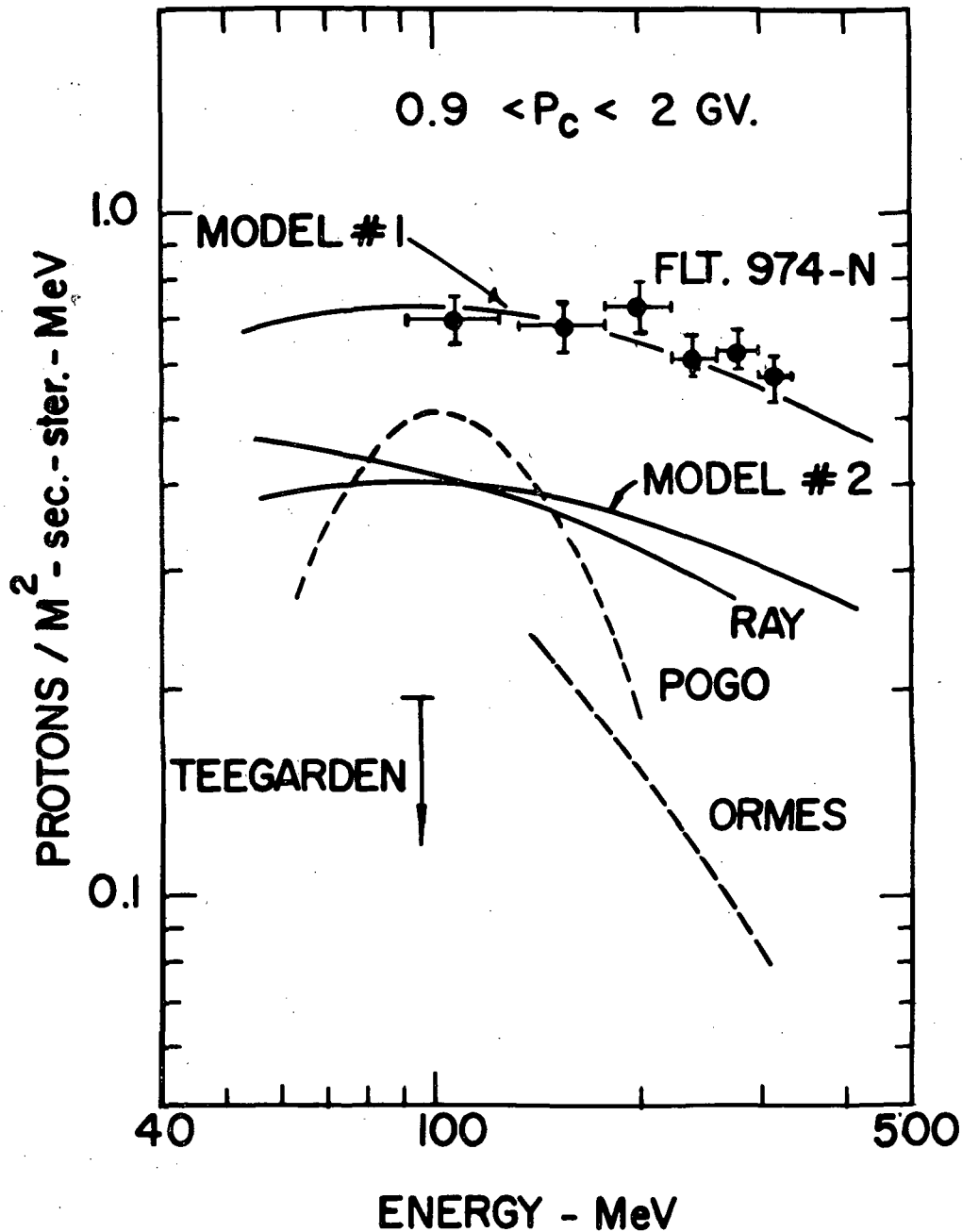


Figure 9. Comparison of measured and calculated albedo spectra deduced at the top of the atmosphere in the Upper Mid-West area. Observations obtained in this work are represented by Flight 974-N. Observations reported by Bingham et al. (1968) on the POGO satellite, Ormes and Webber (1968), and Teegarden (1967) are also shown. Small adjustments of the reported intensities to allow for the effects of solar modulation are described in the text. Solid lines indicate two model calculations discussed in the text as well as the model calculation by Ray (1967).

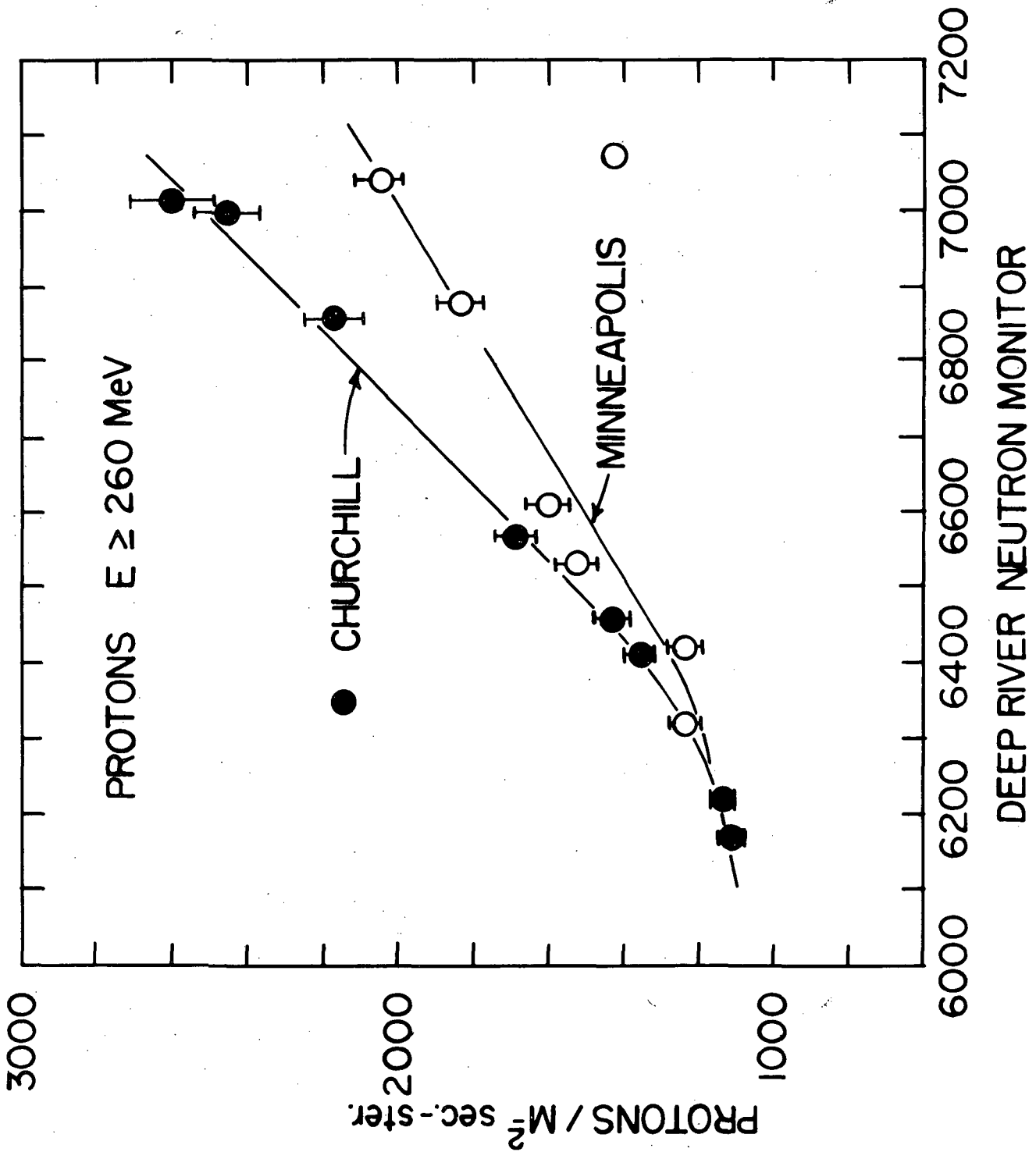


Figure 10. Regression curves of penetrating protons observed at Churchill (solid circles) and Minneapolis (open circles) for the period 1965-1969. The fact that the curves appear to join near solar maximum is used in the text to argue that the albedo and primary fluxes were nearly equal in the energy range 260-720 MeV at that time.

Figure 11. The lower portion is a schematic representation of the penumbral cutoff structure at Sioux Falls, South Dakota calculated by Shea (private communication) indicating the positions of various rigidities used in discussing cutoffs. The upper portion shows the smoothing effect caused by averaging the penumbral structure over a rigidity interval of 100 MV that is typical of the hodoscope. The dashed line indicates the exponential form often used in describing the shape of the cutoff (Earl, 1962).

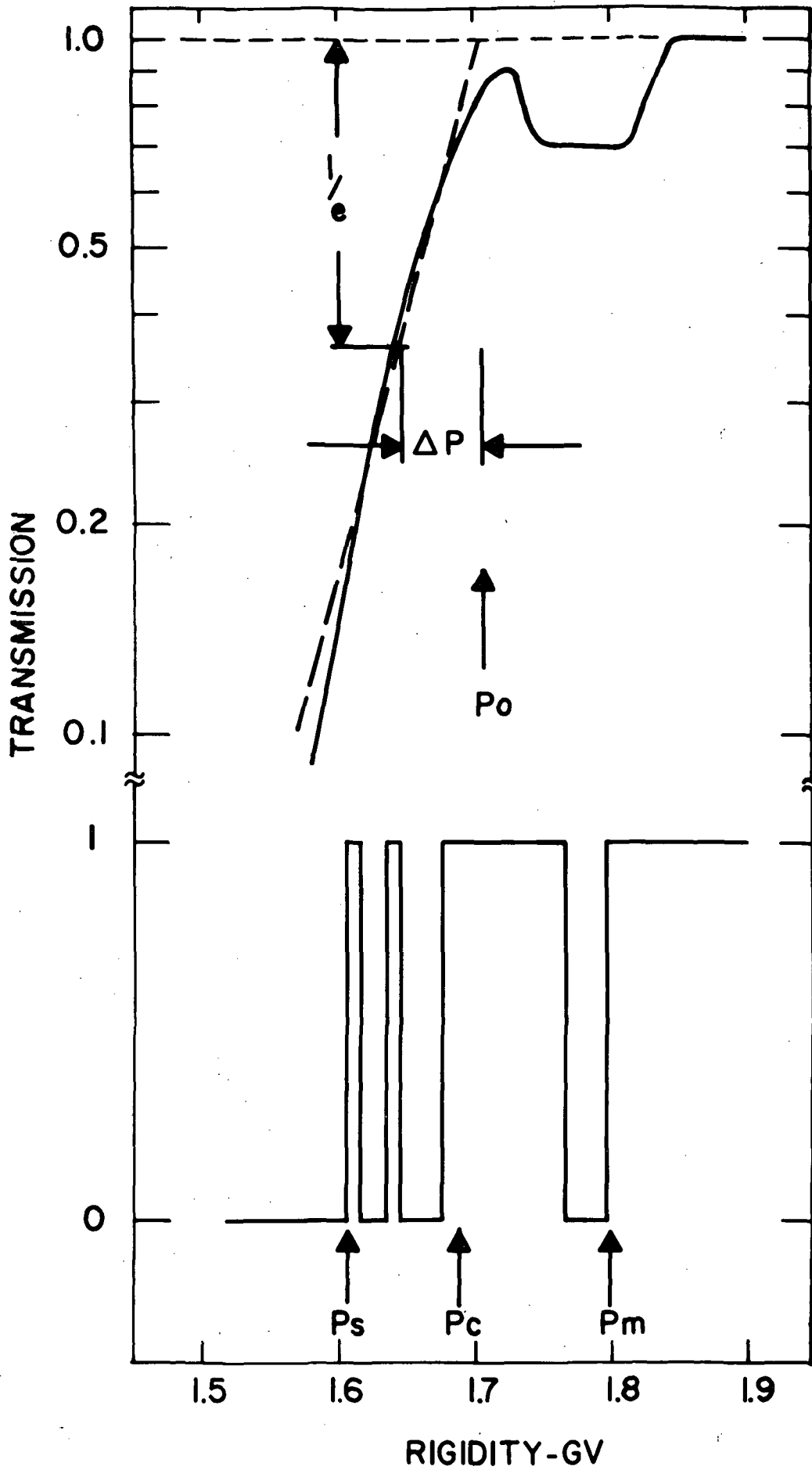


Figure 11

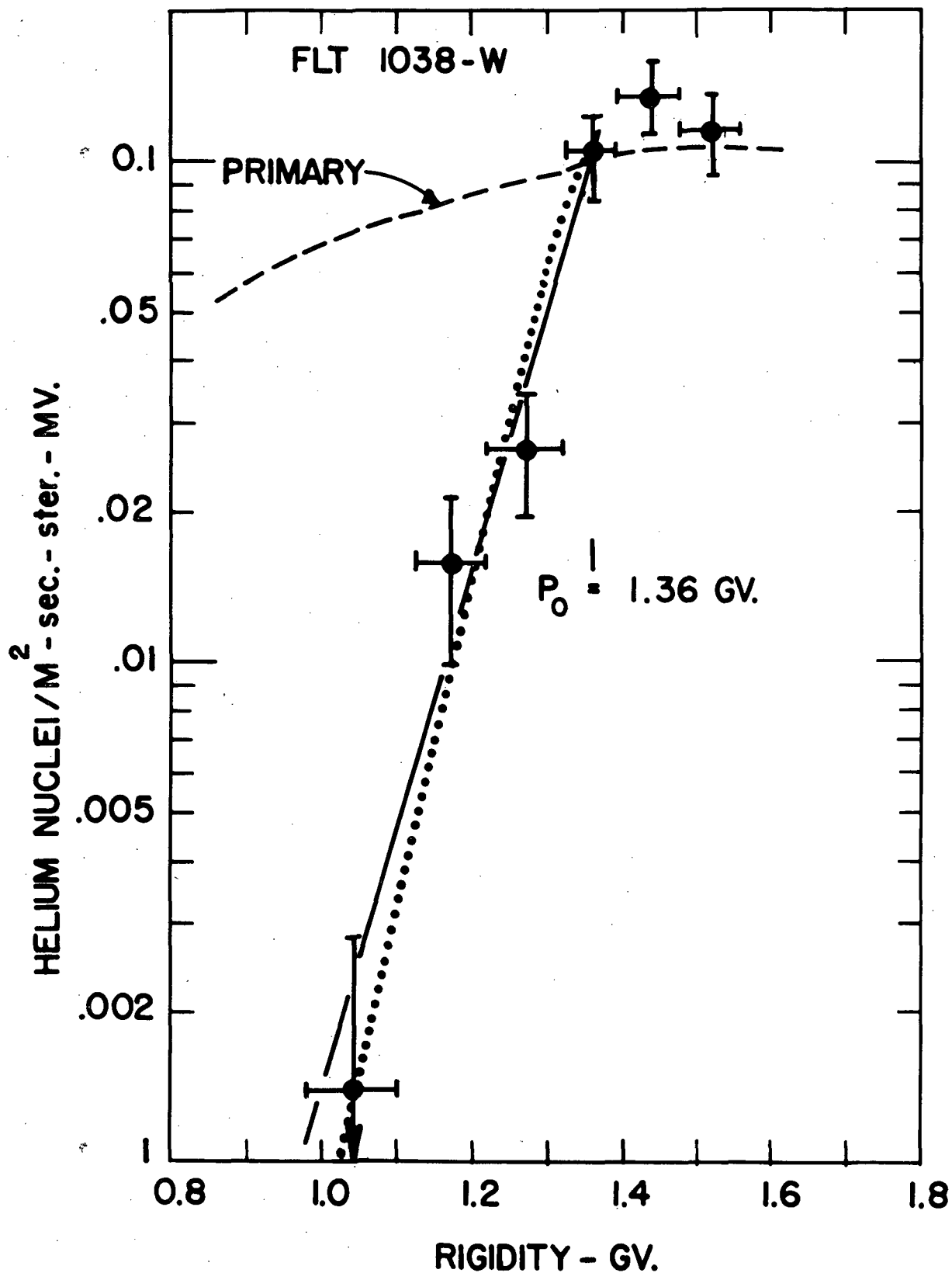


Figure 12. Differential rigidity spectrum of helium nuclei obtained over Minneapolis during Flight 1038-W showing the effect of the geomagnetic cutoff.

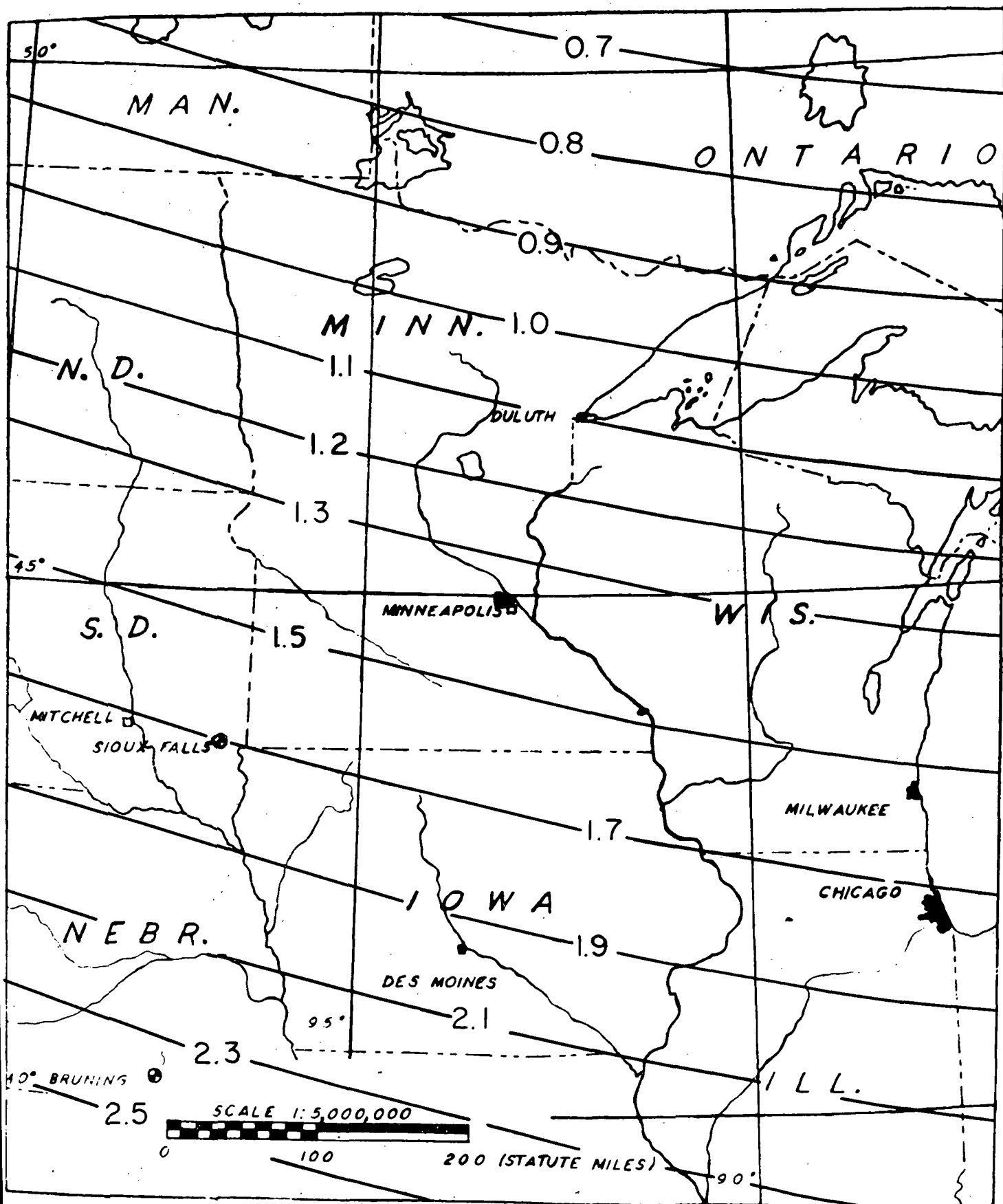


Figure 13 Contours of constant cutoff rigidity over the Upper Mid-West region calculated from Equation V-4 which approximates the cutoff grid calculated by Shea et al. (1968).

Figure 14. Trajectory of Flight 1038-W over St. Paul and Minneapolis, Minnesota.

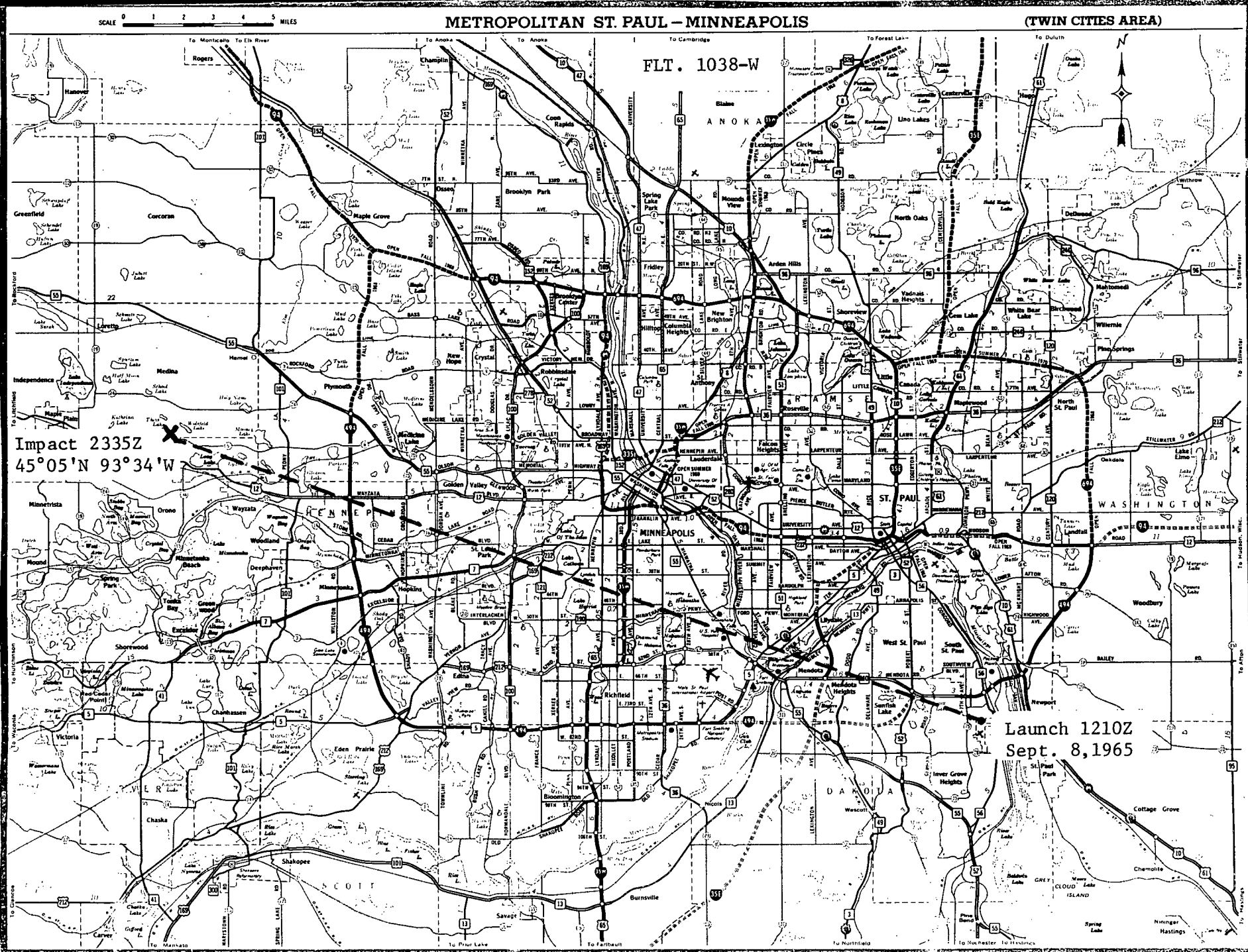
FLT. 1038-W

Impact 2335Z
45°05'N 93°34'W

Launch 1210Z
Sept. 8, 1965

Figure 14

136



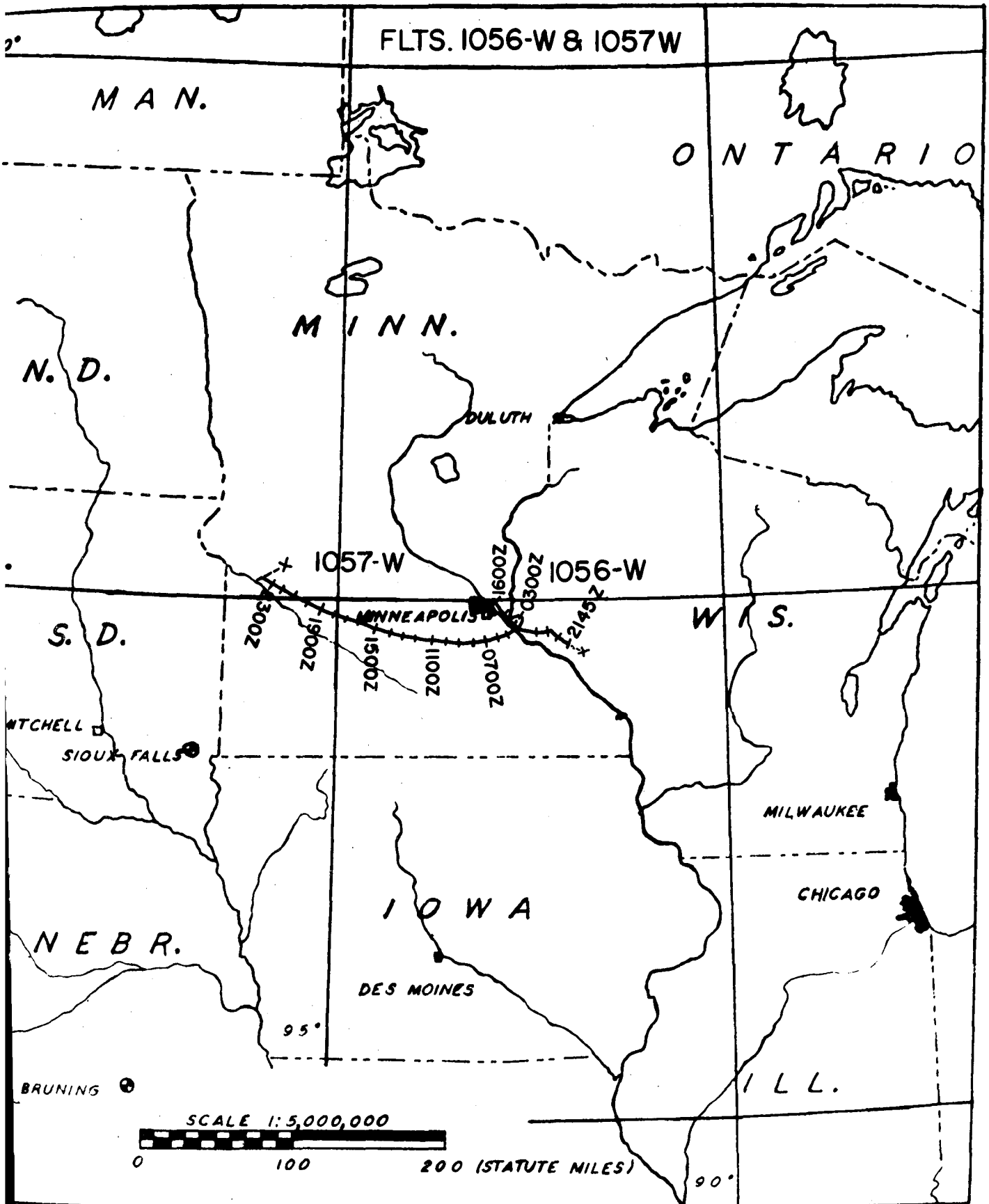


Figure 15. Trajectories of Flights 1056-W and 1057-W launched from Minneapolis, Minnesota.

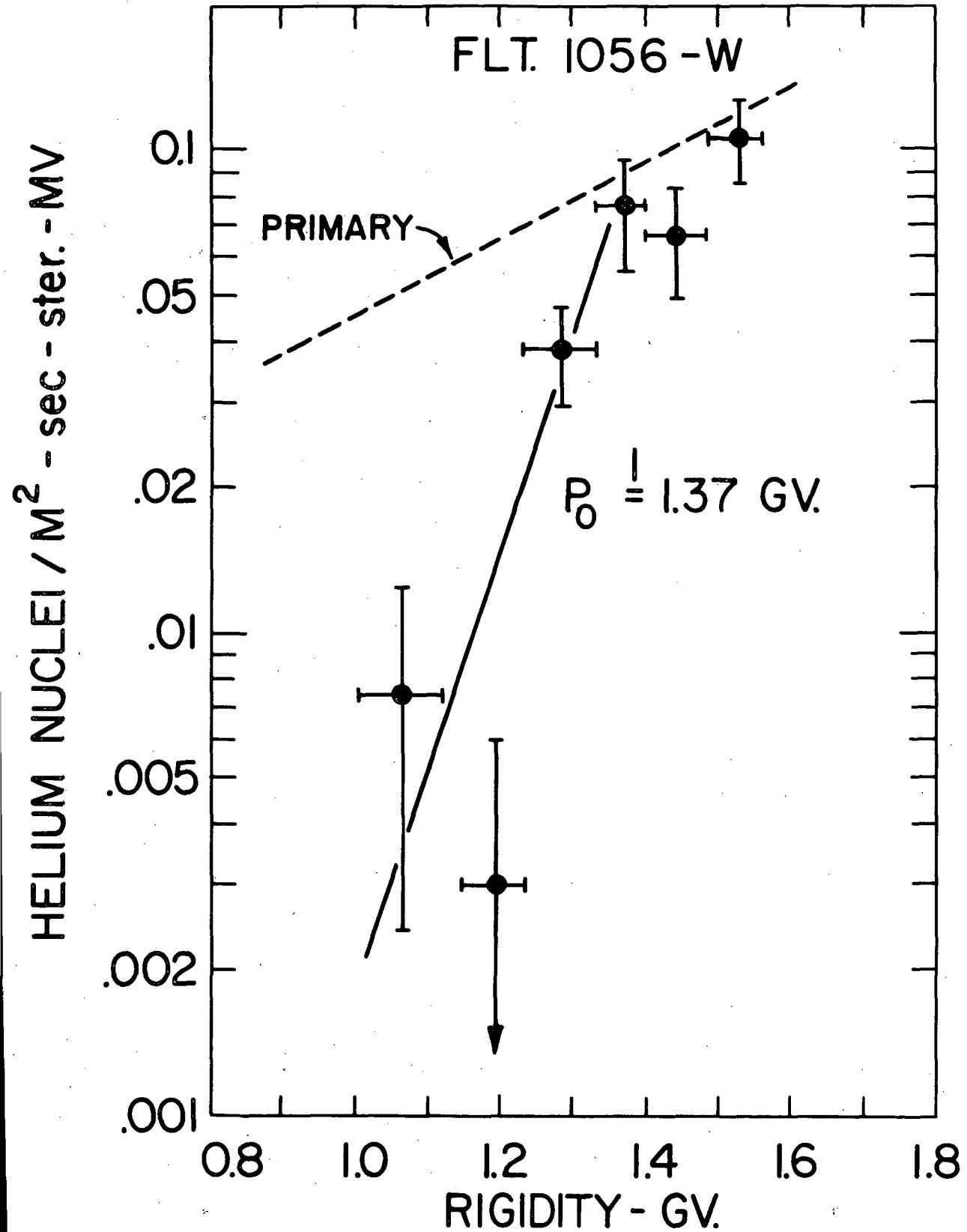


Figure 16. Differential helium rigidity spectrum for Flight 1056-W showing the effect of the geomagnetic cutoff over western Wisconsin.

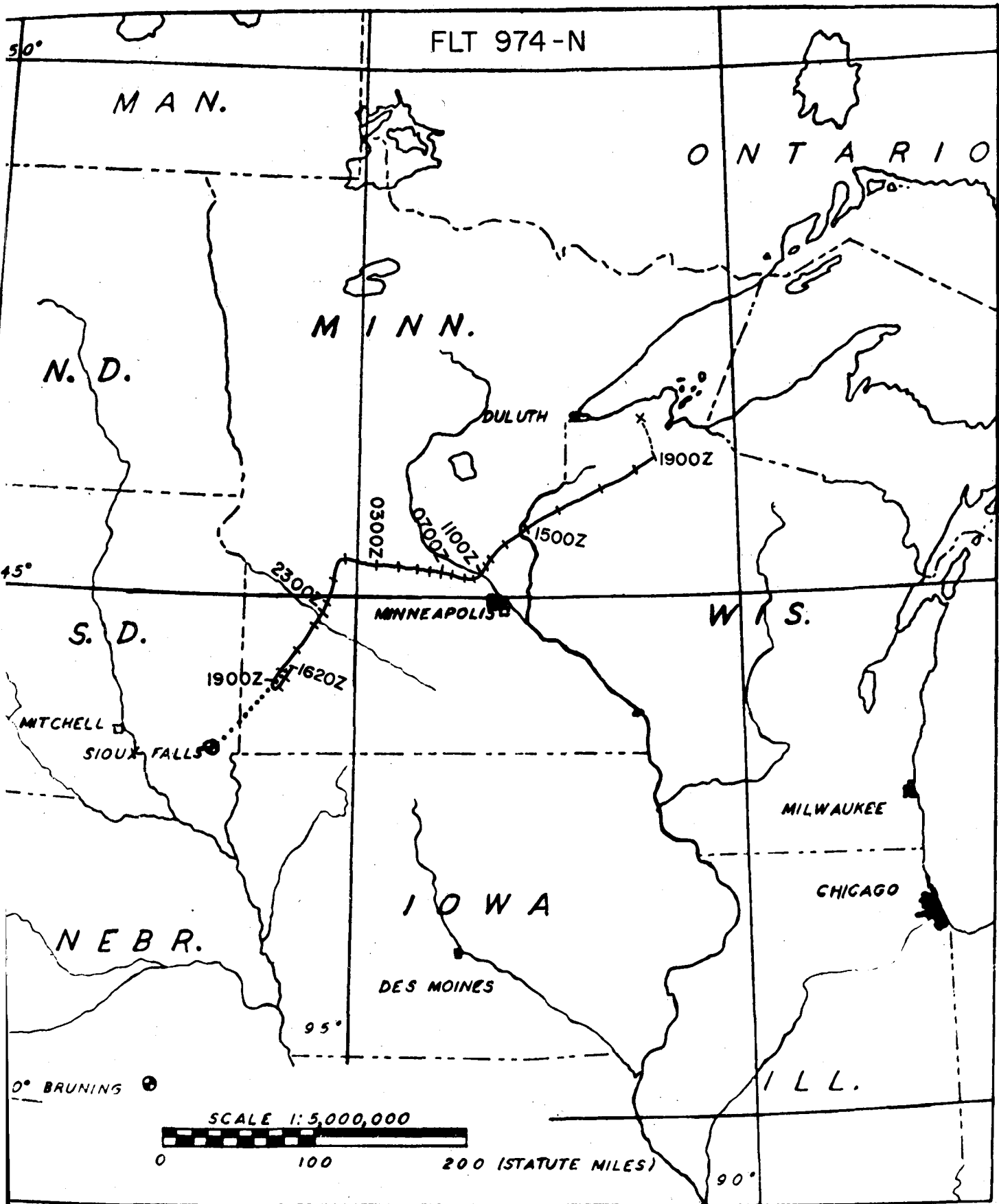


Figure 17. Trajectory of Flight 974-N launched from Sioux Falls, South Dakota.

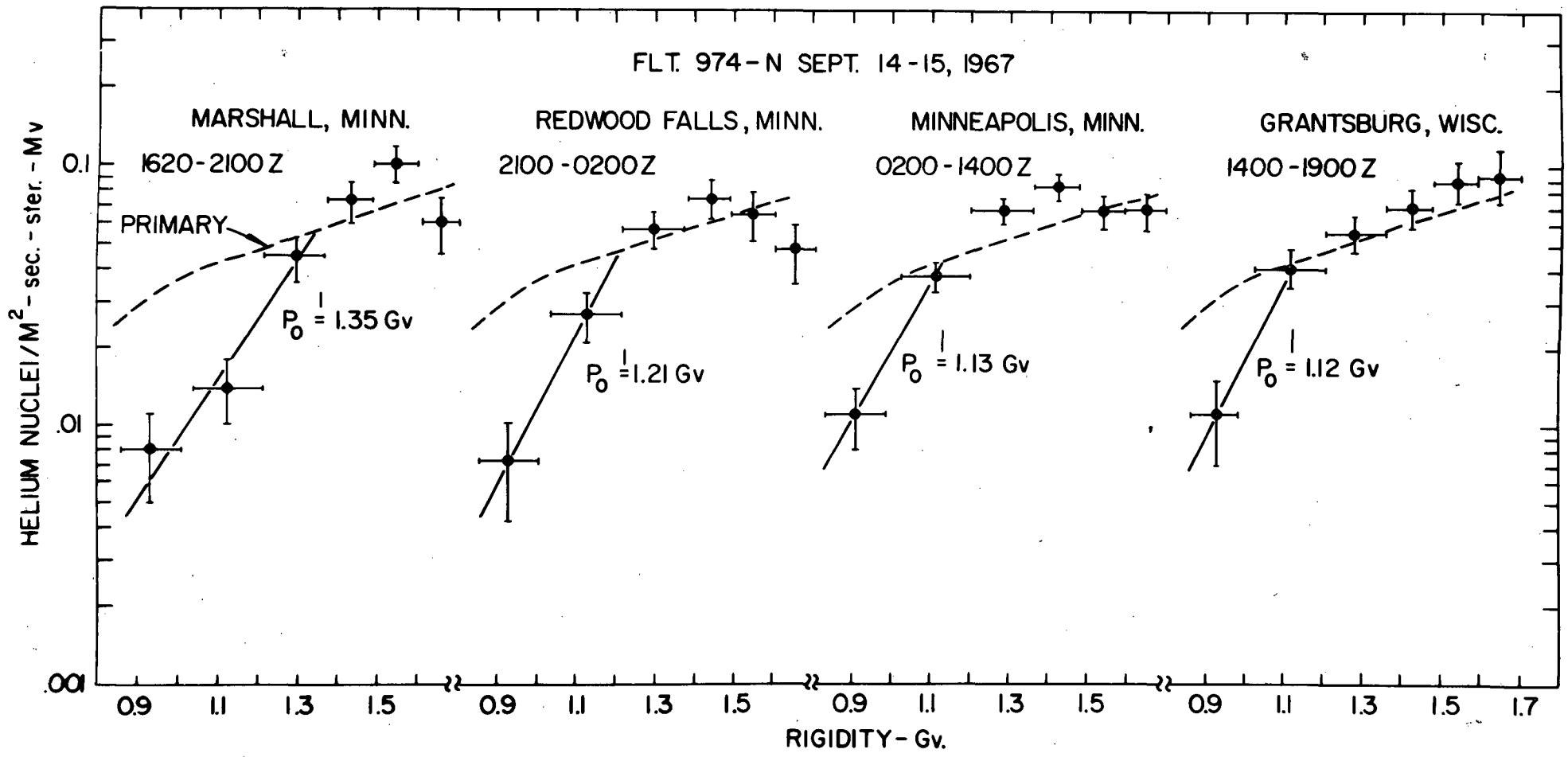


Figure 18. Differential helium rigidity spectra obtained in four sections of Flight 974-N showing the downward progression of the cutoff as the balloon drifted toward the northeast.

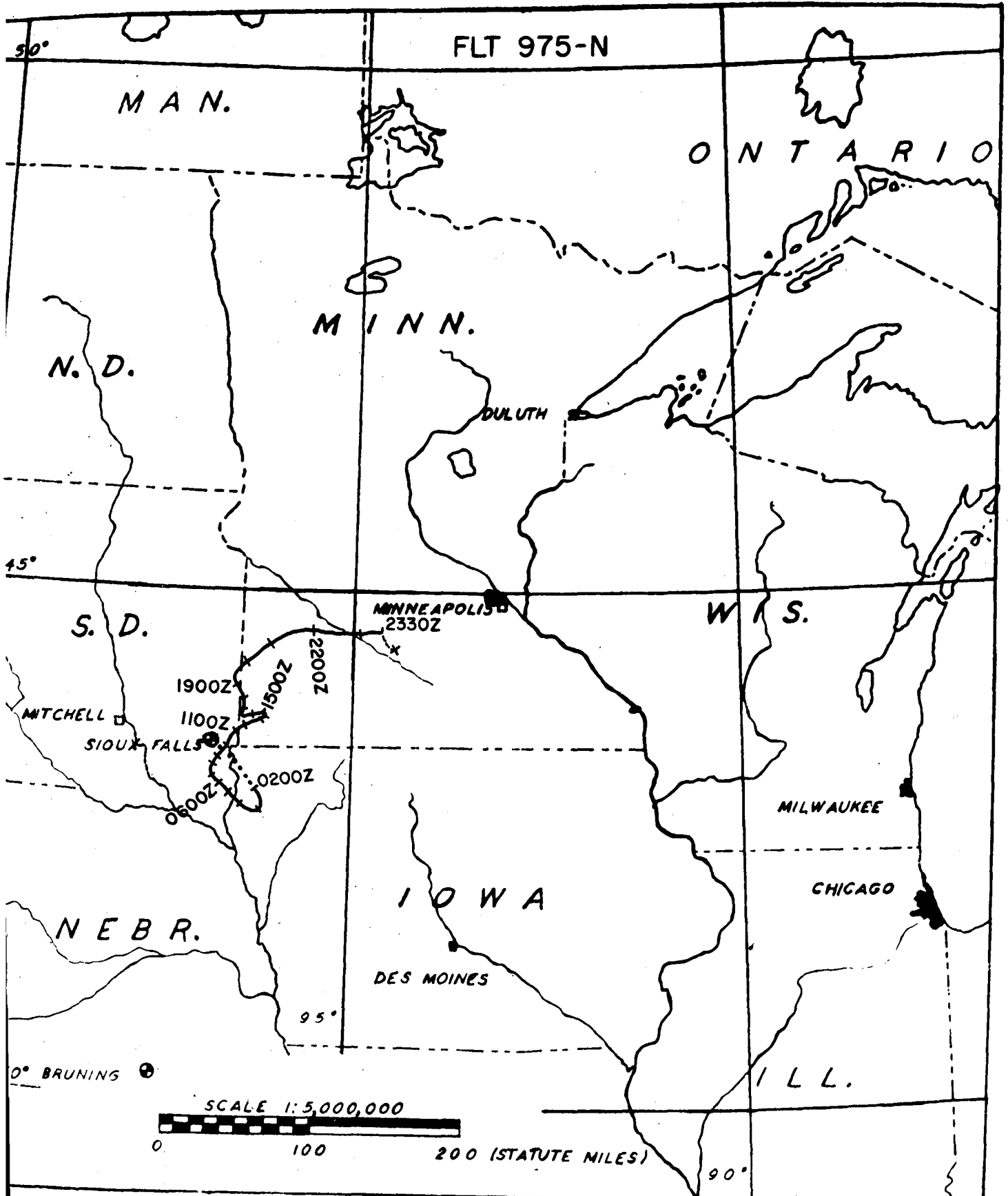


Figure 19. Trajectory of Flight 975-N launched from Sioux Falls, South Dakota.

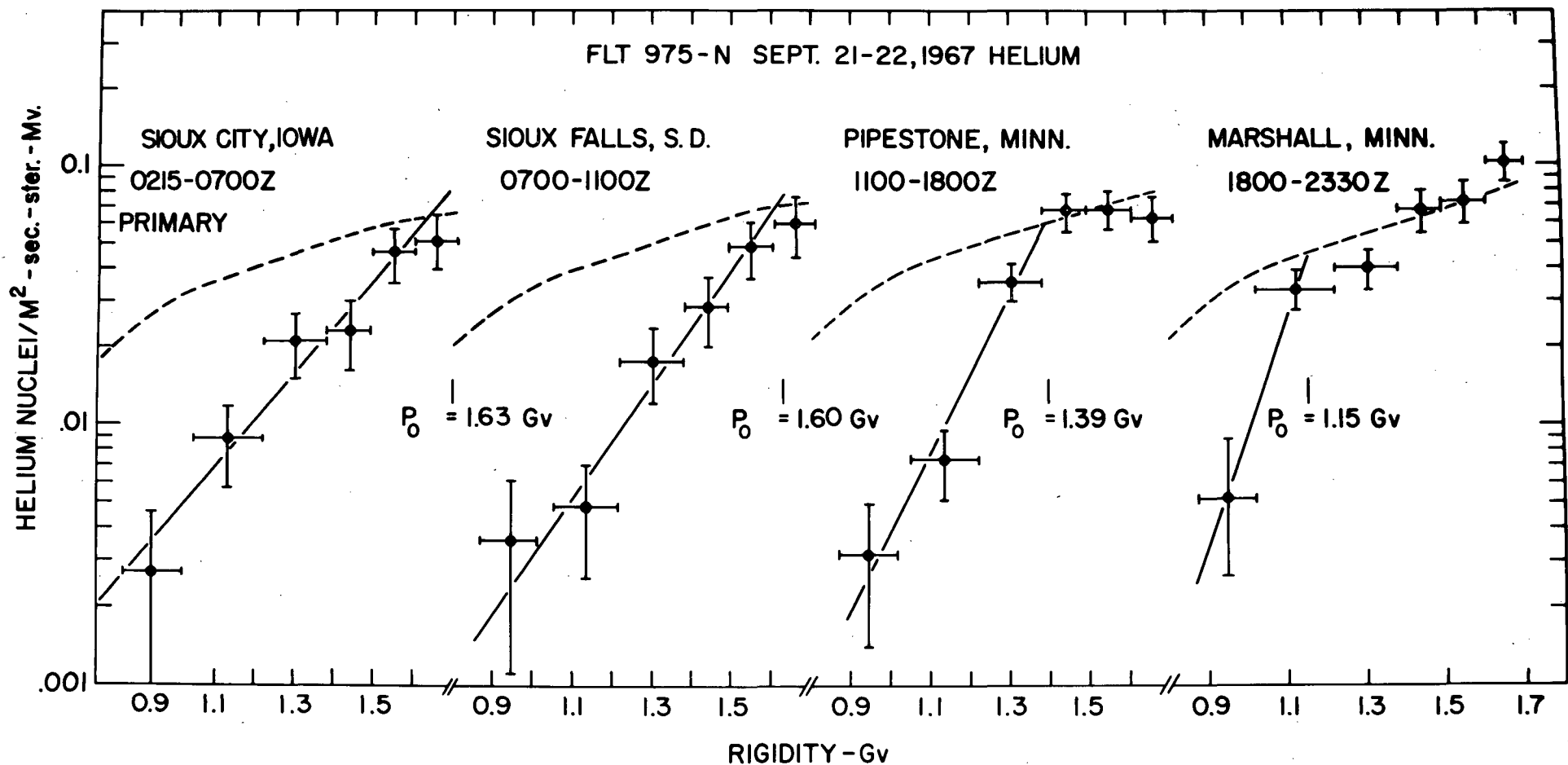


Figure 20. Differential helium rigidity spectra obtained in four sections of Flight 975-N showing the downward progression of the cutoff as the balloon drifted toward the northeast.

Figure 22. Differential helium rigidity spectra obtained in six sections of Flight 1079-W, all of Flight 1078-W, and at Churchill in 1968.

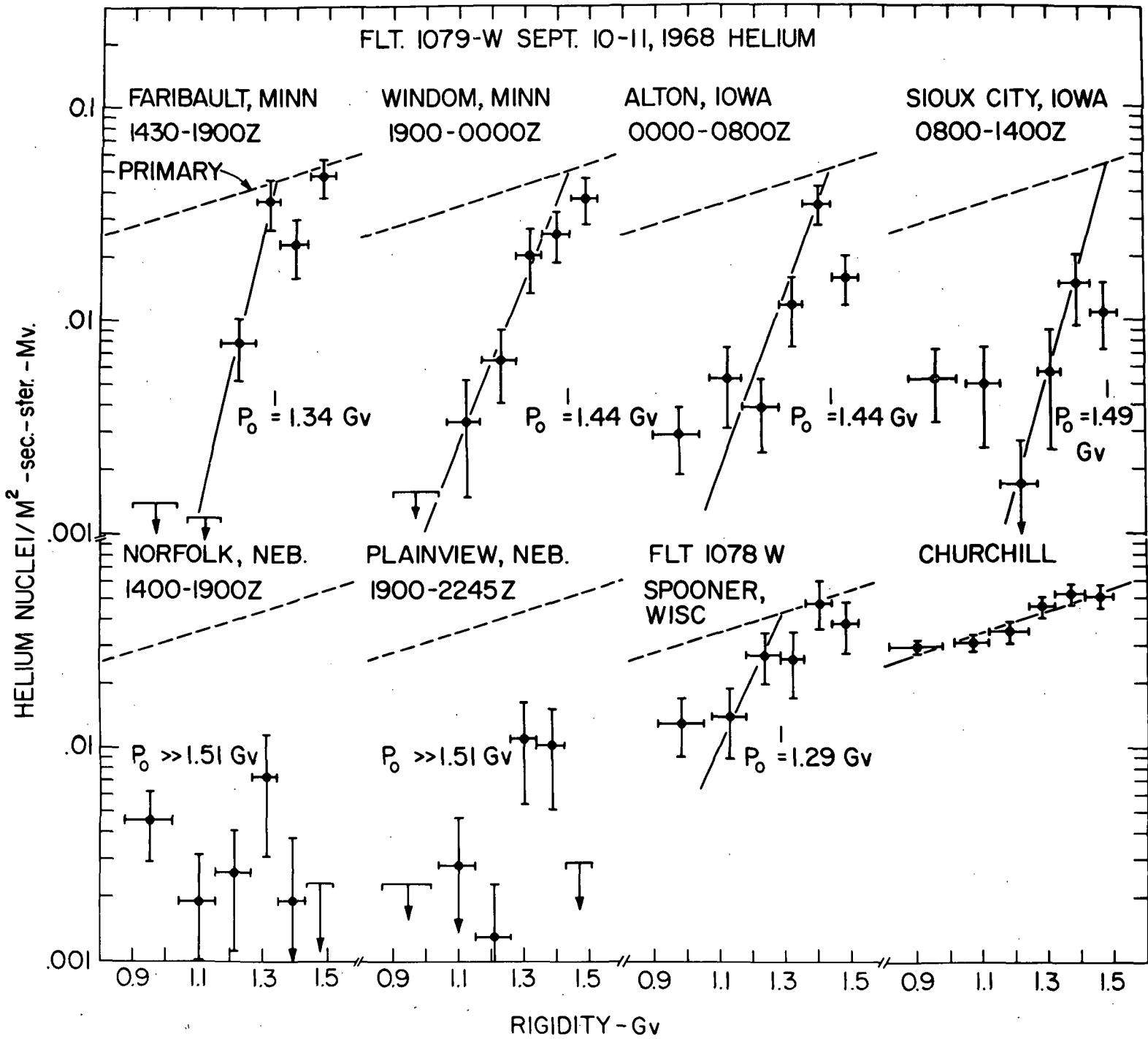


Figure 22

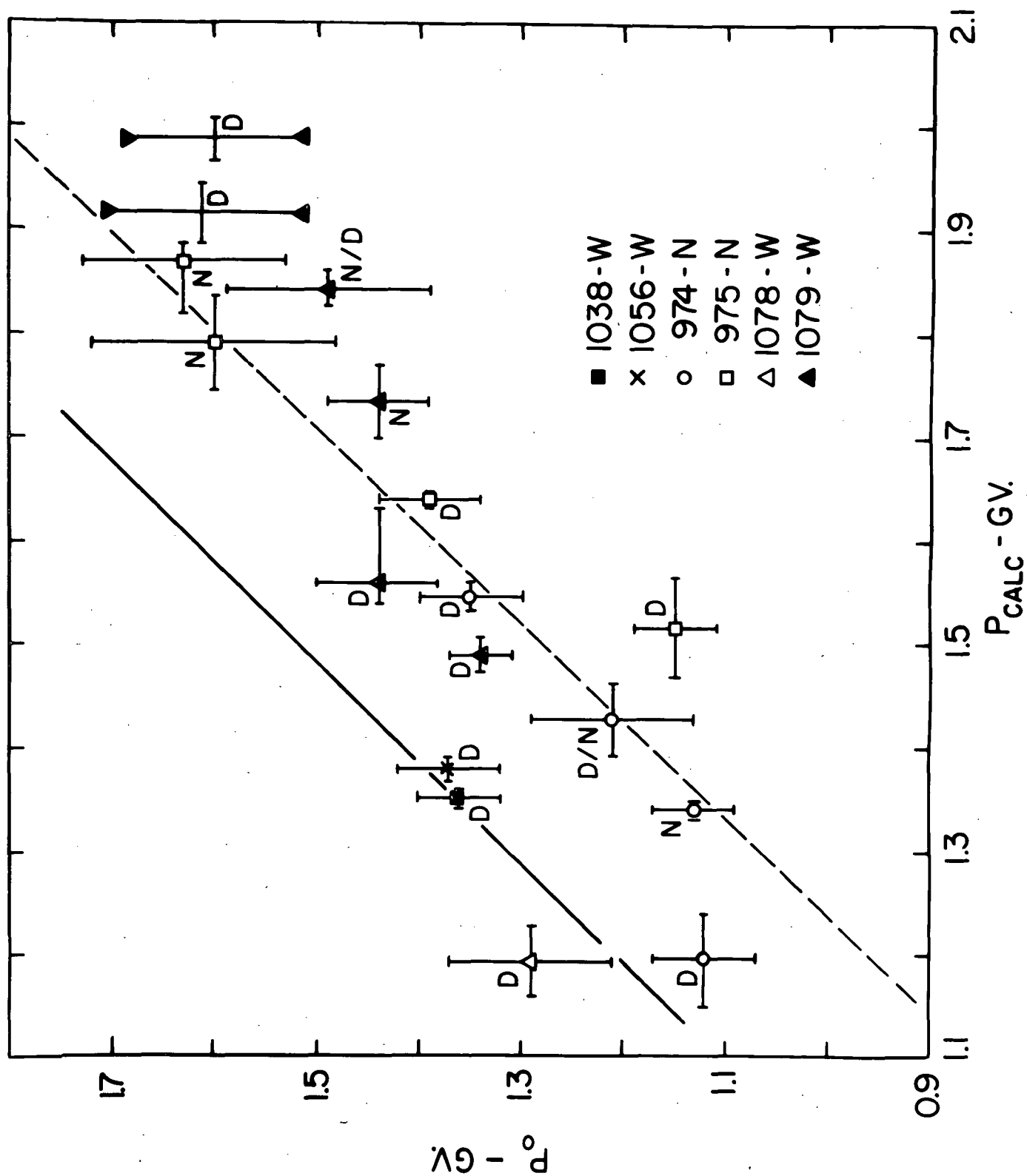


Figure 23. Comparison of the observed cutoff rigidity P_0 and the cutoff rigidity calculated from internal sources P_{calc} from Equation V-4, for all segments of six balloon flights over the Upper Mid-West region. The solid line indicates the expected relation for internal sources of the earth's field alone. The dashed line indicates the average 19% cutoff reduction discussed by Bingham et al. (1968).

Figure 24. Comparison of the observed cutoff rigidity P_{cx} obtained from Equation V-10 with P_{calc} for all segments of six Upper Mid-West flights. The solid line indicates the expected relationship if the cutoff is due to internal sources alone.

Figure 24

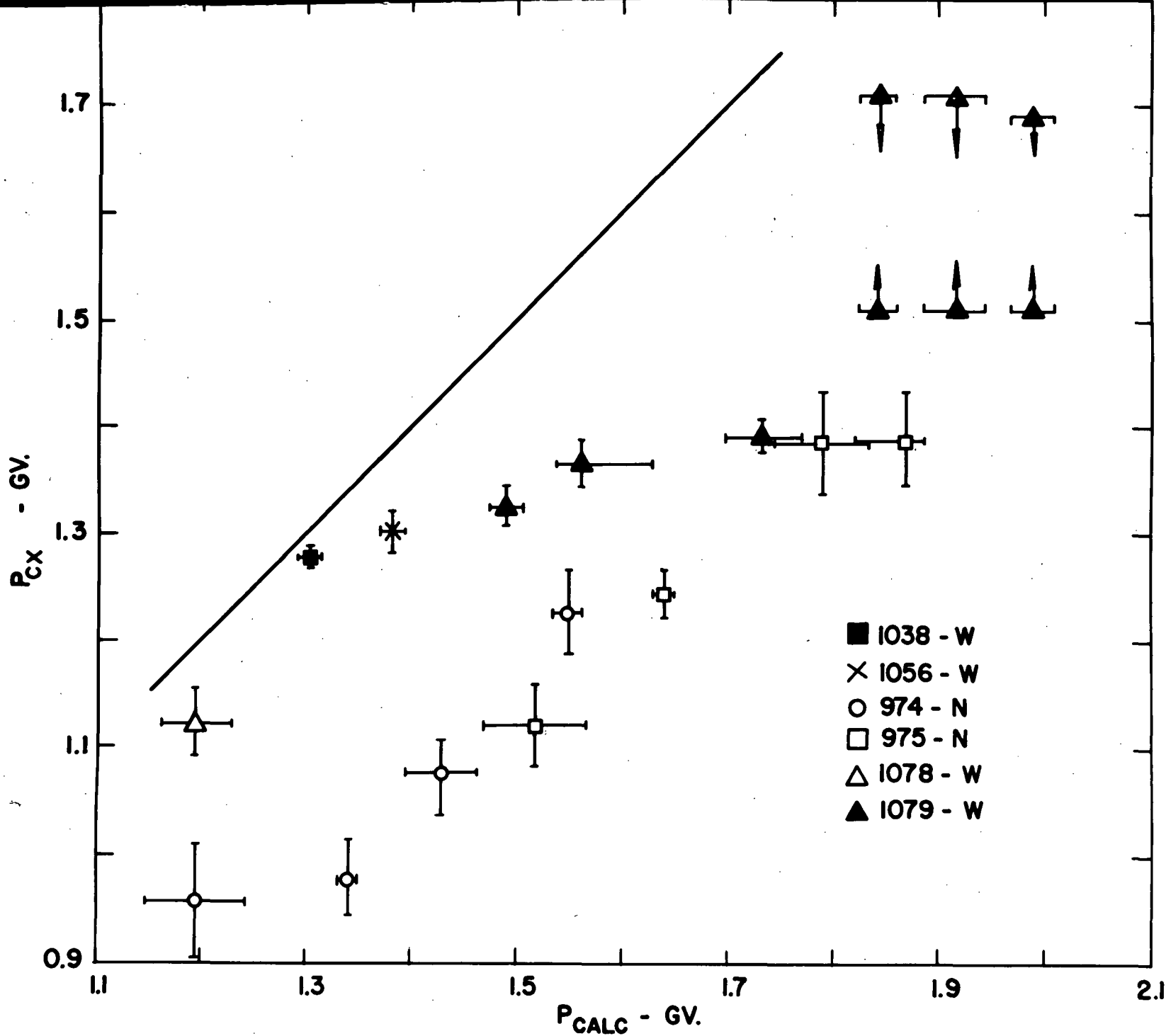


Figure 25. Correlation analysis of cutoff depression (on an inverse scale $P_{\text{calc}}/P_{\text{obs}}$) against equatorial D_{st} for observations obtained during geomagnetically quiet and disturbed times. Numbered diagonal lines indicate the cutoff behavior predicted by the Kellogg and Winckler(1961) model for ring currents of various radii. Numbers shown in parentheses are those radii corrected for the inductive effect of the earth. Solid lines designated Q and D indicate, respectively, the quiet and disturbed time cutoff variations obtained from the hodoscope observations.

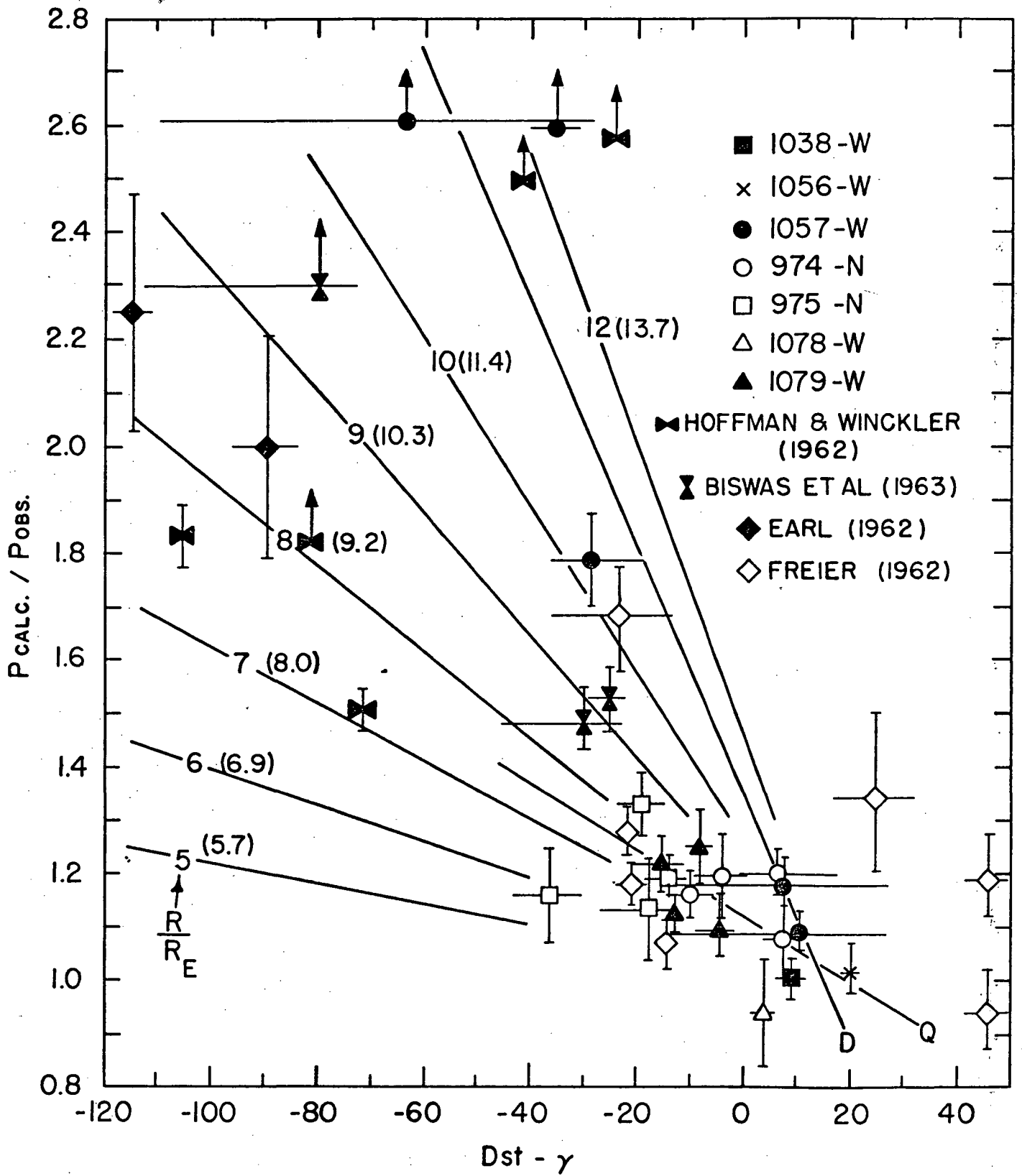


Figure 25

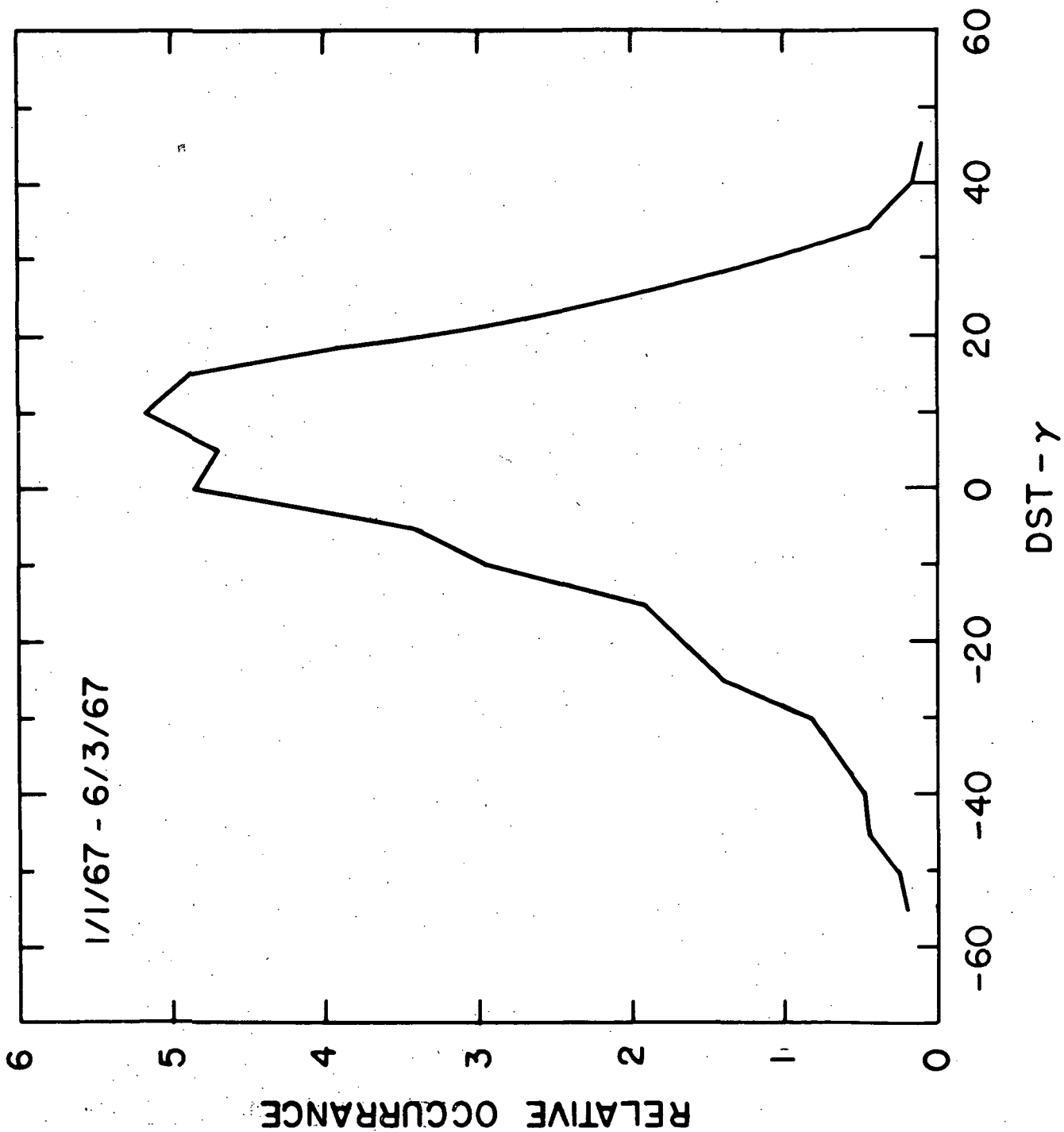


Figure 26. Histogram of the relative occurrence of hourly D_{st} values for the first six months of 1967 used to argue for an offset of $\pm 7.5 \gamma$ in the D_{st} scale.

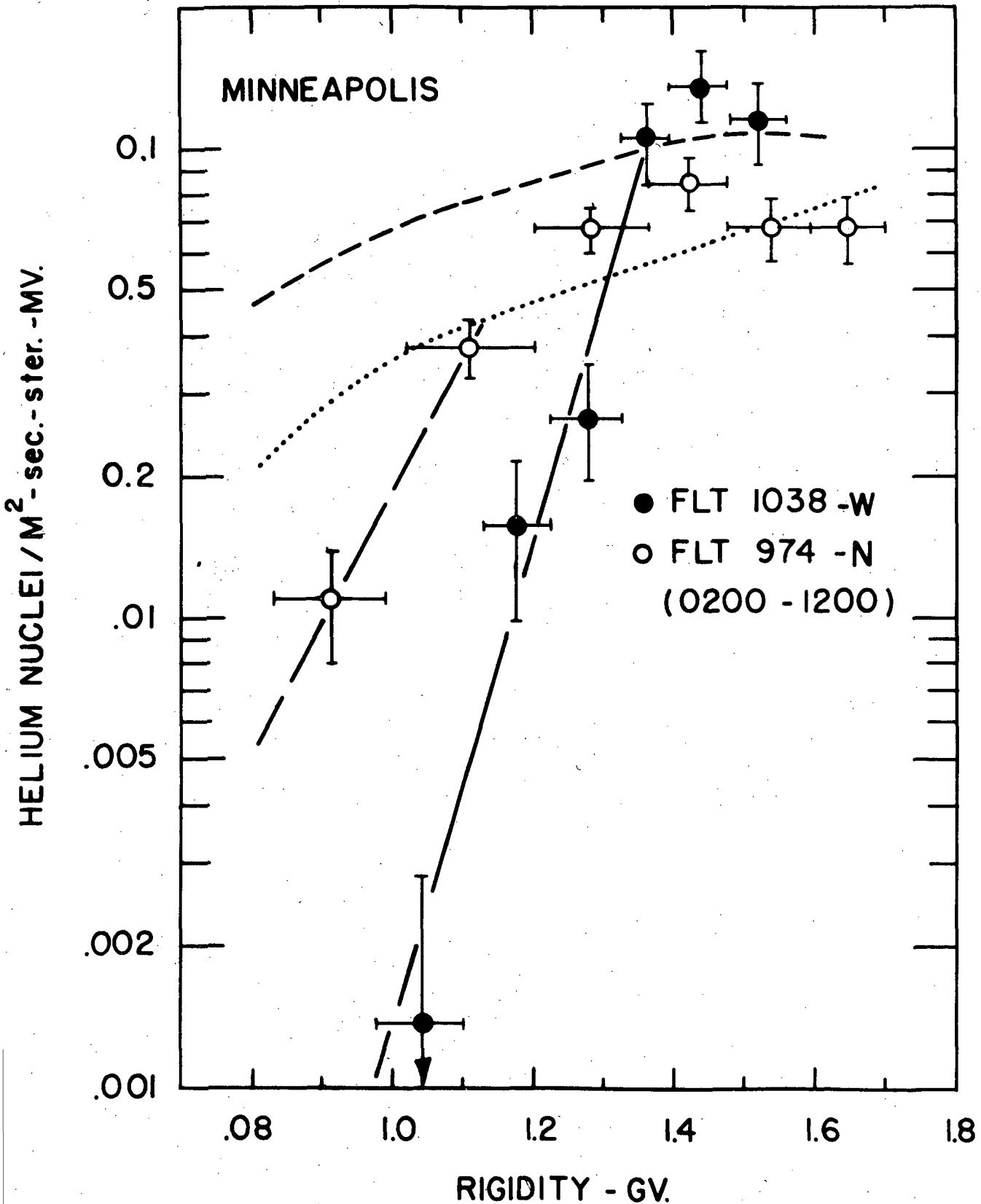


Figure 27. Comparison of the cutoff measured over Minneapolis ($P_c = 1.36$ GV) on two quiet time flights demonstrating the significant cutoff depression in effect during Flight 974-N.

Figure 28. Time history of the solar and geomagnetic event associated with the solar flare that occurred at 1522 U. T. August 28, 1966. See text for further details.

Figure 28

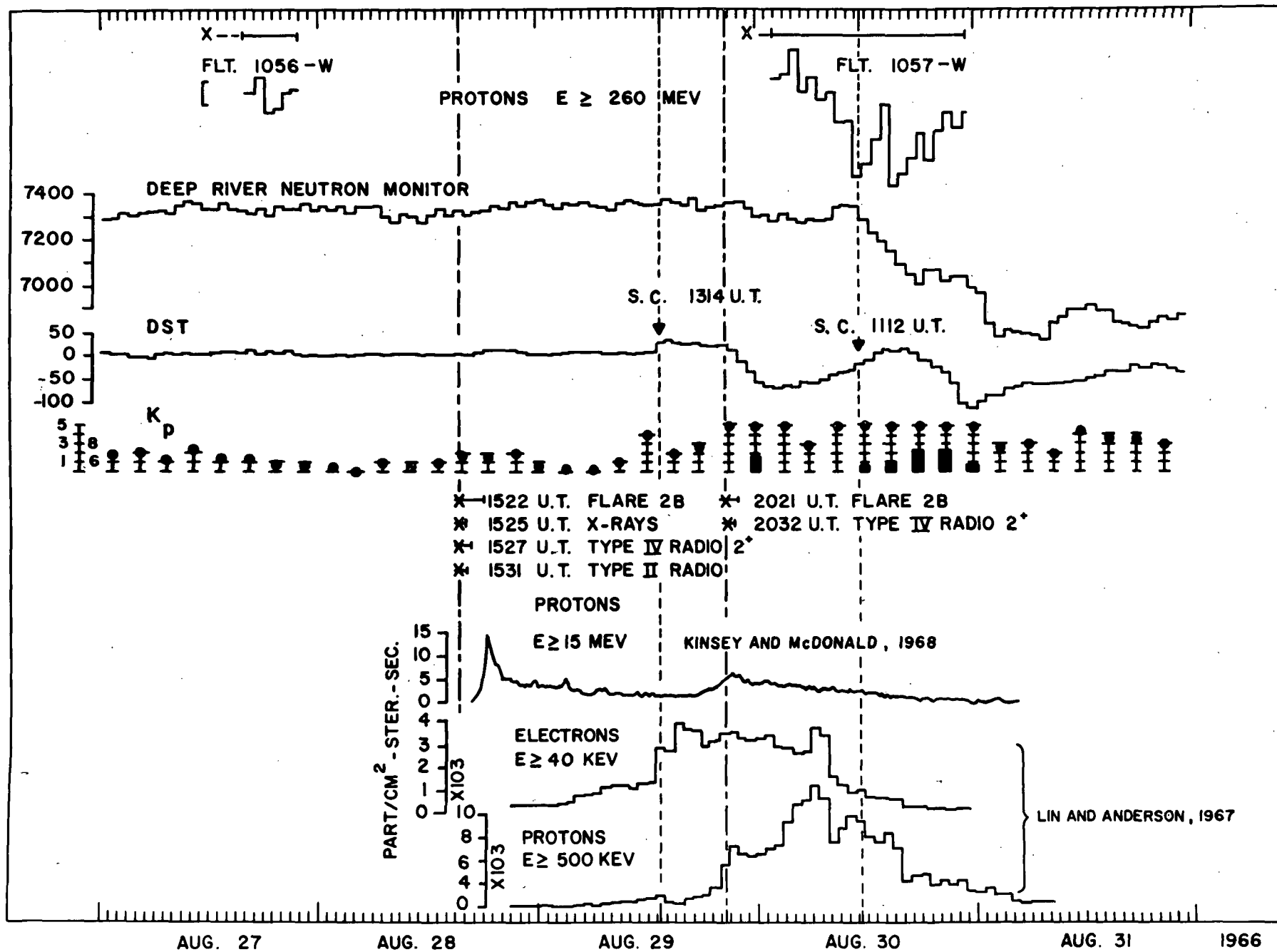


Figure 29. Differential rigidity spectra for protons observed during five segments of Flight 1057-W. Expected primary and albedo spectra are shown as dashed lines to assist in determining the geomagnetic cutoff rigidity for each segment.

FLT. 1057 W

AUG. 30, 1966

PROTONS

0215-0620Z

0620-1020Z

1020-1420Z

1420-1920Z

1920-2340Z

PROTONS / M²-sec. - ster. - Mv

1.0

PRIMARY

ALBEDO

0.1

P₀ < 0.5 GV.

P₀ ≈ 0.8 GV.

P₀ > 0.8 GV.

P₀ > 0.8 GV. P₀ < 0.5 GV.

0.01

0.5

0.7

0.5

0.7

0.5

0.7

0.5

0.7

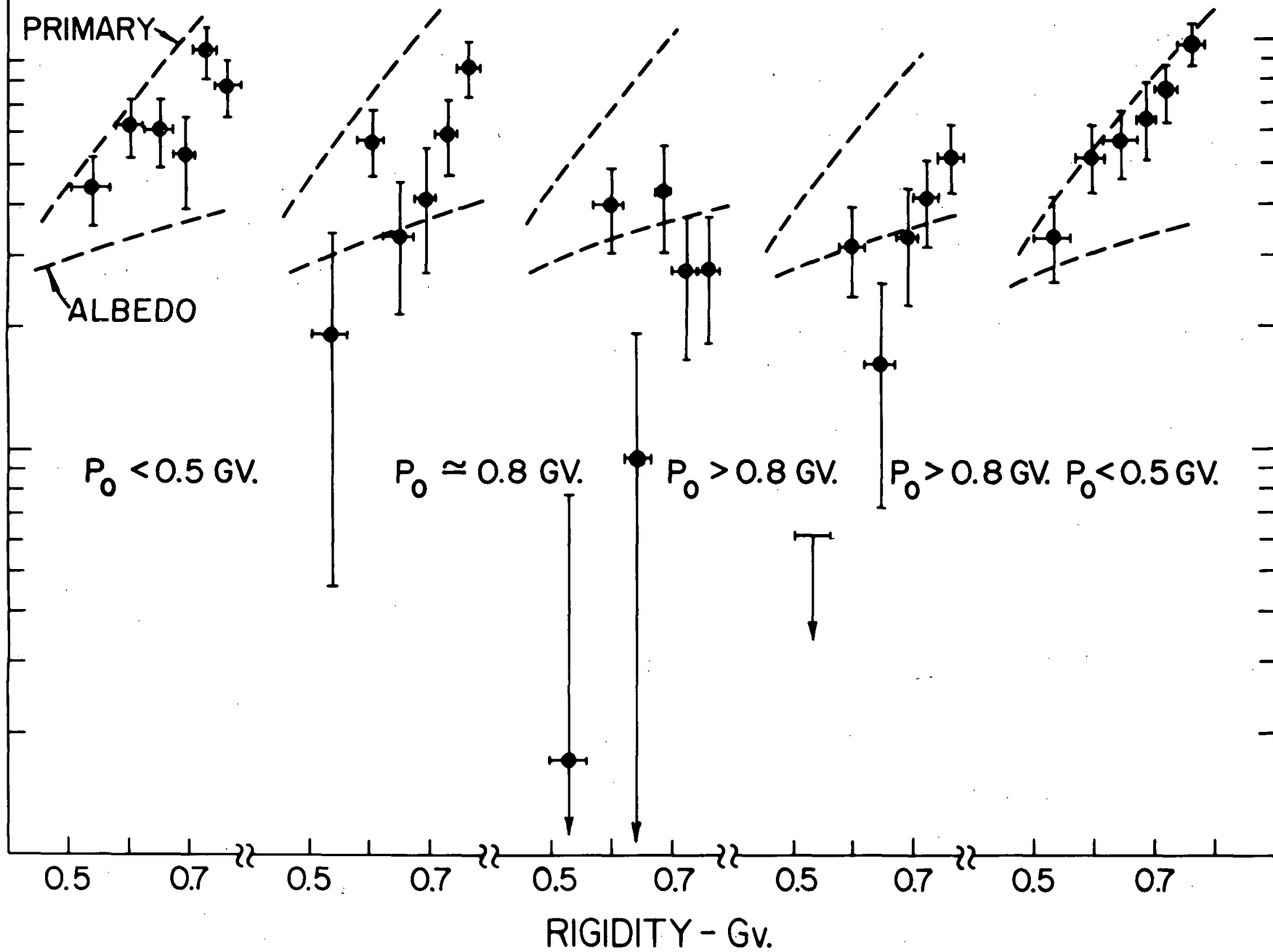
0.5

0.7

RIGIDITY - Gv.

Figure 29

156



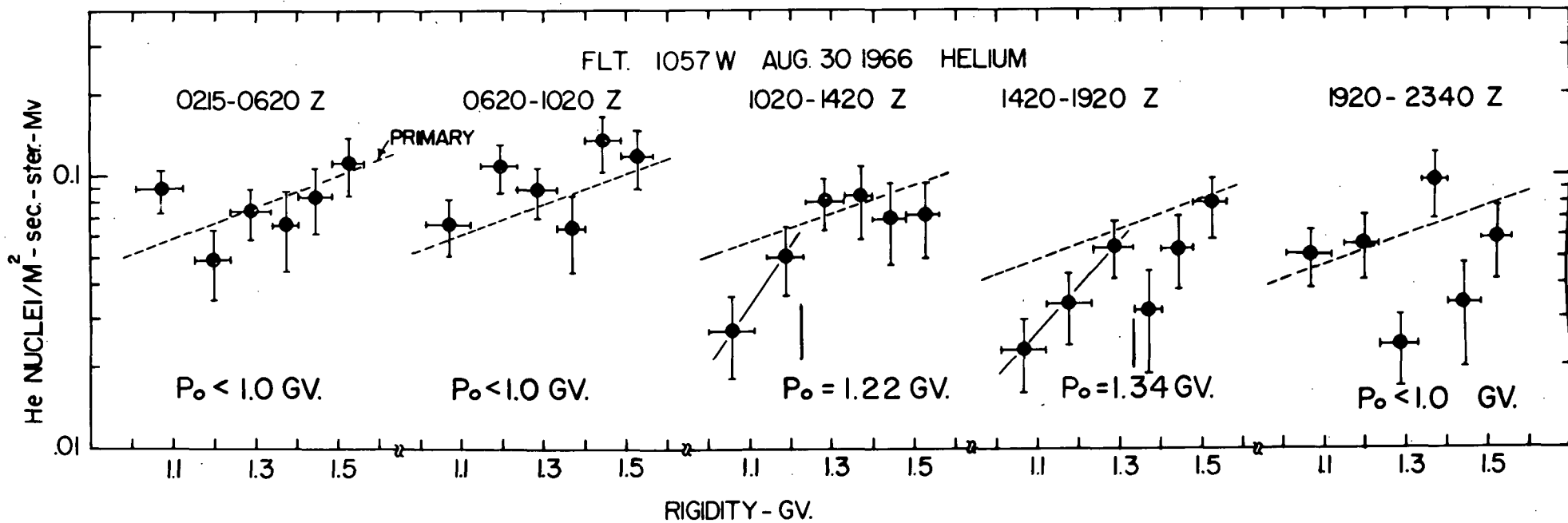


Figure 30. Differential rigidity spectra for helium nuclei for five segments of Flight 1057-W. Dashed lines indicate the expected primary spectra for each segment.

Figure 31. Regression curve of hourly fluxes of penetrating protons observed during Flight 1057-W at Minneapolis (small squares). Fluxes observed at Churchill in 1966 and 1967 (solid circles 1 and 2, respectively) and at Minneapolis during Flight 1056-W (X) are also shown. Diagonal lines indicate regression curves obtained over the long term at Minneapolis and Churchill. The intervening lines indicate regression curves expected for various cutoff rigidities.

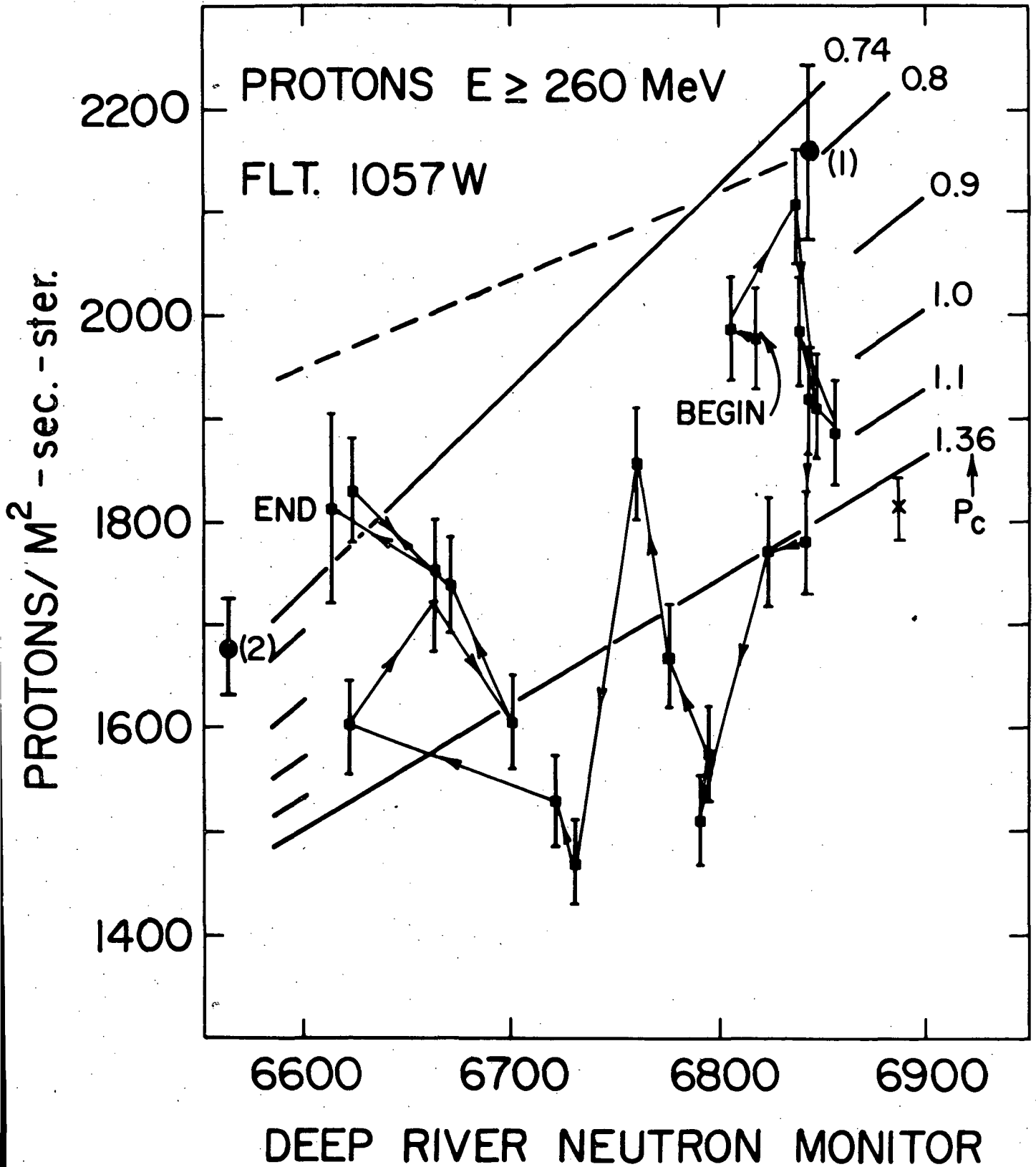


Figure 31

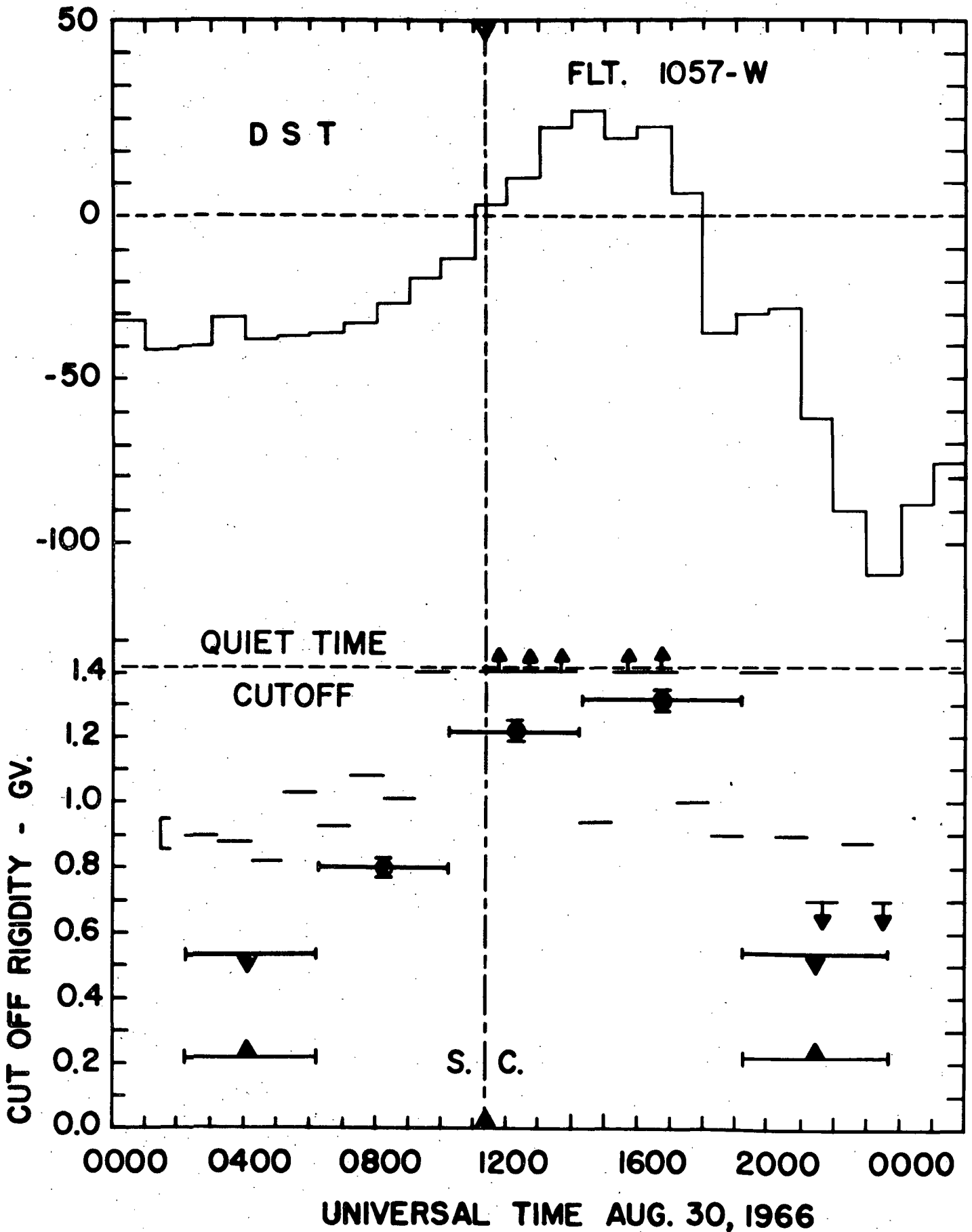


Figure 32. Comparison of the temporal behavior of the geomagnetic cutoff during Flight 1057-W (lower) obtained from the spectral (solid circles) and regression (short lines) analyses with equatorial D_{st} (upper).

Figure 33. Schematic representation of the geomagnetic field in the noon-midnight meridian plane for three idealized cases: A.) dipole field, B.) quiet time solar wind flow (Williams and Mead, 1965), C.) enhanced solar wind flow.

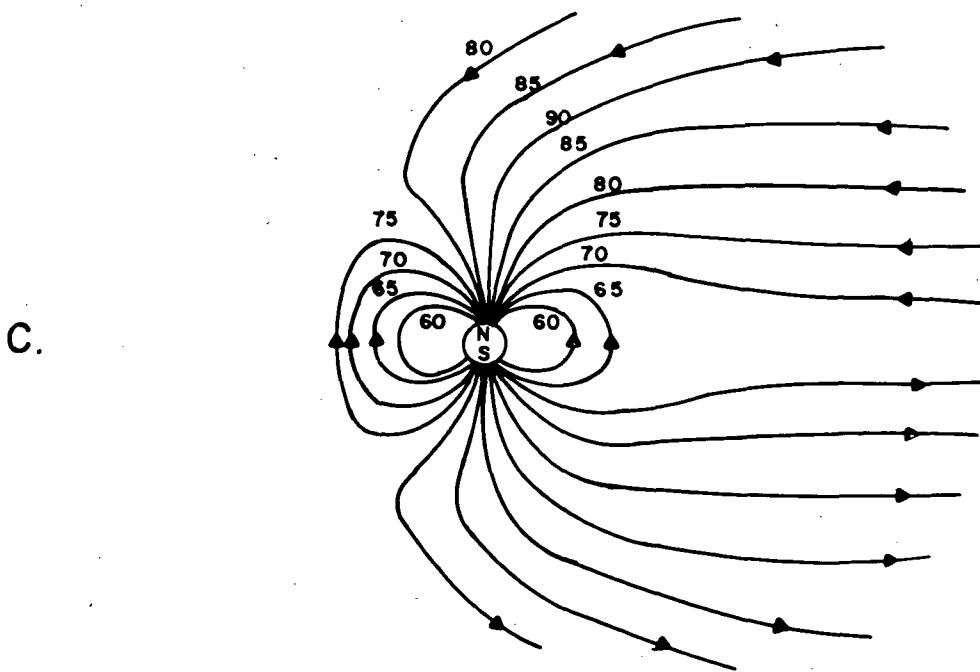
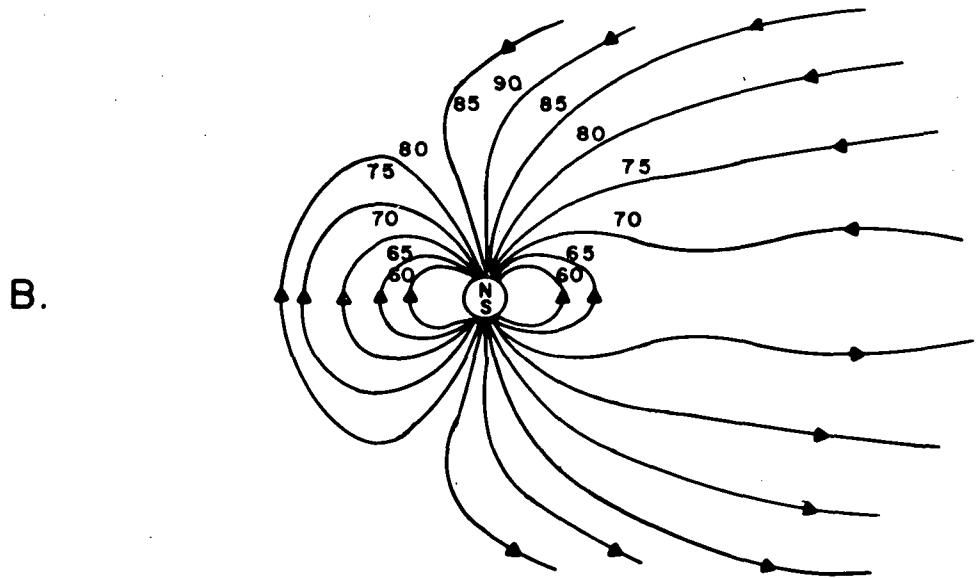
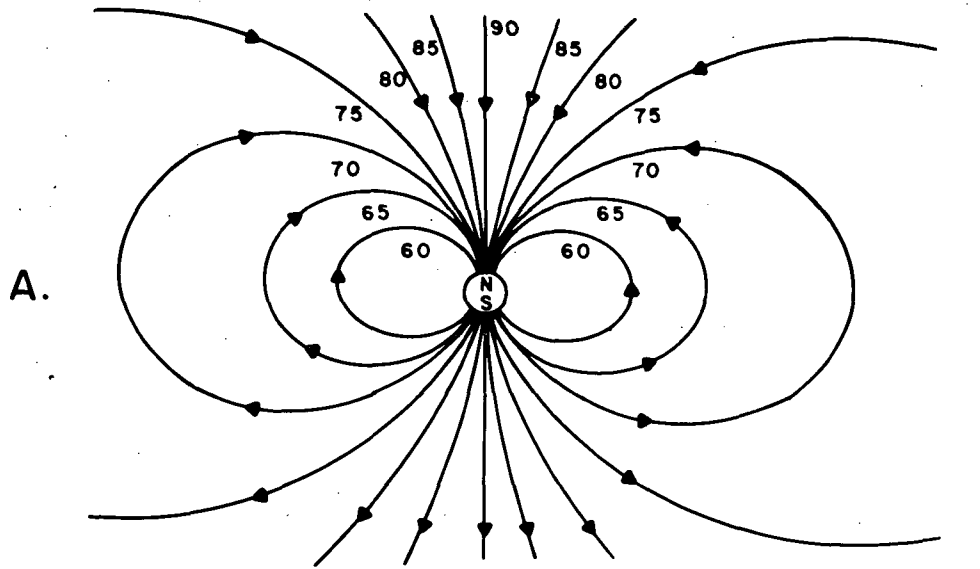


Figure 33

Figure 34. Neutron monitor record for the Canadian net (Steljes, 1966) for August 1966 showing the periods during which hodoscope observations were made.

NEUTRON MONITORS AUGUST 1966

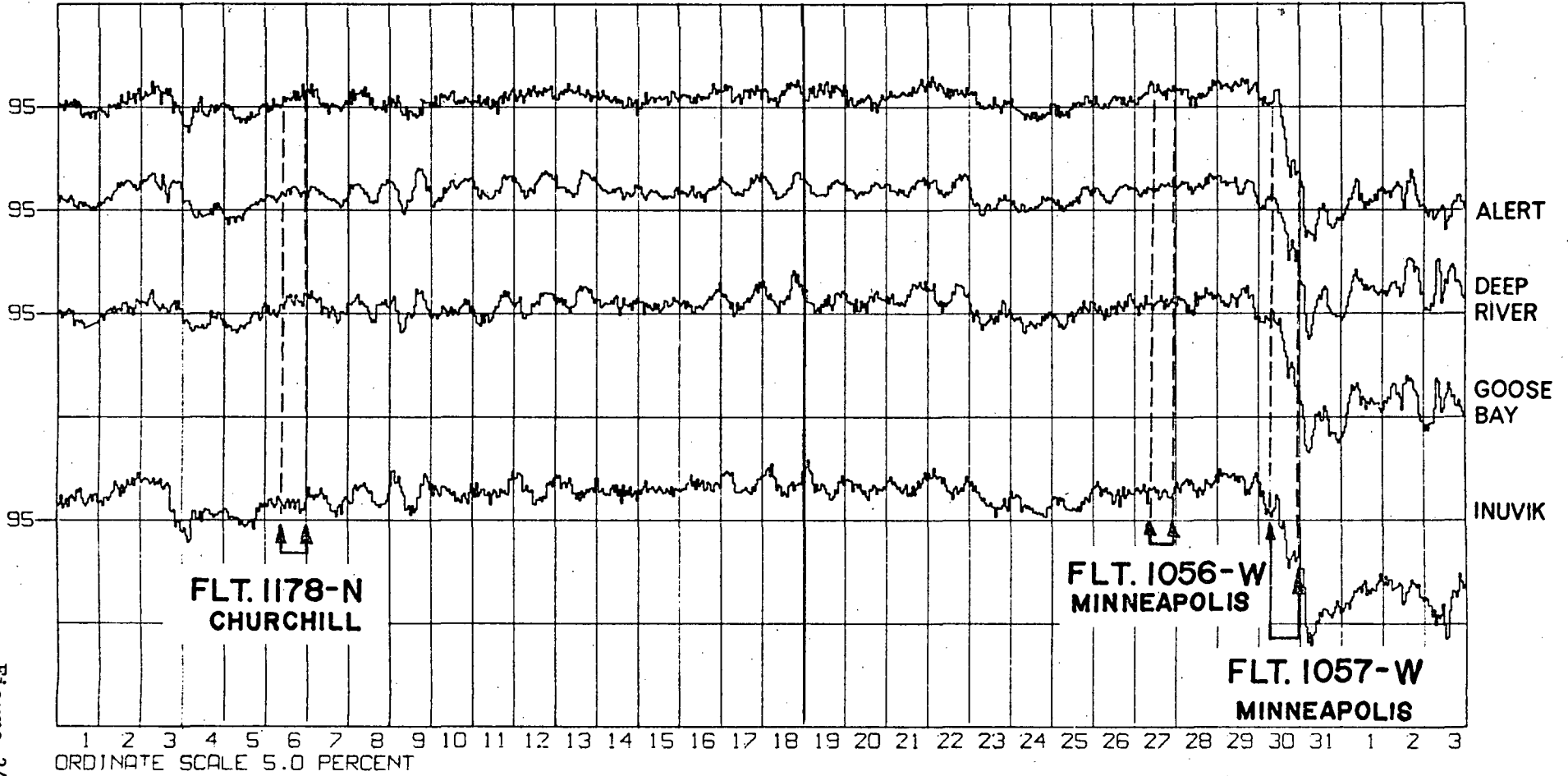


Figure 34

Figure 35. Regression curve for the parameter A in $J=AT$ for protons $100 \leq E \leq 260$ MeV. The fluxes obtained during segments 1 and 5 of Flight 1057-W are shown as crossed circles. Solid circles represent the hodoscope results and open circles are the satellite observations of Hsieh (1970) and Hsieh, Mason, and Simpson (1971). Dashed and dotted lines are regression curves of the form reported by Lockwood et al. (1970).

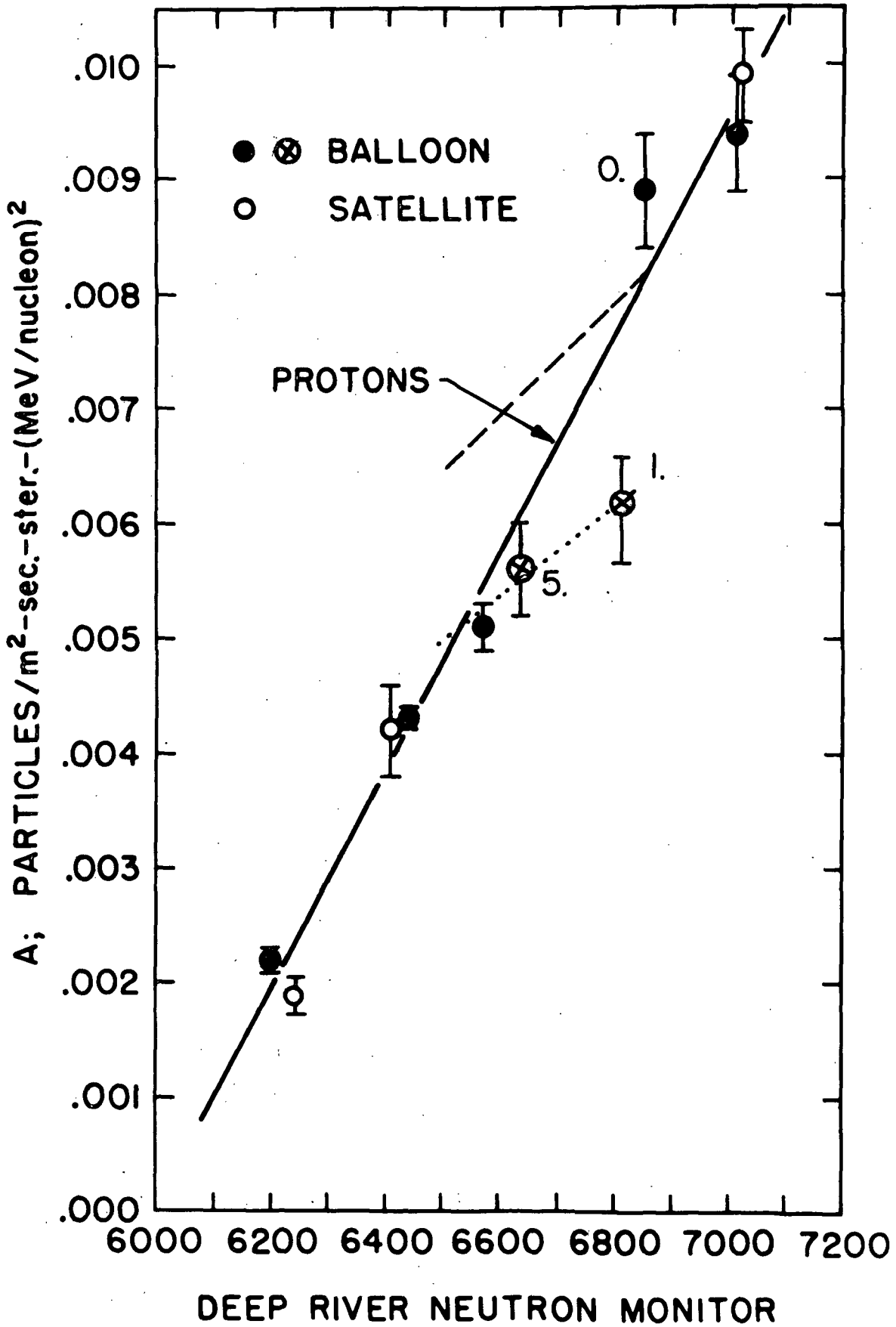


Figure 35

Figure 36. Regression curves of penetrating helium (upper) and RANGE 7-9 helium (lower) during Flight 1057-W (solid circles). Fluxes obtained from Flight 1056-W are shown as X's. Solid lines are the long term regression curves obtained from the hodoscope results (Rygg, 1970). Dashed lines represent regression curves for the short term modulation obtained by Lockwood et al. (1970).

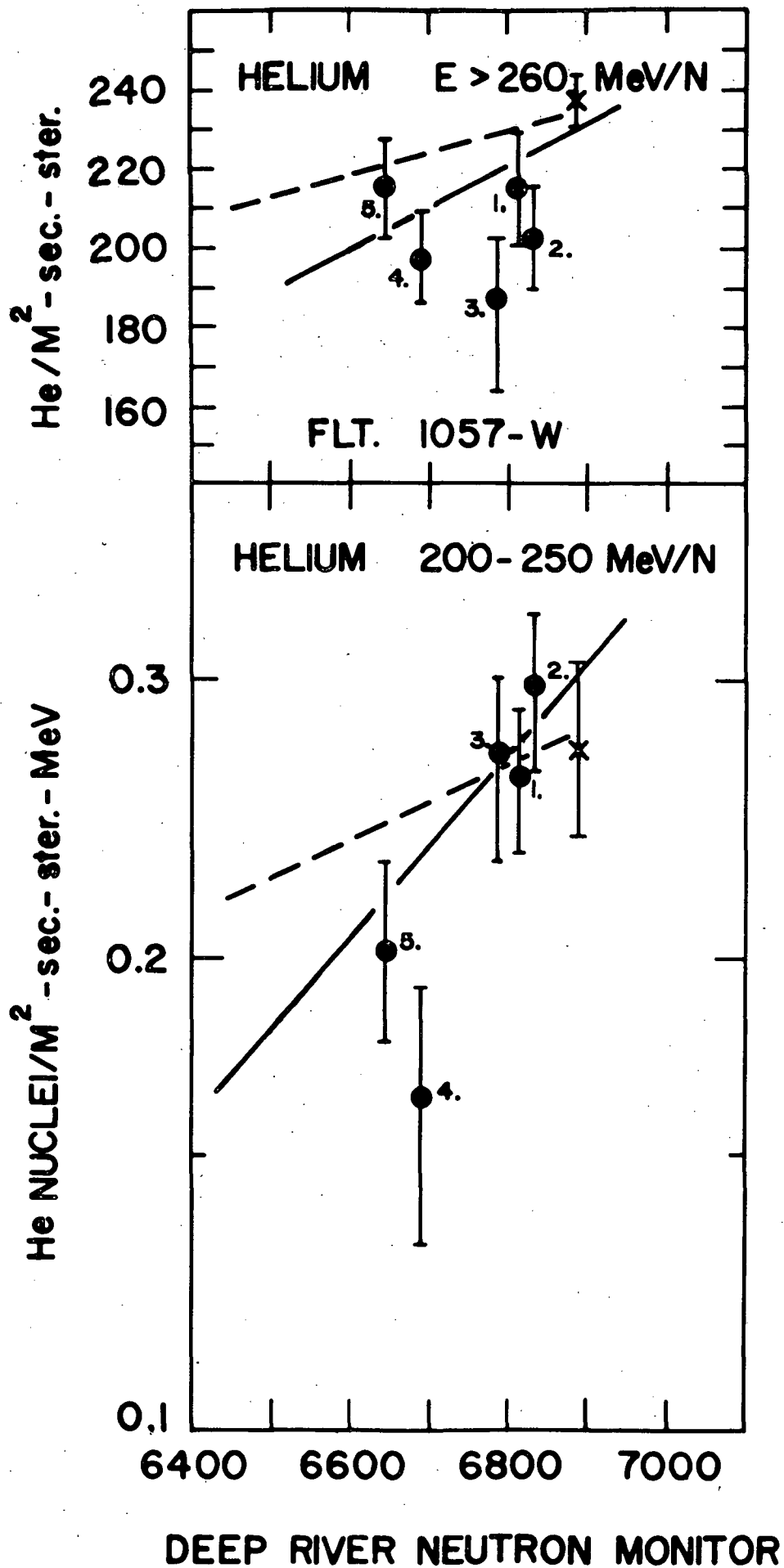


Figure 36